A new 3D equilibrated residual method improving accuracy and efficiency of flux-free error estimates

Núria Parés*, Pedro Díez

Laboratori de Càlcul Numèric (LaCàN), Universitat Politècnica de Catalunya, Campus Nord UPC, E-08034 Barcelona, Spain

Summary

The paper presents a novel strategy providing fully computable upper bounds for the energy norm of the error in the context of three-dimensional linear finite element approximations of the reaction-diffusion equation. The upper bounds are guaranteed regardless the size of the finite element mesh and the given data, and all the constants involved are fully computable. The upper bounds property holds if the shape of the domain is polyhedral and the Dirichlet boundary conditions are piecewise-linear. The new approach is an extension of the flux-free methodology introduced by Parés and Díez[1], which introduces a guaranteed, low-cost and efficient flux-free method substantially reducing the computational cost of obtaining guaranteed bounds using flux-free methods while retaining the good quality of the bounds. Besides extending the 2D methodology, specific new modifications are introduced to further reduce the computational cost in the three-dimensional setting. The presented methodology also provides a new strategy to obtain equilibrated boundary tractions which improves the quality of standard techniques while having a similar computational cost.

KEYWORDS:
Verification, Error estimation, Adaptivity, 3D, Exact/guaranteed/strict bounds, Certificates, Fully computable a posteriori error estimation, Adaptivity, Reaction-diffusion equation, Flux-free, Equilibrated boundary tractions

1 INTRODUCTION

The computation of fully computable *guaranteed/strict* a posteriori error bounds both for the energy norm of the error or for quantities of interest has been a subject of active research in the past years[2,3,4]. The fundamental property of *guaranteed* error estimation is that the final bounds do not depend on generic non-explicit constants and that they hold regardless the size of the finite element mesh (they do not neglect higher order terms nor hold only asymptotically). Moreover, much effort has been devoted to obtain *efficient* guaranteed bounds[5,6,7,8,9,10].

One of the most accurate error estimators currently available is the *flux-free* error estimator introduced by Parés et al.[11] based on the partition of unity property to localize the error equations in nodal-patches of elements called *stars*. This technique has been extensively used in many applications, and even though in its original form only provides asymptotic bounds for the error it has subsequently been modified to provide guaranteed error bounds[12,13,14,15,1].

Flux-free estimators are usually compared with *hybrid-flux* estimators, which are based on obtaining local equilibrated tractions to state the error equations in the elements. In general, the flux-free approach provides better accuracy while the hybrid-flux approach may require lower CPU cost[6,13,14,1]. As in Parés and Díez[1], the objective of the present work is to provide a novel flux-free strategy - now in a three dimensional setting - that while retaining the accuracy of the standard flux-free approach has a computational cost comparable to the cost of hybrid-flux techniques.

Finally, it is shown that the resulting technique also provides a new technique to compute 3D equilibrated boundary tractions to be popular in any equilibrated residual method. One of the most used techniques to compute the equilibrated boundary tractions is described by Ainsworth and Oden[16], Chapter 6. These local fluxes verify the *first-order equilibration conditions* which can be decoupled into local problems posed over nodal-centered patches of elements (patches of elements with a common vertex node called *stars*). Specifically, the equilibrated tractions are written in terms of its moments yielding to a system of equations posed in each star where the number of unknowns of the local problem coincides, in a 3D setting, with the number of faces of the tetrahedra on the star. The new proposed equilibrated technique also solves a local problem in each star but the unknowns are now associated to each vertex of the faces conforming the star (three per face). The increase in the number of local unknowns (three times larger) along with a new efficient minimization criterion allow obtaining a very precise set of equilibrated tractions while not substantially increasing the computational cost.

2 MODEL PROBLEM AND FINITE ELEMENT APPROXIMATION

The *three-dimensional* steady reaction-diffusion equation reads

$$\begin{aligned} -\Delta u + \kappa^2 u &= f \quad \text{in } \Omega, \\ u &= u_{\mathrm{D}} \quad \text{on } \Gamma_{\mathrm{D}}, \\ \boldsymbol{\nabla} u \cdot \boldsymbol{n} &= g_{\mathrm{N}} \quad \text{on } \Gamma_{\mathrm{N}}, \end{aligned} \tag{1}$$

where Ω is an open bounded polyhedral domain whose boundary $\partial\Omega = \overline{\Gamma}_{\mathrm{N}} \cup \overline{\Gamma}_{\mathrm{D}}$ is partitioned into two disjoint sets Γ_{N} and Γ_{D}. The Dirichlet boundary condition u_{D} is assumed to be continuous and piecewise linear on Γ_{D}, $g_{\mathrm{N}} \in \mathcal{L}^2(\Gamma_{\mathrm{N}})$, $f \in \mathcal{L}^2(\Omega)$ and the datum κ is assumed to be a piecewise-constant field. Without loss of generality, κ is also assumed to be non-negative and in order to guarantee the unicity of the solution of (1), either $\kappa > 0$ in a non-zero measure subdomain of Ω or Γ_{D} is a non-empty set. For the sake of simplicity, the Dirichlet boundary conditions are assumed to be piecewise linear so that they are exactly verified using linear finite elements. However, this assumption can be removed[17]. Also, the datum κ is assumed to be piecewise-constant but this assumption can also be removed, see Appendix E.

The variational formulation of the problem is stated as follows: find $u \in \mathcal{U}$ such that

$$a(u, v) = \ell(v) \quad \text{for all } v \in \mathcal{V}, \tag{2}$$

where

$$a(u, v) = \int_\Omega \left(\boldsymbol{\nabla} u \cdot \boldsymbol{\nabla} v + \kappa^2 u v \right) \, d\Omega \quad \text{and} \quad \ell(v) = \int_\Omega f v \, d\Omega + \int_{\Gamma_{\mathrm{N}}} g_{\mathrm{N}} v \, d\Gamma,$$

and $\mathcal{U} = \{u \in \mathcal{H}^1(\Omega),\, u|_{\Gamma_{\mathrm{D}}} = u_{\mathrm{D}}\}$ and $\mathcal{V} = \{v \in \mathcal{H}^1(\Omega),\, v|_{\Gamma_{\mathrm{D}}} = 0\}$ are the solution and test spaces respectively, $\mathcal{H}^1(\Omega)$ being the standard Sobolev space.

The finite element approximation of (2) is defined introducing a conforming tetrahedralization of the computational domain Ω into n_{el} linear shape-regular tetrahedral elements denoted by Ω_k, and considering the associated finite-dimensional spaces $\mathcal{U}^h \subset \mathcal{U}$ and $\mathcal{V}^h \subset \mathcal{V}$ of piecewise-linear continuous functions over this mesh of characteristic mesh size h. It is further assumed that the mesh is such that the reaction coefficient is constant inside each element, and in the following, the local restriction to element Ω_k of the (constant) reaction coefficient is denoted by $\kappa_k = \kappa|_{\Omega_k} \in \mathbb{R}$. Then, the finite element approximation of u is $u_h \in \mathcal{U}^h$ such that

$$a(u_h, v) = \ell(v) \quad \text{for all } v \in \mathcal{V}^h. \tag{3}$$

3 GUARANTEED UPPER BOUNDS FOR THE ENERGY NORM: COMPLEMENTARY ENERGY RELAXATION AND DATA PROJECTION

The standard complementary energy minimization approach[18,19] can be used to derive upper bounds for the energy norm of the error using globally admissible complementary fields[20,21,22,23,24]. This upper bounds can also be derived using the dual variational principle proposed by Prager and Synge[25,26]. Using either of the two previous approaches, it can be stated that any pair of dual complementary estimates $\boldsymbol{q} \in [\mathcal{L}^2(\Omega)]^3$ and $r \in \mathcal{L}^2(\Omega)$ verifying the residual equation

$$\int_\Omega \left(\boldsymbol{q} \cdot \boldsymbol{\nabla} v + \kappa^2 r v \right) d\Omega = \ell(v) - a(u_h, v) = R(v) \quad \forall v \in \mathcal{V} \tag{4}$$

yield an upper bound for the energy norm of the error $e = u - u_h \in \mathcal{V}$, where the energy norm of a function v is defined as $|||v||| = a(v,v)^{1/2}$. Specifically,

$$|||e|||^2 \leq \|\boldsymbol{q}\|^2_{[\mathcal{L}^2(\Omega)]^3} + \|\kappa r\|^2_{\mathcal{L}^2(\Omega)}, \tag{5}$$

where $\|\cdot\|_{[\mathcal{L}^2(\Omega)]^3}$ and $\|\cdot\|_{\mathcal{L}^2(\Omega)}$ denote the standard norms of the Lebesgue spaces $[\mathcal{L}^2(\Omega)]^3$ and $\mathcal{L}^2(\Omega)$ respectively, that is

$$\|\boldsymbol{q}\|^2_{[\mathcal{L}^2(\Omega)]^3} = \int_\Omega \boldsymbol{q}\cdot\boldsymbol{q}\, d\Omega \quad \text{and} \quad \|r\|^2_{\mathcal{L}^2(\Omega)} = \int_\Omega r^2\, d\Omega.$$

A detailed proof of this result is given by Parés and Díez[1] for a 2D setting (valid also for 3D).

Hence, any pair of dual estimates $\boldsymbol{q} \in [\mathcal{L}^2(\Omega)]^3$ and $r \in \mathcal{L}^2(\Omega)$ verifying (4) provide a guaranteed upper bound for the energy norm of the error. However ensuring efficiency and accuracy of guaranteed a posteriori error estimators requires keeping a balance between two aspects in competition: 1) the dual estimates have to be carefully chosen to avoid a large overestimation in (5) (the optimal estimates being $\boldsymbol{q} = \boldsymbol{\nabla} e$ and $r = e$) and 2) the dual estimates have to be *fully computable* and its computational cost should be affordable and as low as possible.

The best approach in terms of accuracy of the error estimator is to use a dual global formulation to compute the dual estimates[19,27,28]. However, this approach is computationally expensive because the methodology to obtain the dual estimates $\boldsymbol{q}$ and r is global. In practice, most methods aim at finding a pair of dual estimates solving only local finite dimensional problems. In particular, it is a common practice to use *piecewise polynomial* fields. That is, for a given suitable interpolation degree q, the goal is to find $\boldsymbol{q} \in [\widehat{\mathbb{P}}^q(\Omega)]^3$ and $r \in \widehat{\mathbb{P}}^{q-1}(\Omega)$ verifying (4) where

$$\widehat{\mathbb{P}}^q(\Omega) = \{v \in \mathcal{L}^2(\Omega),\, v|_{\Omega_k} \in \mathbb{P}^q(\Omega_k)\},$$

$\mathbb{P}^q(\Omega_k)$ being the space of polynomials of degree q over Ω_k, for $k = 1, \dots, n_{\text{el}}$.

It is worth noting that a pair of *piecewise polynomial* dual estimates verifying (4) exist only if the input data f and g_{N} are piecewise polynomial functions. For non-piecewise polynomial data, guaranteed upper bounds using piecewise polynomial dual estimates can also be obtained if the data oscillation errors are isolated from the discretization errors[1,29,30]. Indeed, denote by $\Pi_k^{\hat{q}} : \mathcal{L}^2(\Omega_k) \to \mathbb{P}^{\hat{q}}(\Omega_k)$ the $\mathcal{L}^2(\Omega_k)$-orthogonal projector to the space of polynomials of degree $\hat{q}$ defined over the element Ω_k, and by $\Pi_\gamma^{\bar{q}} : \mathcal{L}^2(\gamma) \to \mathbb{P}^{\bar{q}}(\gamma)$ the $\mathcal{L}^2(\gamma)$-orthogonal projector to the space of polynomials of degree $\bar{q}$ defined over the face γ. Then, the following theorem follows.

Theorem 1. Let $\boldsymbol{q} \in [\mathcal{L}^2(\Omega)]^3$ and $r \in \mathcal{L}^2(\Omega)$ be a pair of dual estimates verifying

$$\int_\Omega \Big(\boldsymbol{q}\cdot\boldsymbol{\nabla} v + \kappa^2 r v\Big)\, d\Omega = R^\Pi(v) \quad \forall v \in \mathcal{V}, \tag{6}$$

where the projected residual $R^\Pi(\cdot)$ is defined as

$$R^\Pi(v) = \sum_{k=1}^{n_{\text{el}}} \left[\int_{\Omega_k} \Pi_k^{\hat{q}}(f - \kappa_k^2 u_h) v\, d\Omega + \sum_{\gamma\subset\partial\Omega_k\cap\Gamma_{\text{N}}} \int_\gamma \Pi_\gamma^{\bar{q}} g_{\text{N}} v\, d\Gamma - \int_{\Omega_k} \boldsymbol{\nabla} u_h\cdot\boldsymbol{\nabla} v\, d\Omega \right],$$

$\hat{q}$ and $\bar{q}$ being two whole numbers. Then, the following upper bound follows

$$|||e|||^2 \leq \sum_{k=1}^{n_{\text{el}}} \eta_k^2,$$

for

$$\eta_k = \sqrt{\|\boldsymbol{q}\|^2_{[\mathcal{L}^2(\Omega_k)]^3} + \kappa_k^2 \|r\|^2_{\mathcal{L}^2(\Omega_k)}} + \text{osc}_k(f) + \sum_{\gamma\subset\partial\Omega_k\cap\Gamma_{\text{N}}} \text{osc}_\gamma(g_{\text{N}}). \tag{7}$$

The oscillation terms are given by

$$\text{osc}_k(f) = C_0 \|f - \kappa_k^2 u_h - \Pi_k^{\hat{q}}(f - \kappa_k^2 u_h)\|_{\mathcal{L}^2(\Omega_k)} \tag{8}$$

and

$$\text{osc}_\gamma(g_{\text{N}}) = \min\left\{C_1, C_2\right\} \|g_{\text{N}} - \Pi_\gamma^{\bar{q}} g_{\text{N}}\|_{\mathcal{L}^2(\gamma)}, \tag{9}$$

for the exactly computable data oscillation constants

$$C_0 = \min\left\{\frac{h_k}{\pi}, \frac{1}{\kappa_k}\right\}, \tag{10}$$

$$C_1^2 = \frac{|\gamma|}{3|\Omega_k|}\frac{1}{\kappa_k}\sqrt{(2\max_{\boldsymbol{x}\in\gamma}|\boldsymbol{x} - \boldsymbol{x}_\gamma|)^2 + (3/\kappa_k)^2} \tag{11}$$

and

$$C_2^2 = \frac{|\gamma|}{3|\Omega_k|} C_0 \left(2\max_{\boldsymbol{x}\in\gamma}|\boldsymbol{x} - \boldsymbol{x}_\gamma| + 3C_0\right), \tag{12}$$

where $\boldsymbol{x}_\gamma$ denotes the vertex of element Ω_k opposite to the face γ, $|\boldsymbol{x}-\boldsymbol{x}_\gamma|$ denotes the $\mathbb{R}^3$ Euclidean norm of the vector $\boldsymbol{x}-\boldsymbol{x}_\gamma$, $|\gamma|$ is the area of the face γ and $h_k = \max_{\boldsymbol{x},\boldsymbol{y}\in\Omega_k} |\boldsymbol{x}-\boldsymbol{y}|$ and $|\Omega_k|$ are the diameter and volume of element Ω_k respectively.

This theorem is the extension to the three dimensional setting of Theorem 1 in Parés and Díez[1]. The proof of the theorem is not included here since it can be easily obtained following Parés and Díez[1] combined with the results presented by Ainsworth and Vejchodský[29,30]. However, it is worth noting that the three dimensional extension of the result incorporates two novelties: 1) the reaction coefficient κ is a piecewise constant function over Ω instead of being just constant and 2) the oscillation term associated to the source data $\mathrm{osc}_k(f)$ includes the projection of the reaction term associated to the finite element approximation.

Remark 1. Note that the notation for the data oscillation constants C_0, C_1 and C_2 is simplified since no explicit dependency on element Ω_k and face γ is done. However, these constants are not the same for each element, C_0 varying in each element Ω_k and C_1 and C_2 being different for each face γ of each element Ω_k.

Remark 2. In the expressions for C_1 and C_2 the term $\max_{\boldsymbol{x}\in\gamma} |\boldsymbol{x}-\boldsymbol{x}_\gamma|$ can be replaced by the diameter of the tetrahedron Ω_k where γ lies, h_k, and still the upper bound property holds.

Remark 3. For $\hat{q} \geq 1$, since the finite element approximation is linear and κ_k is constant, $\Pi_k^{\hat{q}}(\kappa_k^2 u_h) = \kappa_k^2 u_h$ and therefore $\mathrm{osc}_k(f)$ reduces to the standard one

$$\mathrm{osc}_k(f) = C_0 \| f - \Pi_k^{\hat{q}} f \|_{\mathcal{L}^2(\Omega_k)}.$$

Remark 4. For $\kappa_k = 0$, the constants C_0 and C_2 are simply

$$C_0 = \frac{h_k}{\pi} \quad \text{and} \quad C_2^2 = \frac{|\gamma|}{3|\Omega_k|}\frac{h_k}{\pi}\left(2\max_{\boldsymbol{x}\in\gamma}|\boldsymbol{x}-\boldsymbol{x}_\gamma| + 3\frac{h_k}{\pi}\right), \tag{13}$$

and the oscillation error due to the Neumann boundary condition is

$$\mathrm{osc}_\gamma(g_\mathrm{N}) = C_2 \| g_\mathrm{N} - \Pi_\gamma^{\bar{q}} g_\mathrm{N} \|_{\mathcal{L}^2(\gamma)}.$$

From now on, the subscripts of the $\mathcal{L}^2$-norms are simplified to $\|\cdot\|_{[\mathcal{L}^2(\Omega_k)]^3} = \|\cdot\|_k$, $\|\cdot\|_{\mathcal{L}^2(\Omega_k)} = \|\cdot\|_k$ and $\|\cdot\|_{\mathcal{L}^2(\gamma)} = \|\cdot\|_\gamma$, where the local norm of vector and scalar fields in Ω_k, which have the same notation, can be disambiguated by looking into their arguments.

4 LOCAL COMPUTATION OF THE DUAL ESTIMATES q AND R USING A FLUX-FREE APPROACH: A NOVEL CHEAPER/LOW-COST CONSTRUCTION

The piecewise polynomial dual estimates, $\boldsymbol{q}$ and r, are computed imposing equation (6) using a *flux-free* subdomain-based approach[13,14]. The presented method is novel in the sense that it provides a non-unique *explicit/closed* expression for the dual estimates $\boldsymbol{q} \in [\widehat{\mathbb{P}}^q(\Omega)]^3$ and $r \in \widehat{\mathbb{P}}^{q-1}(\Omega)$ verifying (6). Thus, it only requires solving a small linear system of equations to optimize the quality of the bounds.

The present work differs from Parés and Díez[1] in four main aspects: 1) the new method is valid in a 3D context, 2) the reaction dual estimate r is not necessarily taken to be zero, thus overcoming solvability problems when considering low data projection degrees in Theorem 1 and also improving the quality of the final bounds, 3) the reaction term is introduced in the oscillation term (8) allowing to use a lower interpolation degree q for the dual estimates and therefore reducing the computational cost of the technique and finally 4) three different explicit closed forms for the dual estimates are given depending on the projection degrees $\hat{q}$ and $\bar{q}$.

The remainder of the section is structured as follows. Section 4.1 presents the set of decoupled constrained minimization problems that have to be solved (one for each node of the mesh) in order to compute the dual estimates using the flux-free approach. Section 4.2 details the strong form of the constraints of the local optimization problems followed by Section 4.3 which provides a particular closed expression for the dual estimates $\boldsymbol{q}$ and r ensuring that they satisfy the constraints of the optimization problems. These closed formulas allow reducing the constrained optimization problems given in Section 4.1 into simplified smaller constrained quadratic optimization problems described in detail in Section 4.4.

4.1 Flux-free approach: basic equations and notations

Let $\boldsymbol{x}_i$, $i = 1, \dots, n_{\text{np}}$, denote the vertex nodes of the mesh and let ω_i be the support of its associated linear shape function ϕ_i, also referred to as the star associated with node i. Let also $\mathcal{V}(\omega_i)$ and $\widehat{\mathbb{P}}^q(\omega_i)$ denote the local restrictions of the spaces $\mathcal{V}$ and $\widehat{\mathbb{P}}^q(\Omega)$ to the star ω_i, respectively. Then, one can obtain a pair of dual estimates $\boldsymbol{q} \in [\widehat{\mathbb{P}}^q(\Omega)]^3$ and $r \in \widehat{\mathbb{P}}^{q-1}(\Omega)$ verifying (6) by adding a set of local dual estimates $\boldsymbol{q}^i$ and r^i computed independently for each star of the mesh. Specifically,

$$\boldsymbol{q} = \sum_{i=1}^{n_{\text{np}}} \boldsymbol{q}^i \qquad \text{and} \qquad r = \sum_{i=1}^{n_{\text{np}}} r^i, \tag{14}$$

where $\boldsymbol{q}^i \in [\widehat{\mathbb{P}}^q(\omega_i)]^3$ and $r^i \in \widehat{\mathbb{P}}^{q-1}(\omega_i)$ are such that

$$\int_{\omega_i} \left(\boldsymbol{q}^i \cdot \boldsymbol{\nabla} v + \kappa^2 r^i v \right) d\Omega = R^{\Pi}(\phi_i v) \quad \forall v \in \mathcal{V}(\omega_i). \tag{15}$$

Indeed, equation (6) is readily recovered by adding the local star equations (15) and using the partition of unity property, $\sum_{i=1}^{n_{\text{np}}} \phi_i = 1$. It is worth noting that equation (15) does not have a unique solution. In order to select among all the solutions one providing high-quality bounds, this equation is complemented with the minimization of the local norm of the dual estimates $\boldsymbol{q}^i$ and r^i. That is, the global problem of finding $\boldsymbol{q}$ and r verifying equation (6) and minimizing the upper bound for the error given in equation (5) is decomposed into the following local constrained minimization problems

$$\boxed{\begin{array}{c} \underset{\boldsymbol{q}^i \in [\widehat{\mathbb{P}}^q(\omega_i)]^3 \,,\, r^i \in \widehat{\mathbb{P}}^{q-1}(\omega_i)}{\text{Minimize}} \quad \|\boldsymbol{q}^i\|^2_{[\mathcal{L}^2(\omega_i)]^3} + \|\kappa r^i\|^2_{\mathcal{L}^2(\omega_i)} \\ \text{Subject to} \qquad \boldsymbol{q}^i \,,\, r^i \text{ verifying (15).} \end{array}} \tag{16}$$

Remark 5. It is worth noting that although the dual estimates $\boldsymbol{q}^i$ and r^i are selected to minimize the local complementary energy given by $\|\boldsymbol{q}^i\|^2_{[\mathcal{L}^2(\omega_i)]^3} + \|\kappa r^i\|^2_{\mathcal{L}^2(\omega_i)}$, there is no certainty that the accumulated estimates $\boldsymbol{q}$ and r defined in equation (14) will globally minimize the complementary energy used to compute the bounds in (7). As shown in the existing literature[13,12,15,1], the minimization of the local complementary energy given in (16) provides very good effectivities for the final bound, but simple existing techniques[13,12] could be used to further improve the final bound.

Obviously the flux-free approach can only be used if equation (15) admits at least one solution. A strictly positive reaction term $\kappa_k > 0$ in any of the elements Ω_k conforming the star ω_i, ensures the solvability of the local equations (for any $r^i \neq 0$). However, for $\kappa^2 r^i|_{\omega_i} = 0$, the solvability is only directly ensured if the star intersects the Dirichlet boundary. Note that the condition $\kappa^2 r^i|_{\omega_i} = 0$ both includes the case of a zero reaction coefficient $\kappa|_{\omega_i} = 0$ or a particular choice for the reaction estimate of $r^i = 0$. For $\kappa^2 r^i|_{\omega_i} = 0$ and a star not intersecting the Dirichlet boundary, the kernel of the bilinear operator appearing in the l.h.s. of (15) is the one-dimensional space of constants, $\mathbb{P}^0(\omega_i)$, and therefore (15) is solvable only if the following compatibility[31,16] or *star equilibration* condition holds

$$R^{\Pi}(\phi_i) = 0. \tag{17}$$

Since the non-projected residual verifies the Galerkin orthogonality property, that is, $R(v) = 0$ for all $v \in \mathcal{V}^h$, the compatibility condition (17) can be enforced by imposing $R^{\Pi}(\phi_i) = R(\phi_i)$. Therefore, to be able to use the flux-free approach it is sufficient to take $\hat{q}$ and $\bar{q}$ greater or equal than 1. However, important computational savings are obtained when using constant projections and therefore the following solvability assumptions are introduced.

Remark 6 (Solvability assumptions)**.** The computational cost of the a posteriori error estimator decreases for lower values of $\hat{q}$ and $\bar{q}$. However, for $\hat{q} = 0$ or $\bar{q} = 0$, fulfilling (17) requires careful consideration. In general, minimizing cost and guaranteeing solvability suggests taking different values of $\hat{q} = 0$ and $\bar{q} = 0$ in the different elements and faces on Γ_{N}. Hereafter, the following requirements on the values of $\hat{q}$ and $\bar{q}$ on the elements of the mesh and Neumann faces respectively are introduced:

- for every face $\gamma \subset \Gamma_{\text{N}}$, the choice $\bar{q} = 0$ can only be made if either
  - $\kappa^2 r^i\big|_{\omega_i} \neq 0$ for all ω_i such that γ radiates from node $\boldsymbol{x}_i$, that is $\phi_i\big|_{\gamma} \neq 0$ or
  - the Neumann boundary data g_{N} is a constant function on γ
- for every element Ω_k of the mesh, the choice $\hat{q} = 0$ can only be made if either
  - $\kappa^2 r^i\big|_{\omega_i} \neq 0$ for all ω_i containing Ω_k or

– the data source $f - \kappa_k^2 u_h$ is a constant function inside Ω_k, that is $\kappa_k = 0$ along with f being constant in Ω_k.

Finally, it is worth noting that from these requirements, in pure diffusion problems or in problems having a vanishing reaction coefficient in a certain area, it is not possible to use $\hat{q} = 0$ or $\bar{q} = 0$ if the source data is not piecewise constant.

To simplify the presentation, it is assumed that the values of $\hat{q}$ and $\bar{q}$ are constant in all the mesh. However, combining different values of $\hat{q}$ and $\bar{q}$ for some specific faces or elements of the mesh only entails a more involved implementation. This non-constant approach is strongly recommended in some cases, for instance, when non-piecewise constant Neumann boundary conditions are given along with zero values of the reaction term. In this case it is necessary to take $\bar{q} = 1$ along the Neumann boundary, involving the use of quadratic tractions at these faces. The use of linear tractions in the other faces greatly simplifies the computation of the dual estimates in the stars not intersecting the Neumann boundary.

4.2 Strong form of the constraints of the local constrained optimization problems

The constraint (15) to problem (16) is expressed in its weak form. In the following, the strong form of (15) is preferred to handle it analytically. Some new notations must be introduced to derive this strong form.

First, the faces of a star ω_i denoted by $\mathcal{F}(\omega_i)$ are separated into two disjoint sets: $\mathcal{Z}_i$ include the faces not containing $\boldsymbol{x}_i$ as a vertex (or equivalently, the faces where the basis function ϕ_i vanishes), and Γ_i are the faces radiating from node $\boldsymbol{x}_i$ (or equivalently, the faces where ϕ_i is not zero), that is

$$\mathcal{Z}_i = \{\gamma \subset \mathcal{F}(\omega_i)\ ,\ \phi_i|_\gamma = 0\} \quad \text{and} \quad \Gamma_i = \{\gamma \subset \mathcal{F}(\omega_i)\ ,\ \phi_i(\boldsymbol{x}) \neq 0 \text{ for some } \boldsymbol{x} \in \gamma\}.$$

Note that if the star is associated with an interior node, $\mathcal{Z}_i = \partial\omega_i$ and Γ_i are its interior faces.

Also, for each face γ of the mesh, let $\boldsymbol{n}^\gamma$ be an arbitrary but fixed unit normal, with the restriction that if γ is an exterior face, $\boldsymbol{n}^\gamma = \boldsymbol{n}$, that is, it is outward to $\partial\Omega$. In addition, given an element Ω_k and a face of this element $\gamma \subset \partial\Omega_k$, let $\boldsymbol{n}_k^\gamma$ denote the outward unit normal to face γ and let $\sigma_k^\gamma = \boldsymbol{n}^\gamma \cdot \boldsymbol{n}_k^\gamma$ account for the sign associated with the arbitrary choice of $\boldsymbol{n}^\gamma$.

The strong form of the local error equation (15) is then written separately in each element of the star $\Omega_k \subset \omega_i$ by introducing the set of tractions $\{g_\gamma^i\}_{\gamma\subset\mathcal{F}(\omega_i)}$, where g_γ^i is the traction associated with the face γ of the star ω_i in the direction of $\boldsymbol{n}^\gamma$. Introducing the restriction of the dual estimates $\boldsymbol{q}^i$ and r^i to element $\Omega_k \subset \omega_i$, $\boldsymbol{q}_k^i = \boldsymbol{q}^i|_{\Omega_k} \in [\mathbb{P}^q(\Omega_k)]^3$ and $r_k^i = r^i|_{\Omega_k} \in \mathbb{P}^{q-1}(\Omega_k)$, the constraints given in (15) are equivalent to impose in all elements $\Omega_k \subset \omega_i$

$$-\boldsymbol{\nabla}\cdot\left(\boldsymbol{q}_k^i + \phi_i\boldsymbol{\nabla}u_h\right) + \kappa_k^2 r_k^i = \phi_i\Pi_k^{\hat{q}}(f - \kappa_k^2 u_h) - \boldsymbol{\nabla}u_h\cdot\boldsymbol{\nabla}\phi_i \qquad \text{in } \Omega_k, \tag{18a}$$

$$\left(\boldsymbol{q}_k^i + \phi_i\boldsymbol{\nabla}u_h\right)\cdot\boldsymbol{n}_k^\gamma = \sigma_k^\gamma g_\gamma^i \qquad \text{on } \gamma \subset \partial\Omega_k, \tag{18b}$$

along with imposing the following restrictions on the values of the tractions g_γ^i at the boundary of the star

$$g_\gamma^i = 0 \qquad \text{on } \gamma \subset \mathcal{Z}_i, \tag{19a}$$

$$g_\gamma^i = \phi_i\Pi_\gamma^{\bar{q}} g_{\mathrm{N}} \qquad \text{on } \gamma \subset \Gamma_i \cap \Gamma_{\mathrm{N}}. \tag{19b}$$

The proof that, for a given set of tractions $\{g_\gamma^i\}_{\gamma\subset\mathcal{F}(\omega_i)}$ verifying (19), any pair of dual estimates fulfilling (18) are a solution of (15) is given by Parés and Díez[1]. Even though the aforementioned proof refers to the two-dimensional set up, the proof is also valid in the three dimensional framework and is therefore omitted here.

The essential point of the new proposed a posteriori error estimator is that, for values of the polynomial degree of the interior and face projectors, $\hat{q}$ and $\bar{q}$, less or equal than one, it is possible to find a set of tractions $\{g_\gamma^i\}_{\gamma\subset\mathcal{F}(\omega_i)}$ for which equation (18) has an explicit solution (closed formula for $\boldsymbol{q}_k^i$ and r_k^i).

Remark 7. Equations (18) do not uniquely determine $\boldsymbol{q}_k^i \in [\mathbb{P}^q(\Omega_k)]^3$ and $r_k^i \in \mathbb{P}^{q-1}(\Omega_k)$ in terms of the values of the tractions g_γ^i at $\partial\Omega$. Indeed, if Φ_k denotes the space of *hyperstatic fluxes*[28,32]

$$\Phi_k = \{\boldsymbol{q} \in [\mathbb{P}^q(\Omega_k)]^3; -\boldsymbol{\nabla}\cdot\boldsymbol{q} = 0,\ \boldsymbol{q}\cdot\boldsymbol{n}|_{\partial\Omega_k} = 0\},$$

then if $(\boldsymbol{q}_k^i, r_k^i)$ is a pair of dual estimates verifying (18), $(\boldsymbol{q}_k^i + \boldsymbol{q}_k^{hs}, r_k^i)$ also verifies (18) for any $\boldsymbol{q}_k^{hs} \in \Phi_k$, where in the three dimensional setting $\dim(\Phi_k) = q(q-1)(2q+5)/6$. Therefore, Section 4.3 provides an explicit closed formula for one of the particular solutions of (18). This closed formula does not include, for instance, the unknowns associated to the *hyperstatic fluxes* to alleviate the cost of (16), but they could be easily included to improve the estimate[13].

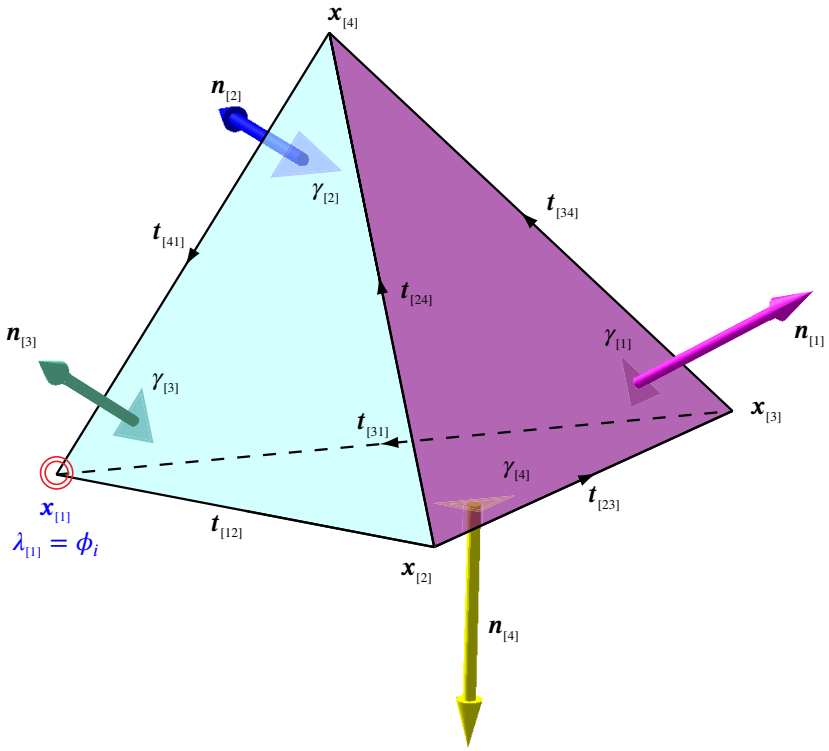

FIGURE 1 Notation for the vertices, edges and faces of an element contained in star ω_i.

TABLE 1 Summary of the cases for which a closed expression for the dual estimates $\boldsymbol{q}_k^i$ and r_k^i is provided.

Case			Neumann BC (19b) $\phi_i \Pi_\gamma^{\bar{q}} g_N$	source term (18a) $\phi_i \Pi_k^{\hat{q}}(f - \kappa_k^2 u_h)$	local tractions g_γ^i	interpolation degree for $\boldsymbol{q}_k^i$
I	$\bar{q}=0$	$\hat{q}=0$	piecewise linear	piecewise linear	linear	$q=2$
II	$\bar{q}=0$	$\hat{q}=1$	piecewise linear	piecewise quadratic	linear	$q=3$
III	$\bar{q}=1$	$\hat{q}=1$	piecewise quadratic	piecewise quadratic	quadratic	$q=3$

4.3 Closed formula for the dual estimates $\boldsymbol{q}_k^i$ and r_k^i (explicit solution of (18))

Let $\mathcal{N} = \{1, 2, \dots, n_{\text{np}}\}$ denote the set of indices of the nodes of the finite element mesh, and let $\mathcal{N}(\gamma) \subset \mathcal{N}$ and $\mathcal{N}(\Omega_k) \subset \mathcal{N}$ denote the set of indices of the nodes of face γ and element Ω_k respectively. Also, let Ω_k be a given tetrahedron in star ω_i defined by the vertices $\boldsymbol{x}_{[1]}$, $\boldsymbol{x}_{[2]}$, $\boldsymbol{x}_{[3]}$ and $\boldsymbol{x}_{[4]}$ where the subscripts within brackets, like in $\boldsymbol{x}_{[1]}$, refer to its local numbering. For simplicity of presentation, it is assumed that $\boldsymbol{x}_{[1]}$ coincides with the central node of the star, that is $\boldsymbol{x}_{[1]} = \boldsymbol{x}_i$. Moreover, for each vertex $\boldsymbol{x}_{[j]}$ the following notations, shown in Figure 1, are considered: $\lambda_{[j]}$ denotes its associated linear shape function and $\gamma_{[j]}$ denotes its opposite face with area $A_{[j]} = |\gamma_{[j]}|$ and unit outward normal vector $\boldsymbol{n}_{[j]}$ (where $\boldsymbol{n}_{[j]} = \boldsymbol{n}_k^{\gamma_{[j]}}$). Also, the edge-vector joining node $\boldsymbol{x}_{[m]}$ to $\boldsymbol{x}_{[n]}$ is denoted by $\boldsymbol{t}_{[mn]} = \boldsymbol{x}_{[n]} - \boldsymbol{x}_{[m]}$. It is worth noting that the shape functions are either denoted by ϕ_* or by $\lambda_{[*]}$ depending on them being the shape functions defined over the whole domain associated to a node using its global numbering or the local shape functions in a particular element where the subscript refers to the local numbering of its associated node.

The closed expression for the dual estimates $\boldsymbol{q}_k^i$ and r_k^i verifying (18) in the tetrahedron Ω_k of star ω_i depends on the source term of (18a) and the Neumann boundary conditions given in (18b). Note that, the source data is known once the value of $\hat{q}$ is fixed. Also, for a given value of $\bar{q}$, the boundary conditions associated to (18) are known on $\Gamma_N \cup \mathcal{Z}_i$. Therefore, the formula for the dual estimates depends on the choice of the projection degree of the input data, that is, it depends on the values of $\hat{q}$ and $\bar{q}$, and on the choice of the free tractions g_γ^i for $\gamma \subset \partial\Omega_k \cap (\Gamma_i \backslash \Gamma_N)$.

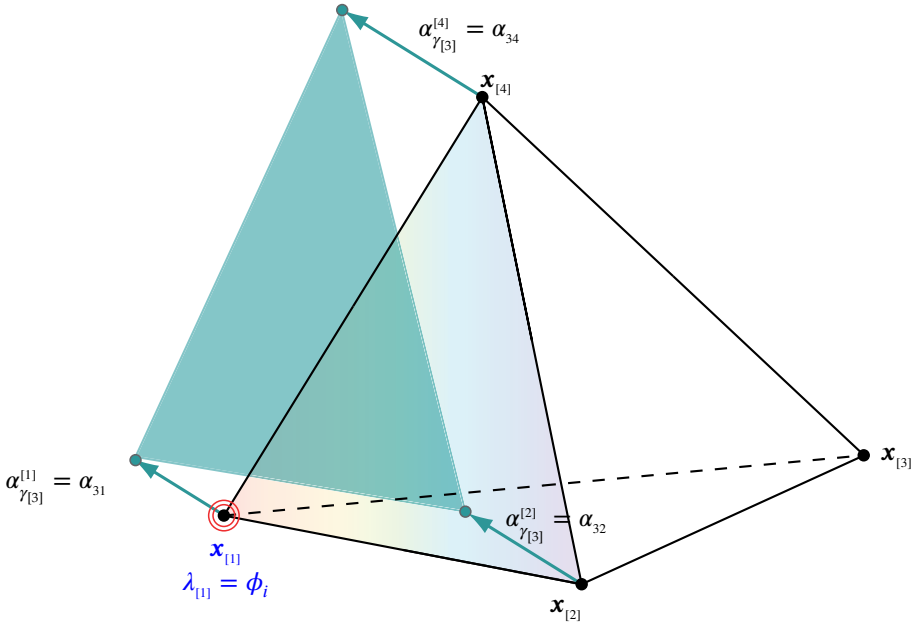

FIGURE 2 Notation for the DOFs of the linear tractions on face $\gamma_{[3]}$.

Table 1 summarizes the three different choices for $\hat{q}$, $\bar{q}$ and g^i_γ considered in this work, and the following subsections provide the closed formulas for these three cases.

4.3.1 Case I. Piecewise constant projection of the data $\hat{q} = \bar{q} = 0$

In this case, for each element of the star $\Omega_k \subset \omega_i$, the formulas defining the pair of local dual estimates $\boldsymbol{q}^i_k$ and r^i_k verifying (18) depend on the fixed source data (which for $\hat{q} = 0$ is a linear function) and the value of the tractions g^i_γ which are taken to be linear functions on the faces of the tetrahedron (since on the Neumann boundaries they have to be linear, see (19b) taking $\bar{q} = 0$). It is worth noting that equation (19) only fixes the value of g^i_γ on the faces $\gamma \subset \Gamma_N \cup \mathcal{Z}_i$ and therefore, the final value of the dual estimates $\boldsymbol{q}^i_k$ and r^i_k is only obtained when the values of the tractions on the free faces (unknowns to be determined) are set.

Specifically, if $\gamma \subset \mathcal{F}(\omega_i)$, g^i_γ is a linear function defined by its values at the vertices of the face $\mathcal{N}(\gamma)$ and therefore

$$g^i_\gamma = \sum_{m \in \mathcal{N}(\gamma)} \alpha^m_{\gamma i} \phi_m, \tag{20}$$

where, with a slight abuse of notation, the two-dimensional Lagrange basis functions on γ are written in terms of the three-dimensional shape functions ϕ_m (without explicitly marking its restriction to face γ). That is, if γ is the face joining nodes m_1, m_2 and m_3, then

$$g^i_\gamma = \alpha^{m_1}_{\gamma i} \phi_{m_1} + \alpha^{m_2}_{\gamma i} \phi_{m_2} + \alpha^{m_3}_{\gamma i} \phi_{m_3}. \tag{21}$$

In particular, for a given element $\Omega_k \subset \omega_i$ and using the notations introduced in Figure 1 (recall that it is assumed that $\boldsymbol{x}_{[1]} = \boldsymbol{x}_i$ and therefore $\gamma_{[1]} \subset \mathcal{Z}_i$), the linear tractions associated to the four faces of this tetrahedron $g^i_\gamma, \gamma \subset \partial\Omega_k$ are locally expressed as

$$\begin{aligned}
g^i_{\gamma_{[1]}} &= 0, \\
g^i_{\gamma_{[2]}} &= \alpha^{[1]}_{\gamma_{[2]} i} \lambda_{[1]} + \alpha^{[3]}_{\gamma_{[2]} i} \lambda_{[3]} + \alpha^{[4]}_{\gamma_{[2]} i} \lambda_{[4]}, \\
g^i_{\gamma_{[3]}} &= \alpha^{[1]}_{\gamma_{[3]} i} \lambda_{[1]} + \alpha^{[2]}_{\gamma_{[3]} i} \lambda_{[2]} + \alpha^{[4]}_{\gamma_{[3]} i} \lambda_{[4]}, \\
g^i_{\gamma_{[4]}} &= \alpha^{[1]}_{\gamma_{[4]} i} \lambda_{[1]} + \alpha^{[2]}_{\gamma_{[4]} i} \lambda_{[2]} + \alpha^{[3]}_{\gamma_{[4]} i} \lambda_{[3]}.
\end{aligned} \tag{22}$$

Therefore, the value of the dual estimates $\boldsymbol{q}^i_k$ and r^i_k on every tetrahedron of the star depends on nine degrees of freedom associated to the linear tractions g^i_γ which are hereafter rewritten to ease the notation as $\alpha_{jl} = \alpha^{[l]}_{\gamma_{[j]} i} = g^i_{\gamma_{[j]}}(\boldsymbol{x}_{[l]})$. Note that the first subscript denotes the local numbering of the face $\gamma_{[j]}$, the second subscript denotes the local numbering of the node $\boldsymbol{x}_{[l]}$ and the superscript referring to the star i is omitted (see Figure 2). These unknowns are stored in vector $\boldsymbol{\alpha}_k$, namely

$$\boldsymbol{\alpha}_k = \left(\alpha_{21}, \alpha_{23}, \alpha_{24}, \alpha_{31}, \alpha_{32}, \alpha_{34}, \alpha_{41}, \alpha_{42}, \alpha_{43}\right)^T. \tag{23}$$

Once the values of $\boldsymbol{\alpha}_k$ are set, the pair of local dual estimates $\boldsymbol{q}_k^i \in [\mathbb{P}^2(\Omega_k)]^3$ and $r_k^i \in \mathbb{P}^1(\Omega_k)$ are defined to be

$$r_k^i = \phi_i r_k^{i1} + r_k^{i0} \tag{24}$$

where r_k^{i1} and r_k^{i0} are two free constant coefficients, and

$$\boldsymbol{q}_k^i = \boldsymbol{q}_k^{iL} + \boldsymbol{q}_k^{iQ}, \tag{25}$$

for

$$\mathbf{q}_k^{iL} = \frac{1}{3|\Omega_k|}\left(\boldsymbol{\rho}_{[1]}^k \lambda_{[1]} + \boldsymbol{\rho}_{[2]}^k \lambda_{[2]} + \boldsymbol{\rho}_{[3]}^k \lambda_{[3]} + \boldsymbol{\rho}_{[4]}^k \lambda_{[4]}\right), \tag{26}$$

and

$$\begin{aligned}\mathbf{q}_k^{iQ} = \frac{F^0}{4}\Big(&\lambda_{[1]}\lambda_{[2]}\boldsymbol{t}_{[12]}\boldsymbol{t}_{[12]}^{\mathsf{T}} + \lambda_{[1]}\lambda_{[3]}\boldsymbol{t}_{[13]}\boldsymbol{t}_{[13]}^{\mathsf{T}} + \lambda_{[1]}\lambda_{[4]}\boldsymbol{t}_{[14]}\boldsymbol{t}_{[14]}^{\mathsf{T}} \\ &+ \lambda_{[2]}\lambda_{[3]}\boldsymbol{t}_{[23]}\boldsymbol{t}_{[23]}^{\mathsf{T}} + \lambda_{[2]}\lambda_{[4]}\boldsymbol{t}_{[24]}\boldsymbol{t}_{[24]}^{\mathsf{T}} + \lambda_{[3]}\lambda_{[4]}\boldsymbol{t}_{[34]}\boldsymbol{t}_{[34]}^{\mathsf{T}}\Big)\nabla\phi_i,\end{aligned} \tag{27}$$

where $F^0 = \Pi_k^0(f - \kappa_k^2 u_h) - \kappa_k^2 r_k^{i1}$ and introducing $\mathcal{R}_{|\gamma} = \sigma_k^\gamma g_\gamma^i - \phi_i \boldsymbol{\nabla} u_h \cdot \boldsymbol{n}_k^\gamma$

$$\begin{aligned}\boldsymbol{\rho}_{[1]}^k &= A_{[2]}\mathcal{R}_{|\gamma_{[2]}}(\boldsymbol{x}_{[1]})\boldsymbol{t}_{[21]} + A_{[3]}\mathcal{R}_{|\gamma_{[3]}}(\boldsymbol{x}_{[1]})\boldsymbol{t}_{[31]} + A_{[4]}\mathcal{R}_{|\gamma_{[4]}}(\boldsymbol{x}_{[1]})\boldsymbol{t}_{[41]}, \\ \boldsymbol{\rho}_{[2]}^k &= A_{[1]}\mathcal{R}_{|\gamma_{[1]}}(\boldsymbol{x}_{[2]})\boldsymbol{t}_{[12]} + A_{[3]}\mathcal{R}_{|\gamma_{[3]}}(\boldsymbol{x}_{[2]})\boldsymbol{t}_{[32]} + A_{[4]}\mathcal{R}_{|\gamma_{[4]}}(\boldsymbol{x}_{[2]})\boldsymbol{t}_{[42]}, \\ \boldsymbol{\rho}_{[3]}^k &= A_{[1]}\mathcal{R}_{|\gamma_{[1]}}(\boldsymbol{x}_{[3]})\boldsymbol{t}_{[13]} + A_{[2]}\mathcal{R}_{|\gamma_{[2]}}(\boldsymbol{x}_{[3]})\boldsymbol{t}_{[23]} + A_{[4]}\mathcal{R}_{|\gamma_{[4]}}(\boldsymbol{x}_{[3]})\boldsymbol{t}_{[43]}, \\ \boldsymbol{\rho}_{[4]}^k &= A_{[1]}\mathcal{R}_{|\gamma_{[1]}}(\boldsymbol{x}_{[4]})\boldsymbol{t}_{[14]} + A_{[2]}\mathcal{R}_{|\gamma_{[2]}}(\boldsymbol{x}_{[4]})\boldsymbol{t}_{[24]} + A_{[3]}\mathcal{R}_{|\gamma_{[3]}}(\boldsymbol{x}_{[4]})\boldsymbol{t}_{[34]}.\end{aligned} \tag{28}$$

Remark 8. The fluxes $\mathbf{q}_k^{iL}$ and $\mathbf{q}_k^{iQ}$ can be rewritten in compact form as

$$\mathbf{q}_k^{iL} = \frac{1}{3|\Omega_k|}\sum_{n=1}^{4}\boldsymbol{\rho}_{[n]}^k\lambda_{[n]} \quad , \quad \boldsymbol{\rho}_{[n]}^k = \sum_{\substack{m=1\\m\neq n}}^{4} A_{[m]}\mathcal{R}_{|\gamma_{[m]}}(\boldsymbol{x}_{[n]})\boldsymbol{t}_{[mn]} \text{ and } \mathbf{q}_k^{iQ} = \frac{F^0}{4}\mathbf{M}^{\mathbf{q}}\nabla\phi_i. \tag{29}$$

where the matrix $\mathbf{M}^{\mathbf{q}}$ is defined as

$$\mathbf{M}^{\mathbf{q}} = \sum_{n=1}^{4}\sum_{\substack{m=2\\m>n}}^{4}\lambda_{[n]}\lambda_{[m]}\boldsymbol{t}_{[nm]}\boldsymbol{t}_{[nm]}^{\mathsf{T}}.$$

The key point is that these dual estimates $\boldsymbol{q}_k^i$ and r_k^i verify (18) if the following weighted projected equilibration condition

$$\int_{\Omega_k}\left[\phi_i F^0 - \kappa_k^2 r_k^{i0} - \nabla u_h \cdot \nabla\phi_i\right]\, d\Omega + \sum_{\gamma\subset\partial\Omega_k}\int_\gamma \sigma_k^\gamma g_\gamma^i\, d\Gamma = 0 \tag{30}$$

holds. This result is stated in the following theorem and proven in Appendix A.

Theorem 2. Let $\Omega_k \subset \omega_i$ be an element of the star associated to node $\boldsymbol{x}_i$ and let $\boldsymbol{q}_k^i$ and r_k^i be the weighted dual estimates defined by equations (24) and (25).Then, for any choice of the local tractions g_γ^i verifying the weighted projected equilibration condition (30) , $\boldsymbol{q}_k^i$ and r_k^i verify equation (18) for the particular choice $\hat{q} = 0$.

Remark 9. A set of local weighted tractions $\{g_\gamma^i\}_{\gamma\subset\mathcal{F}(\omega_i)}$ verifying both (19) and (30) exist if problem (18) (resp. (15)) admits a solution. As mentioned in Remark 6, the values of $\hat{q} = \bar{q} = 0 < 1$ do not ensure that the global compatibility condition (17) holds, and therefore solvability is only guaranteed if either 1) $\kappa^2 r^i\big|_{\omega_i} \neq 0$, or 2) $\Gamma_i \cap \Gamma_{\mathrm{D}} \neq \emptyset$ or 3) for every element $\Omega_k \subset \omega_i$, $\kappa_k = 0$ along with the data source f being a constant function in Ω_k so that $f - \kappa_k^2 u_h$ is constant and, for every face $\gamma \subset \Gamma_i \cap \Gamma_{\mathrm{N}}$ the Neumann boundary data g_{N} is a constant function on γ. Therefore, one can only use the more computational efficient choice $r_k^{i0} = r_k^{i1} = 0$ in equation (24) if no solvability problems are found. A simple to implement strategy is to set $r_k^{i0} = r_k^{i1} = 0$ if $f - \kappa_k^2 u_h$ and g_{N} are piecewise constant functions on the whole mesh and boundary respectively, and otherwise take $r_k^{i0} \neq 0$ in all the elements of the mesh. In this case, the constant r_k^{i1} appearing in (24) is optional and can be set to zero to simplify the implementation of the method. Of course, a more sophisticated approach considering different values of r_k^{i0} and r_k^{i1} over the mesh, depending if solvability issues are encountered, would reduce the computational cost of the local problems to be solved. Finally, recall that for pure diffusion problems with non piecewise-constant data solvability cannot be ensured and therefore only Cases II or III may be considered.

4.3.2 Case II. Mixed piecewise linear/constant projection of the data $\hat{q} = 1, \bar{q} = 0$

In this case, the formulas defining the pair of local dual estimates $\boldsymbol{q}_k^i$ and r_k^i verifying (18) depend on the fixed source data (which for $\hat{q} = 1$ is a quadratic function) and the value of the tractions g_γ^i which, as in Case I, are taken to be linear functions on the faces of the tetrahedron (since on the Neumann boundaries they have to be linear, see (19b) taking $\bar{q} = 0$). Therefore, the value of the dual estimates $\boldsymbol{q}_k^i$ and r_k^i on every tetrahedron of the star depends, as in Case I, on the nine degrees of freedom stored in vector $\boldsymbol{\alpha}_k$, see equation (23).

Once the values of $\boldsymbol{\alpha}_k$ are set, the pair of local dual estimates $\boldsymbol{q}_k^i \in [\mathbb{P}^3(\Omega_k)]^3$ and $r_k^i \in \mathbb{P}^2(\Omega_k)$ are defined to be

$$r_k^i = \phi_i r_k^{iL} + r_k^{i0}, \tag{31}$$

where r_k^{i0} is a free constant parameter and r_k^{iL} is a free linear function defined as

$$r_k^{iL} = r_{[1]}\lambda_{[1]} + r_{[2]}\lambda_{[2]} + r_{[3]}\lambda_{[3]} + r_{[4]}\lambda_{[4]},$$

and the flux $\boldsymbol{q}_k^i$ is decomposed into a linear plus a cubic part as

$$\boldsymbol{q}_k^i = \boldsymbol{q}_k^{iL} + \boldsymbol{q}_k^{iC} \tag{32}$$

where $\mathbf{q}_k^{iL}$ is the same flux introduced in Case I, see equation (26), and

$$\mathbf{q}_k^{iC} = \frac{1}{4}\mathbf{M}^{\mathbf{q}}\nabla v^Q, \tag{33}$$

for

$$v^Q = \frac{2}{5}\phi_i F^1 + \frac{1}{10}(F^1_{[1]}\ F^1_{[2]}\ F^1_{[3]}\ F^1_{[4]})\begin{pmatrix} 4 & 0 & 0 & 0 \\ 0 & 0 & -1 & -1 \\ 0 & -1 & 0 & -1 \\ 0 & -1 & -1 & 0 \end{pmatrix}\begin{pmatrix} \lambda_{[1]} \\ \lambda_{[2]} \\ \lambda_{[3]} \\ \lambda_{[4]} \end{pmatrix}, \tag{34}$$

and

$$F^1 = \Pi_k^1(f - \kappa_k^2 u_h) - \kappa_k^2 r_k^{iL} = F^1_{[1]}\lambda_{[1]} + F^1_{[2]}\lambda_{[2]} + F^1_{[3]}\lambda_{[3]} + F^1_{[4]}\lambda_{[4]}. \tag{35}$$

Note that the notation $F^1_{[j]} = F^1(\boldsymbol{x}_{[j]}),\ j = 1, \dots, 4$ has been introduced to simplify the notation.

As in Case I, the key point is that these pair of dual estimates $\boldsymbol{q}_k^i$ and r_k^i verify (18) if the following weighted projected equilibration condition

$$\int_{\Omega_k} \left[\phi_i F^1 - \kappa_k^2 r_k^{i0} - \nabla u_h \cdot \nabla \phi_i\right]\, d\Omega + \sum_{\gamma \subset \partial\Omega_k} \int_\gamma \sigma_k^\gamma g_\gamma^i\, d\Gamma = 0 \tag{36}$$

holds. This result is stated in the following theorem and proven in Appendix B.

Theorem 3. Let $\Omega_k \subset \omega_i$ be an element of the star associated to node $\boldsymbol{x}_i$ and let $\boldsymbol{q}_k^i$ and r_k^i be the weighted dual estimates defined by equations (31) and (32). Then, for any choice of the local linear tractions g_γ^i verifying the weighted projected equilibration condition (36) , $\boldsymbol{q}_k^i$ and r_k^i verify equation (18) for the particular choice $\hat{q} = 1$.

Remark 10. The existence of a set of local weighted tractions $\{g_\gamma^i\}_{\gamma \subset \mathcal{F}(\omega_i)}$ verifying both (19b) and (36) is always ensured if $\hat{q}$ and $\bar{q}$ take values larger than one (see Remark 6). Since in this case $\bar{q} = 0$, solvability is only ensured if either 1) $\kappa^2 r^i\big|_{\omega_i} \neq 0$, or 2) $\Gamma_i \cap \Gamma_D \neq \emptyset$ or 3) for every face $\gamma \subset \Gamma_i \cap \Gamma_N$ the Neumann boundary data g_N is a constant function on γ. Therefore, one can only use the more computational efficient choice $r_k^{i0} = r_k^{iL} = 0$ in equation (31) if either $\Gamma_i \cap \Gamma_D \neq \emptyset$ or if in the case the star intersects the Neumann boundary, the Neumann boundary conditions are piecewise constant. Finally, as in Remark 9, for pure diffusion problems with non piecewise-constant Neumann data, solvability cannot be ensured and therefore Case III has to be considered at least on those elements touching the Neumann boundary.

4.3.3 Case III. Piecewise linear projection of the data $\hat{q} = \bar{q} = 1$

As discussed in Remark 10, the choice $\bar{q} = 0$ can only be made if the Neumann tractions g_N are piecewise constant on the faces of the domain or if the reaction coefficient is not zero in the elements containing the Neumann faces with non-constant tractions. Otherwise it is necessary to set $\bar{q} = 1$ at least on the faces of Γ_N where the non-constant tractions are applied. Note that setting $\bar{q} = 1$ in the constraints (19b) involves using quadratic equilibrated tractions over the faces of the star. If $\gamma \subset \mathcal{F}(\omega_i)$ is the face joining nodes $\boldsymbol{x}_{m_1}$, $\boldsymbol{x}_{m_2}$ and $\boldsymbol{x}_{m_3}$, the traction g_γ^i is a quadratic function defined by its values at these vertices and at the corresponding mid-edge nodes $\boldsymbol{x}_{m_j m_l} = (\boldsymbol{x}_{m_j} + \boldsymbol{x}_{m_l})/2$ (see figure 3). That is,

$$g_\gamma^i = \alpha_{\gamma i}^{m_1}\phi_{m_1}^q + \alpha_{\gamma i}^{m_2}\phi_{m_2}^q + \alpha_{\gamma i}^{m_3}\phi_{m_3}^q + \alpha_{\gamma i}^{m_1 m_2}\phi_{m_1 m_2}^q + \alpha_{\gamma i}^{m_1 m_3}\phi_{m_1 m_3}^q + \alpha_{\gamma i}^{m_2 m_3}\phi_{m_2 m_3}^q, \tag{37}$$

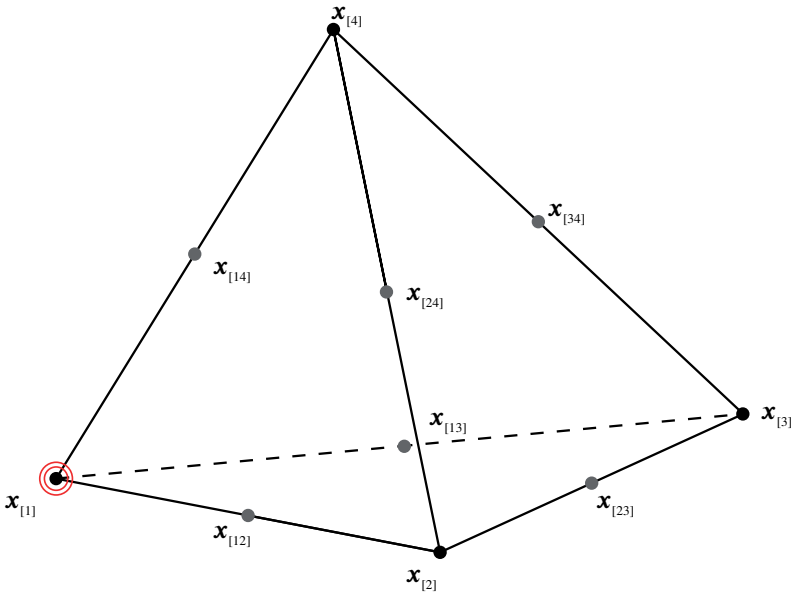

FIGURE 3 Notation of the vertices and mid-edge nodes of a ten node tetrahedral element contained in star ω_i.

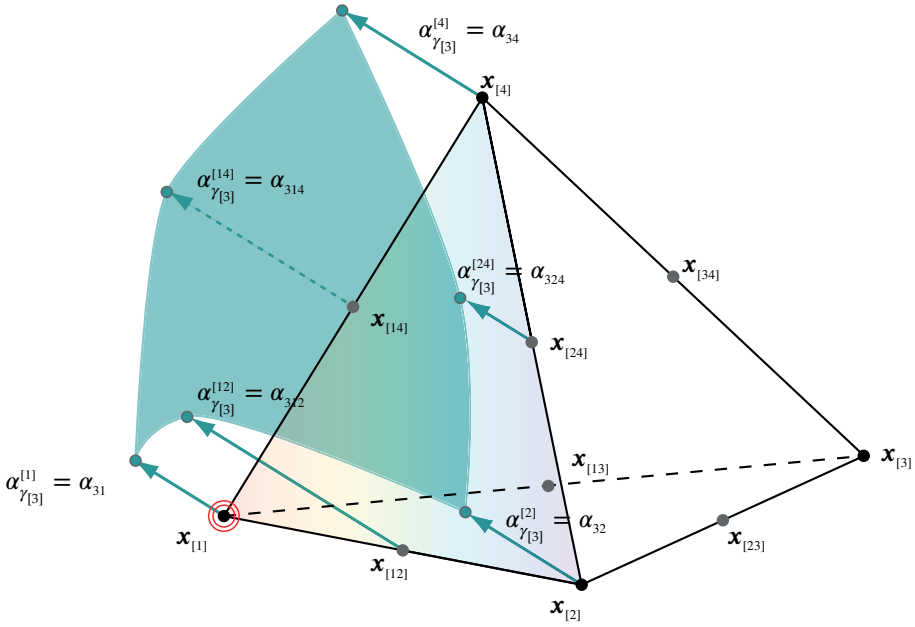

FIGURE 4 Notation for the quadratic tractions on face $\gamma_{[3]}$.

where $\phi^q_{m_j}$ and $\phi^q_{m_j m_l}$ for $j, l = 1, \ldots, 4$ are the quadratic shape functions associated to the vertices and mid-edge nodes respectively. For simplicity of presentation the same notation g^i_γ is used for the linear tractions from Cases I and II and the quadratic tractions of Case III, since it can be easily disambiguated by the Case the user considers.

Thus, the local traction g^i_γ on a face γ can be expressed using six degrees of freedom as shown in Figure 4. Specifically, recalling that $g^i_{\gamma_{[1]}} = 0$ and introducing the simplified notation $\alpha^{[l]}_{\gamma_{[j]}i} = g^i_{\gamma_{[j]}}(\boldsymbol{x}_{[l]}) = \alpha_{jl}$, where the first subscript denotes the local numbering of the face $\gamma_{[j]}$, the second subscript denotes the local numbering for the node $\boldsymbol{x}_{[l]}$ (which can now be comprised of one or two numbers) and the superscript referring to the star i is omitted, the unknown coefficients defining the quadratic tractions g^i_γ in element Ω_k can be stored in the following vector

$$\boldsymbol{\alpha}^q_k = \left(\alpha_{21}, \alpha_{23}, \alpha_{24}, \alpha_{213}, \alpha_{214}, \alpha_{234}, \alpha_{31}, \alpha_{32}, \alpha_{34}, \alpha_{312}, \alpha_{314}, \alpha_{324}, \alpha_{41}, \alpha_{42}, \alpha_{43}, \alpha_{412}, \alpha_{413}, \alpha_{423}\right)^{\mathsf{T}}. \tag{38}$$

Remark 11. In this case since $\hat{q} = \bar{q} = 1$, the local problem (15) (or respectively (18) along with (19)) has no solvability issues even if no reaction term is present in the equation (see Remark 6). Therefore it is possible to set $r_k^i = 0$ in equation (18) reducing the problem to find a dual estimate $\boldsymbol{q}_k^i$ verifying the following simplified version of (18)

$$-\boldsymbol{\nabla}\cdot\left(\boldsymbol{q}_k^i + \phi_i\boldsymbol{\nabla}u_h\right) = \phi_i\Pi_k^1(f-\kappa_k^2u_h) - \boldsymbol{\nabla}u_h\cdot\boldsymbol{\nabla}\phi_i \qquad \text{in } \Omega_k, \tag{39a}$$

$$\left(\boldsymbol{q}_k^i + \phi_i\boldsymbol{\nabla}u_h\right)\cdot\boldsymbol{n}_k^\gamma = \sigma_k^\gamma g_\gamma^i \qquad \text{on } \gamma\subset\partial\Omega_k. \tag{39b}$$

Once the values of $\boldsymbol{\alpha}_k^q$ are set, for each element of the star $\Omega_k \subset \omega_i$ and using the notations introduced in Figures 1 and 3, the local equilibrated flux $\boldsymbol{q}_k^i \in [\mathbb{P}^3(\Omega_k)]^3$ verifying equation (39) is defined adding three different contributions

$$\boldsymbol{q}_k^i = \boldsymbol{q}_k^{iQq} + \boldsymbol{q}_k^{iC} + \boldsymbol{q}_k^{i\nabla}. \tag{40}$$

The contribution $\boldsymbol{q}_k^{iQq}$ is a quadratic flux enforcing the quadratic boundary conditions, see equation (39b), given by

$$\mathbf{q}_k^{iQq} = \frac{1}{3|\Omega_k|}\Big(\sum_{n=1}^{4}\boldsymbol{\rho}_{[n]}^k\lambda_{[n]} + \sum_{n=1}^{4}\sum_{\substack{m=2\\ m>n}}^{4}\boldsymbol{\rho}_{[nm]}^k\lambda_{[nm]}^q\Big), \tag{41}$$

where $\boldsymbol{\rho}_{[n]}^k$ is defined in equation (29) and

$$\boldsymbol{\rho}_{[nm]}^k = \sum_{\substack{j=1\\ j\neq n,m}}^{4} A_{[j]}\left(\mathcal{R}_{|\gamma_{[j]}}(\boldsymbol{x}_{[nm]}) - \frac{1}{2}\mathcal{R}_{|\gamma_{[j]}}(\boldsymbol{x}_{[n]}) - \frac{1}{2}\mathcal{R}_{|\gamma_{[j]}}(\boldsymbol{x}_{[m]})\right)\frac{\boldsymbol{t}_{[jn]}+\boldsymbol{t}_{[jm]}}{2}. \tag{42}$$

The cubic flux $\boldsymbol{q}_k^{iC}$ is the same as in Case II, see equation (33), and the third flux $\boldsymbol{q}_k^{i\nabla}$, introduced to compensate the divergence of the now quadratic flux $\boldsymbol{q}_k^{iQq}$, is given by

$$\mathbf{q}_k^{i\nabla} = \frac{1}{4}\mathbf{M}^{\mathbf{q}}\boldsymbol{\nu}^\nabla, \tag{43}$$

for

$$\boldsymbol{\nu}^\nabla = \frac{4}{27|\Omega_k|^3}\sum_{n=1}^{4}\sum_{m=n+1}^{4}A_{[n]}A_{[m]}(\boldsymbol{n}_{[m]}\boldsymbol{n}_{[n]}^\mathsf{T} + \boldsymbol{n}_{[n]}\boldsymbol{n}_{[m]}^\mathsf{T})\boldsymbol{\rho}_{[nm]}^k. \tag{44}$$

As in the previous Cases I and II, the key point is that the dual estimate $\boldsymbol{q}_k^i$ verifies equation (39) if the following weighted projected equilibration condition

$$\int_{\Omega_k}\left[\phi_i\Pi_k^1(f-\kappa_k^2u_h) - \nabla u_h\cdot\nabla\phi_i\right]\,d\Omega + \sum_{\gamma\subset\partial\Omega_k}\int_\gamma\sigma_k^\gamma g_\gamma^i\,d\Gamma = 0 \tag{45}$$

holds. The proof is similar to the ones given in Appendices A and B and is not given here for brevity.

Remark 12. Is is worth noting that both the quadratic flux $\mathbf{q}_k^{iQq}$ given in equation (41) and the additional term $\boldsymbol{q}_k^{i\nabla}$ given in equation (43) can also be defined with respect to the modified $\boldsymbol{\rho}_{[nm]}^k$ vectors obtained by replacing the term $(\boldsymbol{t}_{[jn]}+\boldsymbol{t}_{[jm]})/2$ by either $\boldsymbol{t}_{[jn]}$ or $\boldsymbol{t}_{[jm]}$. For instance,

$$\boldsymbol{\rho}_{[nm]}^k = \sum_{\substack{j=1\\ j\neq n,m}}^{4} A_{[j]}\left(\mathcal{R}_{|\gamma_{[j]}}(\boldsymbol{x}_{[nm]}) - \frac{1}{2}\mathcal{R}_{|\gamma_{[j]}}(\boldsymbol{x}_{[n]}) - \frac{1}{2}\mathcal{R}_{|\gamma_{[j]}}(\boldsymbol{x}_{[m]})\right)\boldsymbol{t}_{[jn]}. \tag{46}$$

The only requirement being consistency with any desired choice, that is, the same definition has to be used for both $\mathbf{q}_k^{iQq}$ and $\mathbf{q}_k^{i\nabla}$.

4.4 Condensed local constrained minimization problems

The closed formulas for the dual estimates $\boldsymbol{q}_k^i$ and r_k^i given in Section 4.3, ensuring the verification of equation (15) or its equivalent strong form given by equations (18) and (19), allow alleviating the cost of solving the constrained optimization problems posed in (16). Specifically, both the original number of unknowns and the number of constraints (given by equations (18) and (19)) are greatly reduced, and the problem reduces to solving small constrained quadratic optimization problems (with very few unknowns and constraints). Indeed, on one hand, the unknowns of the original constrained optimization problem (16) are the unknowns defining $\boldsymbol{q}^i \in [\widehat{\mathbb{P}}^q(\omega_i)]^3$ and $r^i \in \widehat{\mathbb{P}}^{q-1}(\omega_i)$ in each element of the star. Therefore, for a general value of q the number of degrees of freedom is

$$\Big(\underbrace{3\frac{(q+1)(q+2)(q+3)}{6}}_{\dim([\mathbb{P}^q(\Omega_k)]^3)} + \underbrace{\frac{q(q+1)(q+2)}{6}}_{\dim(\mathbb{P}^{q-1}(\Omega_k))}\Big)\times n_{\text{el}}^i$$

where n^i_{el} denotes the number of elements in star ω_i. Also, the number of constraints given by equation (18a) coincides with $\dim(\mathbb{P}^{q-1}(\Omega_k))$ and the number of constraints of (18b) coincides with $\dim(\mathbb{P}^q(\gamma)) = (q+1)(q+2)/2$ in each face of the element. However, note that for every element of the star one of the constraints posed by (18a) and (18b) is redundant. Also, note that actually equation (18b) does not pose any constraint in the edges of the Dirichlet boundary and that an interior edge $\gamma = \partial\Omega_k \cap \partial\Omega_{k'}$ has two associated constraints which in fact impose normal continuity of $\boldsymbol{q}$ on the interior edges of the star. Therefore, taking also into account that one of the constraints of the global star problem is redundant, the total number of constraints of the original problem is

$$\Big(\underbrace{\frac{q(q+1)(q+2)}{6}}_{(18a)} + \underbrace{2(q+1)(q+2)}_{(18b)} - 1\Big) \times n^i_{\text{el}} - \frac{(q+1)(q+2)}{2}(n^i_{\text{fa}} - n^{i\text{N}}_{\text{fa}}) - 1,$$

where n^i_{fa} denotes the number of faces contained in Γ_i and $n^{i\text{N}}_{\text{fa}}$ denotes the number of faces contained in $\Gamma_i \cap \Gamma_{\text{N}}$.

Remark 13. The original constrained optimization problem (16) can be solved using Lagrange multipliers, but following Parés et al.[13], Section 6, it is also possible to solve it taking advantage of the decomposition of the space $\mathcal{H}(\text{div}, \Omega_k)$ used in the context of mixed or hybrid elements. In this case, the constraints given in (18) and (19) can be explicitly imposed yielding to an unconstrained optimization problem with the following number of degrees of freedom

$$\Big(\underbrace{\frac{q(q-1)(2q+5)}{6}}_{\dim(\Phi_k)} + \underbrace{\frac{q(q+1)(q+2)}{6}}_{\dim(\mathbb{P}^{q-1}(\Omega_k))}\Big) \times n^i_{\text{el}} + \underbrace{\frac{(q+1)(q+2)}{2}}_{\dim(\mathbb{P}^q(\gamma))} \times (n^i_{\text{fa}} - n^{i\text{N}}_{\text{fa}}).$$

On the other hand, the number of unknowns of the new approach are:

Case I: $3 \times n^i_{\text{fa}} + 2 \times n^i_{\text{el}}$ (unknowns associated to $\boldsymbol{\alpha}_k$ and reaction term r^{i1}_k and r^{i0}_k)

Case II: $3 \times n^i_{\text{fa}} + 4 \times n^i_{\text{el}}$ (unknowns associated to $\boldsymbol{\alpha}_k$ and reaction term r^{i0}_k and r^{iL}_k)

Case III: $6 \times n^i_{\text{fa}}$ (unknowns associated to $\boldsymbol{\alpha}^q_k$),

and the number of constraints is one per element of the star (see (30), (36) or (45)) plus the constraints on the Neumann boundary of the domain (see (19b)) if the star intersects Γ_{N}.

Table 2 briefly compares the computational effort required to solve the local problems of the presented approach with respect to the original approach for an interior star for which $n^i_{\text{fa}} = 3n^i_{\text{el}}/2$. In all the cases, the cost of computing a strict upper bound for the energy norm of the error is governed by the cost of the local systems of equations that have to be solved, and therefore, the cost of explicitly evaluating the dual estimates and computing its norm is not incorporated in the computational cost. Additionally, when the solution of a constrained optimization problem is needed the computational cost is evaluated, assuming that the Lagrange multiplier method is used to enforce the constraints. Of course, this is not an efficient implementation of the local problems and the cost of the algorithms involving these optimization strategies could be reduced selecting a more efficient strategy to enforce the constraints.

TABLE 2 Cost comparison in terms of degrees of freedom and constraints for an interior star.

	Original ($q=2$)		Original ($q=3$)		Case I	Case II	Case III
	Standard	Optimized	Standard	Optimized	($q=2$)	($q=3$)	($q=3$)
Number of unknowns	$34n^i_{\text{el}}$	$16n^i_{\text{el}}$	$70n^i_{\text{el}}$	$36n^i_{\text{el}}$	$13/2n^i_{\text{el}}$	$17/2n^i_{\text{el}}$	$9n^i_{\text{el}}$
Number of constraints	$18n^i_{\text{el}}$	–	$34n^i_{\text{el}}$	–	n^i_{el}	n^i_{el}	n^i_{el}
d.o.f. Lagrange multipliers	$52n^i_{\text{el}}$	$16n^i_{\text{el}}$	$104n^i_{\text{el}}$	$36n^i_{\text{el}}$	$15/2n^i_{\text{el}}$	$19/2n^i_{\text{el}}$	$10n^i_{\text{el}}$
Linear Solver $\mathcal{O}((dof)^3)$	$140608n^i_{\text{el}}$	$4096n^i_{\text{el}}$	$1124864n^i_{\text{el}}$	$46656n^i_{\text{el}}$	$422n^i_{\text{el}}$	$858n^i_{\text{el}}$	$1000n^i_{\text{el}}$

This section is devoted to exhaustively describe the transformation of (16) into a simple constrained quadratic minimization problem in terms of the local unknowns involved in the explicit expressions of $\boldsymbol{q}^i_k$ and r^i_k (the unknowns associated to $\{g^i_\gamma\}_{\gamma \subset \mathcal{F}(\omega_i)}$ and the constants describing r^i_k).

Problem (16) aims at finding the pair of polynomial dual estimates $\boldsymbol{q}^i \in [\widehat{\mathbb{P}}^q(\omega_i)]^3$, $r^i \in \widehat{\mathbb{P}}^{q-1}(\omega_i)$ with associated minimal squared $\mathcal{L}^2$-norm while verifying (15). To simplify the complexity of this problem, instead of allowing $\boldsymbol{q}^i$ and r^i to be general polynomial estimates, they are restricted to be of the form of the estimates presented in Section 4.3 (the local restriction of r^i and $\boldsymbol{q}^i$ in each element of the star are given by equations (24) and (25) for Case I, (31) and (32) for Case II and $r^i = 0$ and (40) for Case III). Of course enforcing these particular forms of the estimates will, in general, provide a larger value for the squared norm of the estimates than the norm given solving the full original problem (16). However, as will be seen in the numerical examples, the results for the upper bounds are very similar while the computational cost is greatly reduced.

Therefore, in the new modified problem, the unknowns of the problem are no longer the degrees of freedom of the pair of dual estimates $\boldsymbol{q}^i \in [\widehat{\mathbb{P}}^q(\omega_i)]^3$ and $r^i \in \widehat{\mathbb{P}}^{q-1}(\omega_i)$ but the set of local weighted tractions $\{g^i_\gamma\}_{\gamma\subset\mathcal{F}(\omega_i)}$ associated to each face γ of the star ω_i and the degrees of freedom defining the reaction r^i_k. Note that once $\{g^i_\gamma\}_{\gamma\subset\mathcal{F}(\omega_i)}$ and r^i_k are fixed, $\boldsymbol{q}^i_k$ is uniquely defined by the formulas given in Section 4.3. Also enforcing these particular forms of r^i and $\boldsymbol{q}^i$ directly enforces the verification of (15) as long as $\{g^i_\gamma\}_{\gamma\subset\mathcal{F}(\omega_i)}$ fulfill 1) the boundary values given in equation (19) and 2) the weighted projected equilibration conditions (given in equations (30), (36) and (45) for the three considered cases). Hence, instead of aiming at finding $\boldsymbol{q}^i$ and r^i verifying (15) the new problem aims at finding $\{g^i_\gamma\}_{\gamma\subset\mathcal{F}(\omega_i)}$ and r^i_k verifying both (19) and the corresponding weighted projected equilibration conditions.

Specifically, the constrained optimization problem given in (16) is simplified to

$$\boxed{\begin{array}{ll}\underset{g^i_\gamma,\, r^i_k}{\text{Minimize}} & \displaystyle\sum_{\Omega_k\subset\omega_i} \|\boldsymbol{q}^i_k(g^i_\gamma, r^i_k)\|^2_k + \kappa_k^2\|r^i_k\|^2_k \\ \text{Subject to} & g^i_\gamma \text{ verifying the boundary conditions (19)} \\ & g^i_\gamma \text{ and } r^i_k \text{ verifying the equilibration conditions (30), (36) or (45).}\end{array}} \tag{47}$$

The degrees of freedom of (47) are the values of g^i_γ (three or six DOFs per face of the star depending on the case) and the degrees of freedom of r^i_k which if necessary can be set to zero or a constant per element, being clearly smaller than the $(4q+9)(q+2)(q+1)/6$ times the number of elements in the star (with $q \geq 2$) of (16). Also, the number of constraints is greatly reduced since the boundary conditions (19) only restrict the value of g^i_γ at the boundary of the star (excluding the faces in the Dirichlet boundary) and the equilibration conditions state only one condition per element of the star.

Remark 14. It is tacitly assumed that problem (47) has at least one solution, that is, it is assumed that the restrictions given by equations (19) and the corresponding equilibration condition (30), (36) or (45) form a set of compatible restrictions. The reader is referred to Remarks 6, 9, 10 and 11 for specific details.

Remark 15. The equilibration conditions given in (30), (36) or (45) are a direct consequence of (18) being solvable and can be stated as a unified condition. Indeed, integrating equation (18a) over element Ω_k yields

$$\int_{\Omega_k}\left[\phi_i\Pi^{\hat{q}}_k(f-\kappa_k^2u_h) - \boldsymbol{\nabla}u_h\cdot\boldsymbol{\nabla}\phi_i - \kappa_k^2 r^i_k\right]d\Omega + \int_{\Omega_k}\boldsymbol{\nabla}\cdot\left(\boldsymbol{q}^i_k + \phi_i\boldsymbol{\nabla}u_h\right)d\Omega = 0$$

which after applying the divergence theorem and the boundary conditions (18b) gives the condition

$$\int_{\Omega_k}\left[\phi_i\Pi^{\hat{q}}_k(f-\kappa_k^2u_h) - \boldsymbol{\nabla}u_h\cdot\boldsymbol{\nabla}\phi_i - \kappa_k^2 r^i_k\right]d\Omega + \sum_{\gamma\subset\partial\Omega_k}\int_\gamma \sigma^\gamma_k g^i_\gamma\, d\Gamma = 0. \tag{48}$$

Equations (30), (36) or (45) are found substituting the particular values of $\hat{q}$ and the corresponding expression of r^i_k into the previous unified equation.

The remainder of the section thoroughly details for the three different considered cases: 1) the degrees of freedom for the problems given in (47), 2) the expressions of its quadratic objective function

$$\|\boldsymbol{q}^i_k(g^i_\gamma, r^i_k)\|^2_k + \kappa_k^2\|r^i_k\|^2_k \tag{49}$$

and 3) the expressions of its constraints in terms of the local degrees of freedom.

4.4.1 Case I. Piecewise constant projection of the data $\hat{q} = \bar{q} = 0$

Given a star ω_i and a tetrahedron of this star $\Omega_k \subset \omega_i$, the linear tractions associated to the faces of this tetrahedron $g^i_\gamma, \gamma \subset \partial\Omega_k$ are given in (22). Therefore, every tetrahedron of the star has nine degrees of freedom associated to the linear tractions g^i_γ which are stored in vector $\boldsymbol{\alpha}_k$, see equation (23).

With these notations, the expression for the linear part of the flux $\boldsymbol{q}_k^{iL}$ given in equation (26) can be simplified noting that in this case, introducing (22) into (28) and recalling that $\phi_i(\boldsymbol{x}_{[j]}) = \delta_{1j}$ yields

$$\begin{aligned}
\boldsymbol{\rho}_{[1]}^k &= A_{[2]}(\sigma_k^{\gamma_{[2]}}\alpha_{21} - \boldsymbol{\nabla} u_h \cdot \boldsymbol{n}_{[2]})\boldsymbol{t}_{[21]} + A_{[3]}(\sigma_k^{\gamma_{[3]}}\alpha_{31} - \boldsymbol{\nabla} u_h \cdot \boldsymbol{n}_{[3]})\boldsymbol{t}_{[31]} + A_{[4]}(\sigma_k^{\gamma_{[4]}}\alpha_{41} - \boldsymbol{\nabla} u_h \cdot \boldsymbol{n}_{[4]})\boldsymbol{t}_{[41]},\\
\boldsymbol{\rho}_{[2]}^k &= A_{[3]}\sigma_k^{\gamma_{[3]}}\alpha_{32}\boldsymbol{t}_{[32]} + A_{[4]}\sigma_k^{\gamma_{[4]}}\alpha_{42}\boldsymbol{t}_{[42]},\\
\boldsymbol{\rho}_{[3]}^k &= A_{[2]}\sigma_k^{\gamma_{[2]}}\alpha_{23}\boldsymbol{t}_{[23]} + A_{[4]}\sigma_k^{\gamma_{[4]}}\alpha_{43}\boldsymbol{t}_{[43]},\\
\boldsymbol{\rho}_{[4]}^k &= A_{[2]}\sigma_k^{\gamma_{[2]}}\alpha_{24}\boldsymbol{t}_{[24]} + A_{[3]}\sigma_k^{\gamma_{[3]}}\alpha_{34}\boldsymbol{t}_{[34]}
\end{aligned}$$

and therefore

$$\begin{aligned}
\mathbf{q}_k^{iL} &= \frac{1}{3|\Omega_k|}\Big(\lambda_{[1]}A_{[2]}\sigma_k^{\gamma_{[2]}}\boldsymbol{t}_{[21]},\ \lambda_{[3]}A_{[2]}\sigma_k^{\gamma_{[2]}}\boldsymbol{t}_{[23]},\ \lambda_{[4]}A_{[2]}\sigma_k^{\gamma_{[2]}}\boldsymbol{t}_{[24]},\ \lambda_{[1]}A_{[3]}\sigma_k^{\gamma_{[3]}}\boldsymbol{t}_{[31]},\ \lambda_{[2]}A_{[3]}\sigma_k^{\gamma_{[3]}}\boldsymbol{t}_{[32]},\\
&\qquad \lambda_{[4]}A_{[3]}\sigma_k^{\gamma_{[3]}}\boldsymbol{t}_{[34]},\ \lambda_{[1]}A_{[4]}\sigma_k^{\gamma_{[4]}}\boldsymbol{t}_{[41]},\ \lambda_{[2]}A_{[4]}\sigma_k^{\gamma_{[4]}}\boldsymbol{t}_{[42]},\ \lambda_{[3]}A_{[4]}\sigma_k^{\gamma_{[4]}}\boldsymbol{t}_{[43]}\Big)\boldsymbol{\alpha}_k\\
&\quad + \frac{1}{3|\Omega_k|}\lambda_{[1]}\Big(A_{[2]}\boldsymbol{\nabla} u_h \cdot \boldsymbol{n}_{[2]}\boldsymbol{t}_{[12]} + A_{[3]}\boldsymbol{\nabla} u_h \cdot \boldsymbol{n}_{[3]}\boldsymbol{t}_{[13]} + A_{[4]}\boldsymbol{\nabla} u_h \cdot \boldsymbol{n}_{[4]}\boldsymbol{t}_{[14]}\Big)\\
&= \frac{1}{3|\Omega_k|}\ \left(\mathbf{M}^{\mathbf{q}L}\,\boldsymbol{\Lambda}^{\mathbf{q}L}\,\boldsymbol{\alpha}_k + \lambda_{[1]}\,\mathbf{b}^{\mathbf{q}L}\right),
\end{aligned} \tag{50}$$

where

$$\begin{aligned}
\mathbf{M}^{\mathbf{q}L} &= \Big(A_{[2]}\sigma_k^{\gamma_{[2]}}\boldsymbol{t}_{[21]},\ A_{[2]}\sigma_k^{\gamma_{[2]}}\boldsymbol{t}_{[23]},\ A_{[2]}\sigma_k^{\gamma_{[2]}}\boldsymbol{t}_{[24]},\ A_{[3]}\sigma_k^{\gamma_{[3]}}\boldsymbol{t}_{[31]},\ A_{[3]}\sigma_k^{\gamma_{[3]}}\boldsymbol{t}_{[32]},\ A_{[3]}\sigma_k^{\gamma_{[3]}}\boldsymbol{t}_{[34]},\\
&\qquad A_{[4]}\sigma_k^{\gamma_{[4]}}\boldsymbol{t}_{[41]},\ A_{[4]}\sigma_k^{\gamma_{[4]}}\boldsymbol{t}_{[42]},\ A_{[4]}\sigma_k^{\gamma_{[4]}}\boldsymbol{t}_{[43]}\Big),\\
\boldsymbol{\Lambda}^{\mathbf{q}L} &= \mathbf{diag}(\lambda_{[1]}, \lambda_{[3]}, \lambda_{[4]}, \lambda_{[1]}, \lambda_{[2]}, \lambda_{[4]}, \lambda_{[1]}, \lambda_{[2]}, \lambda_{[3]}),\\
\mathbf{b}^{\mathbf{q}L} &= A_{[2]}\boldsymbol{\nabla} u_h \cdot \boldsymbol{n}_{[2]}\boldsymbol{t}_{[12]} + A_{[3]}\boldsymbol{\nabla} u_h \cdot \boldsymbol{n}_{[3]}\boldsymbol{t}_{[13]} + A_{[4]}\boldsymbol{\nabla} u_h \cdot \boldsymbol{n}_{[4]}\boldsymbol{t}_{[14]}.
\end{aligned} \tag{51}$$

Also, the expression for the quadratic flux $\boldsymbol{q}_k^{iQ}$ given in equation (27) or (29) can be simplified writing the gradient $\nabla\phi_i$ in terms of geometrical data, see equation (A10), and using the geometrical properties given in equation (A2). Indeed, from equation (A2) it holds that

$$A_{[1]}\mathbf{M}^{\mathbf{q}}\boldsymbol{n}_{[1]} = \sum_{n=1}^{4}\sum_{\substack{m=2\\ m>n}}^{4}\lambda_{[n]}\lambda_{[m]}\boldsymbol{t}_{[nm]}(A_{[1]}\boldsymbol{t}_{[nm]}^{\mathsf{T}}\boldsymbol{n}_{[1]}) = 3|\Omega_k|\sum_{m=2}^{4}\lambda_{[1]}\lambda_{[m]}\boldsymbol{t}_{[1m]}$$

and therefore introducing (A10) into (29) yields

$$\mathbf{q}_k^{iQ} = -\frac{F^0}{4}\frac{A_{[1]}}{3|\Omega_k|}\mathbf{M}^{\mathbf{q}}\boldsymbol{n}_{[1]} = -\frac{F_0}{4}\sum_{m=2}^{4}\lambda_{[1]}\lambda_{[m]}\boldsymbol{t}_{[1m]}. \tag{52}$$

Introducing the expressions for the fluxes $\mathbf{q}_k^{iL}$ and $\mathbf{q}_k^{iQ}$ given in equations (50) and (52) into the local squared norms given in equation (49) allows expressing the contribution of element Ω_k to the objective function of the total star as a quadratic function depending on the nine unknowns given in $\boldsymbol{\alpha}_k$ and r_k^{i1} and r_k^{i0} (denoted as r_1 and r_0 in the following to simplify the notation). Indeed, inserting equations (24) and (25) into (49) and expanding the expression for the squared norms yields

$$\begin{aligned}
\|\boldsymbol{q}_k^i\|_k^2 + \kappa_k^2\|r_k^i\|_k^2 &= \|\boldsymbol{q}_k^{iL} + \boldsymbol{q}_k^{iQ}\|_k^2 + \kappa_k^2\|\phi_i r_1 + r_0\|_k^2\\
&= \|\boldsymbol{q}_k^{iL}\|_k^2 + \|\boldsymbol{q}_k^{iQ}\|_k^2 + 2(\boldsymbol{q}_k^{iL}, \boldsymbol{q}_k^{iQ})_k + \frac{\kappa_k^2|\Omega_k|}{10}\left(r_1^2 + 5r_1r_0 + 10r_0^2\right),
\end{aligned}$$

where $(\cdot,\cdot)_k$ represents the $[\mathcal{L}^2(\Omega_k)]^3$ scalar product and the properties $4\int_{\Omega_k}\phi_i d\Omega = |\Omega_k|$ and $10\|\phi_i\|_k^2 = |\Omega_k|$ have been used. Additionally, using equations (50) and (52) and introducing the expanded vector of unknowns $\widehat{\boldsymbol{\alpha}}_k = \left(\boldsymbol{\alpha}_k^{\mathsf{T}}, r_1, r_0\right)^{\mathsf{T}}$, the three terms of the previous expression can be computed as

$$\begin{aligned}
&\|\boldsymbol{q}_k^{iL}\|_k^2 = \widehat{\boldsymbol{\alpha}}_k^{\mathsf{T}}\widehat{\mathbf{M}}_k^L\widehat{\boldsymbol{\alpha}}_k + \widehat{\boldsymbol{\alpha}}_k^{\mathsf{T}}\widehat{\mathbf{b}}_k^L + \mathrm{c}_k^L,\\
&(\boldsymbol{q}_k^{iL}, \boldsymbol{q}_k^{iQ})_k = \widehat{\boldsymbol{\alpha}}_k^{\mathsf{T}}\widehat{\mathbf{M}}_k^{LQ}\widehat{\boldsymbol{\alpha}}_k + \widehat{\boldsymbol{\alpha}}_k^{\mathsf{T}}\widehat{\mathbf{b}}_k^{LQ} + \Pi_k^0(f - \kappa_k^2 u_h)\mathrm{c}_k^{LQ},\\
&\|\boldsymbol{q}_k^{iQ}\|_k^2 = \widehat{\boldsymbol{\alpha}}_k^{\mathsf{T}}\widehat{\mathbf{M}}_k^Q\widehat{\boldsymbol{\alpha}}_k + \widehat{\boldsymbol{\alpha}}_k^{\mathsf{T}}\widehat{\mathbf{b}}_k^Q + (\Pi_k^0(f - \kappa_k^2 u_h))^2\mathrm{c}_k^Q,
\end{aligned} \tag{53}$$

where the expressions for the matrices, vectors and constants appearing in these equations are given in Appendix C for simplicity of presentation. Therefore the squared norm of the local weighted fluxes is given by

$$\begin{aligned}\|\boldsymbol{q}_k^i\|_k^2+\kappa_k^2\|r_k^i\|_k^2 &= \widehat{\boldsymbol{\alpha}}_k^\mathsf{T}(\widehat{\mathbf{M}}_k^L+2\widehat{\mathbf{M}}_k^{LQ}+\widehat{\mathbf{M}}_k^Q+\frac{\kappa_k^2|\Omega_k|}{10}\begin{bmatrix}\mathbf{0}_{9\times9} & \mathbf{0}_{9\times1} & \mathbf{0}_{9\times1}\\ \mathbf{0}_{1\times9} & 1 & 5/2\\ \mathbf{0}_{1\times9} & 5/2 & 10\end{bmatrix})\widehat{\boldsymbol{\alpha}}_k \\ &+\widehat{\boldsymbol{\alpha}}_k^\mathsf{T}(\widehat{\mathbf{b}}_k^L+2\widehat{\mathbf{b}}_k^{LQ}+\widehat{\mathbf{b}}_k^Q)+\text{constant term.}\end{aligned} \tag{54}$$

Equation (54) provides a closed explicit formula for the local contribution of element Ω_k to the global objective function to be minimized in the star, see equation (47). Element Ω_k also contributes to the optimization problem with one equation coming from the constraint given in (30). Appendix D shows that, after computing the integrals appearing in equation (30), this weighted projected equilibration condition can be rewritten in terms of the unknowns $\widehat{\boldsymbol{\alpha}}_k$ as

$$\begin{aligned}&|\Omega_k|\left(\frac{1}{4}\Pi_k^0(f-\kappa_k^2u_h)-\nabla u_h\cdot\nabla\phi_i\right)-\kappa_k^2|\Omega_k|\left(\frac{1}{4}r_1+r_0\right)\\ &+\frac{1}{3}A_{[2]}\sigma_k^{\gamma_{[2]}}(\alpha_{21}+\alpha_{23}+\alpha_{24})+\frac{1}{3}A_{[3]}\sigma_k^{\gamma_{[3]}}(\alpha_{31}+\alpha_{32}+\alpha_{34})+\frac{1}{3}A_{[4]}\sigma_k^{\gamma_{[4]}}(\alpha_{41}+\alpha_{42}+\alpha_{43})=0.\end{aligned} \tag{55}$$

4.4.2 Case II. Mixed piecewise linear/constant projection of the data $\hat{q}=1, \bar{q}=0$

As in Case I, the local tractions at face γ of a tetrahedron $\partial\Omega_k \subset \omega_i$ are linear and can be expressed as detailed in equation (22). Thus its degrees of freedom can be again stored using vector $\boldsymbol{\alpha}_k$ defined in (23). With these notations, the contributions to the flux $\boldsymbol{q}_k^i$ given in (32) can be rewritten in terms of the nine unknowns given in $\boldsymbol{\alpha}_k$ plus the five unknowns describing the reaction term r_k^i ($r_{[1]}$, $r_{[2]}$, $r_{[3]}$, $r_{[4]}$ and $r_0 = r_k^{i0}$), see (31). These unknowns are stored in the expanded vector

$$\widehat{\boldsymbol{\alpha}}_k = \left(\boldsymbol{\alpha}_k^\mathsf{T}, r_{[1]}, r_{[2]}, r_{[3]}, r_{[4]}, r_0\right)^\mathsf{T}.$$

Specifically, the linear part of the flux $\boldsymbol{q}_k^{iL}$ given in equation (26), which coincides with the one from Case I, can be rewritten in a matrix-vector form as detailed in (50).

Also, the cubic flux $\mathbf{q}_k^{iC}$ given in (33) depends on $\widehat{\boldsymbol{\alpha}}_k$ via the function F^1 (since from equation (35), $F^1_{[j]} = F^1(\boldsymbol{x}_{[j]}) = \Pi_k^1(f-\kappa_k^2u_h)(\boldsymbol{x}_{[j]})-\kappa_k^2r_{[j]}$). Thus, the flux $\mathbf{q}_k^{iC}$ can be rewritten in terms of $\widehat{\boldsymbol{\alpha}}_k$ by making its dependence on F^1 explicit. Specifically, introducing the value of ∇v^Q given in (B20) into (33) and using the following geometrical properties

$$\boldsymbol{t}_{[mn]}^\mathsf{T}\boldsymbol{n}_{[l]}=0 \text{ if } m,n\neq l \quad\text{and}\quad A_{[l]}\boldsymbol{t}_{[ln]}^\mathsf{T}\boldsymbol{n}_{[l]}=3|\Omega_k|\,,\; A_{[l]}\boldsymbol{t}_{[nl]}^\mathsf{T}\boldsymbol{n}_{[l]}=-3|\Omega_k| \text{ for } n\neq l \tag{56}$$

yields

$$\mathbf{q}_k^{iC}=-\frac{1}{40}\mathbf{M}^{\mathbf{q}C}(4\mathbf{M}_2^{v^Q}+4\lambda_{[1]}\mathbf{I}_4+\mathbf{M}_1^{v^Q})\left(\boldsymbol{\Pi}^1-\kappa_k^2(r_{[1]}\,r_{[2]}\,r_{[3]}\,r_{[4]})^\mathsf{T}\right), \tag{57}$$

where $\mathbf{I}_4$ is the 4×4 identity matrix, matrices $\mathbf{M}_1^{v^Q}$ and $\mathbf{M}_2^{v^Q}$ are defined in equations (B16) and (B21) and

$$\begin{aligned}\mathbf{M}^{\mathbf{q}C} &= (\,\lambda_{[1]}\lambda_{[2]}\boldsymbol{t}_{[12]}+\lambda_{[1]}\lambda_{[3]}\boldsymbol{t}_{[13]}+\lambda_{[1]}\lambda_{[4]}\boldsymbol{t}_{[14]}\,,\;-\lambda_{[1]}\lambda_{[2]}\boldsymbol{t}_{[12]}+\lambda_{[2]}\lambda_{[3]}\boldsymbol{t}_{[23]}+\lambda_{[2]}\lambda_{[4]}\boldsymbol{t}_{[24]}\,,\\ &\quad-\lambda_{[1]}\lambda_{[3]}\boldsymbol{t}_{[13]}-\lambda_{[2]}\lambda_{[3]}\boldsymbol{t}_{[23]}+\lambda_{[3]}\lambda_{[4]}\boldsymbol{t}_{[34]}\,,\;-\lambda_{[1]}\lambda_{[4]}\boldsymbol{t}_{[14]}-\lambda_{[2]}\lambda_{[4]}\boldsymbol{t}_{[24]}-\lambda_{[3]}\lambda_{[4]}\boldsymbol{t}_{[34]}\,),\\ \boldsymbol{\Pi}^1 &= \left(\Pi_k^1(f-\kappa_k^2u_h)(\boldsymbol{x}_{[1]})\,,\;\Pi_k^1(f-\kappa_k^2u_h)(\boldsymbol{x}_{[2]})\,,\;\Pi_k^1(f-\kappa_k^2u_h)(\boldsymbol{x}_{[3]})\,,\;\Pi_k^1(f-\kappa_k^2u_h)(\boldsymbol{x}_{[4]})\right)^\mathsf{T}.\end{aligned}$$

Introducing the expressions for the fluxes $\mathbf{q}_k^{iL}$ and $\mathbf{q}_k^{iC}$ given in equations (50) and (57) into the local squared norms given in equation (49) allows expressing the contribution of element Ω_k to the norm associated to the star as a quadratic function depending on $\widehat{\boldsymbol{\alpha}}_k$. Indeed, inserting equations (31) and (32) into (49) and expanding the expression for the squared norms yields

$$\|\boldsymbol{q}_k^i\|_k^2+\kappa_k^2\|r_k^i\|_k^2=\|\boldsymbol{q}_k^{iL}\|_k^2+\|\boldsymbol{q}_k^{iC}\|_k^2+2(\boldsymbol{q}_k^{iL},\boldsymbol{q}_k^{iC})_k+\kappa_k^2\|\phi_ir_k^{iL}+r_0\|_k^2,$$

where

$$\begin{aligned}\|\boldsymbol{q}_k^{iL}\|_k^2 &= \widehat{\boldsymbol{\alpha}}_k^\mathsf{T}\widehat{\mathbf{M}}_k^L\widehat{\boldsymbol{\alpha}}_k+\widehat{\boldsymbol{\alpha}}_k^\mathsf{T}\widehat{\mathbf{b}}_k^L+\mathrm{c}_k^L,\\ (\boldsymbol{q}_k^{iL},\boldsymbol{q}_k^{iC})_k &= \widehat{\boldsymbol{\alpha}}_k^\mathsf{T}\widehat{\mathbf{M}}_k^{LC}\widehat{\boldsymbol{\alpha}}_k+\widehat{\boldsymbol{\alpha}}_k^\mathsf{T}\widehat{\mathbf{b}}_k^{LC}+c_k^{LC},\\ \|\boldsymbol{q}_k^{iC}\|_k^2 &= \widehat{\boldsymbol{\alpha}}_k^\mathsf{T}\widehat{\mathbf{M}}_k^C\widehat{\boldsymbol{\alpha}}_k+\widehat{\boldsymbol{\alpha}}_k^\mathsf{T}\widehat{\mathbf{b}}_k^C+c_k^C,\\ \|\phi_ir_k^{iL}+r_0\|_k^2 &= \widehat{\boldsymbol{\alpha}}_k^\mathsf{T}\widehat{\mathbf{M}}_k^r\widehat{\boldsymbol{\alpha}}_k.\end{aligned} \tag{58}$$

The expressions for the matrices, vectors and constants appearing in the previous equations are given in Appendix C for simplicity of presentation. Therefore the squared norm of the local weighted fluxes is given by

$$\begin{aligned}\|\boldsymbol{q}_k^i\|_k^2+\kappa_k^2\|r_k^i\|_k^2 &= \widehat{\boldsymbol{\alpha}}_k^{\mathsf{T}}(\widehat{\mathbf{M}}_k^L + 2\widehat{\mathbf{M}}_k^{LC} + \widehat{\mathbf{M}}_k^C + \kappa_k^2\widehat{\mathbf{M}}_k^r)\widehat{\boldsymbol{\alpha}}_k \\ &+\widehat{\boldsymbol{\alpha}}_k^{\mathsf{T}}(\widehat{\mathbf{b}}_k^L + 2\widehat{\mathbf{b}}_k^{LC} + \widehat{\mathbf{b}}_k^C) + \text{constant term.}\end{aligned} \tag{59}$$

Equation (59) provides a closed explicit formula for the local contribution of element Ω_k to the global objective function to be minimized in (47). As in Case I, element Ω_k also contributes to the optimization problem with one equation coming from the constraint given in (36). Appendix D shows that this weighted projected equilibration condition can be rewritten in terms of $\widehat{\boldsymbol{\alpha}}_k$ as

$$\begin{aligned}&\frac{|\Omega_k|}{20}\left(2F_{[1]}^1 + F_{[2]}^1 + F_{[3]}^1 + F_{[4]}^1 - 20\kappa_k^2 r_0 - 20\nabla u_h\cdot\nabla\phi_i\right)\\ &+\frac{1}{3}A_{[2]}\sigma_k^{\gamma_{[2]}}(\alpha_{21}+\alpha_{23}+\alpha_{24}) + \frac{1}{3}A_{[3]}\sigma_k^{\gamma_{[3]}}(\alpha_{31}+\alpha_{32}+\alpha_{34}) + \frac{1}{3}A_{[4]}\sigma_k^{\gamma_{[4]}}(\alpha_{41}+\alpha_{42}+\alpha_{43}) = 0.\end{aligned} \tag{60}$$

4.4.3 Case III. Piecewise linear projection of the data $\hat{q} = \bar{q} = 1$

Given a star ω_i and a tetrahedron of this star $\Omega_k \subset \omega_i$, the quadratic tractions associated to the faces of this tetrahedron $g_\gamma^i, \gamma \subset \partial\Omega_k$ are given in equation (37). Therefore, every tetrahedron of the star has eighteen degrees of freedom associated to the quadratic tractions g_γ^i which are stored in vector $\boldsymbol{\alpha}_k^q$, see equation (38). It is also worth noting that in this case $r_k^i = 0$ and therefore the only unknowns of the local optimization problem are given by $\boldsymbol{\alpha}_k^q$.

With these notations, the three contributions to the flux $\boldsymbol{q}_k^i$ given in (40) can be rewritten in matrix form in terms of $\boldsymbol{\alpha}_k^q$ as

$$\mathbf{q}_k^{iC} = -\frac{1}{40}\mathbf{M}^{\mathbf{q}C}(4\mathbf{M}_2^{vQ} + 4\lambda_{[1]}\mathbf{I}_4 + \mathbf{M}_1^{vQ})\mathbf{\Pi}^1, \tag{61a}$$

$$\mathbf{q}_k^{iQq} = \frac{1}{3|\Omega_k|}\left(\left(\mathbf{M}_1^{\mathbf{q}Q}\,\mathbf{\Lambda}^{\mathbf{q}Q} + \mathbf{M}_2^{\mathbf{q}Q}\right)\boldsymbol{\alpha}_k^q + \mathbf{b}^{\mathbf{q}Q}\right), \tag{61b}$$

$$\mathbf{q}_k^{i\nabla} = -\frac{1}{18|\Omega_k|^2}\,\mathbf{M}^{\mathbf{q}}\,\mathbf{M}^{\mathbf{q}\nabla}\boldsymbol{\alpha}_k^q. \tag{61c}$$

Indeed, since the definition of $\mathbf{q}_k^{iC}$ is the same for Cases II and III, equation (61a) is directly obtained from equation (57) recalling that in this case $r_{[j]} = 0$, $j = 1,\dots,4$. Also, $\boldsymbol{\rho}_{[n]}^k$ and $\boldsymbol{\rho}_{[nm]}^k$ given in equations (29) and (46) respectively can be expressed as

$$\boldsymbol{\rho}_{[n]}^k = \sum_{\substack{m=2\\ m\neq n}}^{4} A_{[m]}(\sigma_k^{\gamma_{[m]}}\alpha_{mn} - \delta_{1n}\nabla u_h\cdot\boldsymbol{n}_k^{\gamma_{[m]}})\boldsymbol{t}_{[mn]} \tag{62}$$

and

$$\boldsymbol{\rho}_{[nm]}^k = \frac{1}{2}\sum_{\substack{j=2\\ j\neq n,m}}^{4} A_{[j]}\sigma_k^{\gamma_{[j]}}\left(2\alpha_{jnm} - \alpha_{jn} - \alpha_{jm}\right)\boldsymbol{t}_{[jn]}, \tag{63}$$

and therefore

$$\begin{aligned}\mathbf{q}_k^{iQq} = \frac{1}{3|\Omega_k|}\Bigg(&\sum_{n=1}^{4}\sum_{\substack{m=2\\ m\neq n}}^{4} A_{[m]}\sigma_k^{\gamma_{[m]}}\boldsymbol{t}_{[mn]}\lambda_{[n]}\alpha_{mn} - \sum_{m=2}^{4} A_{[m]}\nabla u_h\cdot\boldsymbol{n}_k^{\gamma_{[m]}}\boldsymbol{t}_{[m1]}\lambda_{[1]}\\ &+\frac{1}{2}\sum_{n=1}^{4}\sum_{\substack{m=2\\ m>n}}^{4}\sum_{\substack{j=2\\ j\neq n,m}}^{4} A_{[j]}\sigma_k^{\gamma_{[j]}}\boldsymbol{t}_{[jn]}\lambda_{[nm]}^q\left(2\alpha_{jnm} - \alpha_{jn} - \alpha_{jm}\right)\Bigg).\end{aligned}$$

Then, equation (61b) holds for

$$
\begin{aligned}
\mathbf{M}_1^{\mathbf{q}\mathcal{Q}} &= \Big(A_{[2]}\sigma_k^{\gamma_{[2]}}\boldsymbol{t}_{[21]}\,,\; A_{[2]}\sigma_k^{\gamma_{[2]}}\boldsymbol{t}_{[23]}\,,\; A_{[2]}\sigma_k^{\gamma_{[2]}}\boldsymbol{t}_{[24]}\,,\; A_{[2]}\sigma_k^{\gamma_{[2]}}\boldsymbol{t}_{[21]}\,,\; A_{[2]}\sigma_k^{\gamma_{[2]}}\boldsymbol{t}_{[21]}\,,\; A_{[2]}\sigma_k^{\gamma_{[2]}}\boldsymbol{t}_{[23]}\,, \\
&\qquad A_{[3]}\sigma_k^{\gamma_{[3]}}\boldsymbol{t}_{[31]}\,,\; A_{[3]}\sigma_k^{\gamma_{[3]}}\boldsymbol{t}_{[32]}\,,\; A_{[3]}\sigma_k^{\gamma_{[3]}}\boldsymbol{t}_{[34]}\,,\; A_{[3]}\sigma_k^{\gamma_{[3]}}\boldsymbol{t}_{[31]}\,,\; A_{[3]}\sigma_k^{\gamma_{[3]}}\boldsymbol{t}_{[31]}\,,\; A_{[3]}\sigma_k^{\gamma_{[3]}}\boldsymbol{t}_{[32]}\,, \\
&\qquad A_{[4]}\sigma_k^{\gamma_{[4]}}\boldsymbol{t}_{[41]}\,,\; A_{[4]}\sigma_k^{\gamma_{[4]}}\boldsymbol{t}_{[42]}\,,\; A_{[4]}\sigma_k^{\gamma_{[4]}}\boldsymbol{t}_{[43]}\,,\; A_{[4]}\sigma_k^{\gamma_{[4]}}\boldsymbol{t}_{[41]}\,,\; A_{[4]}\sigma_k^{\gamma_{[4]}}\boldsymbol{t}_{[41]}\,,\; A_{[4]}\sigma_k^{\gamma_{[4]}}\boldsymbol{t}_{[42]} \Big) \\
\boldsymbol{\Lambda}^{\mathbf{q}\mathcal{Q}} &= \mathbf{diag}(\lambda_{[1]},\lambda_{[3]},\lambda_{[4]},\lambda^q_{[13]},\lambda^q_{[14]},\lambda^q_{[34]},\lambda_{[1]},\lambda_{[2]},\lambda_{[4]},\lambda^q_{[12]},\lambda^q_{[14]},\lambda^q_{[24]},\lambda_{[1]},\lambda_{[2]},\lambda_{[3]},\lambda^q_{[12]},\lambda^q_{[13]},\lambda^q_{[23]}) \\
\mathbf{M}_2^{\mathbf{q}\mathcal{Q}} &= \Big(A_{[2]}\sigma_k^{\gamma_{[2]}}\boldsymbol{t}_{[21]}(\lambda^q_{[13]}+\lambda^q_{[14]})\,,\; A_{[2]}\sigma_k^{\gamma_{[2]}}(\boldsymbol{t}_{[23]}\lambda^q_{[34]}+\boldsymbol{t}_{[21]}\lambda^q_{[13]})\,,\; A_{[2]}\sigma_k^{\gamma_{[2]}}(\boldsymbol{t}_{[23]}\lambda^q_{[34]}+\boldsymbol{t}_{[21]}\lambda^q_{[14]})\,,\; \mathbf{0}\,,\; \mathbf{0}\,,\; \mathbf{0}\,, \\
&\qquad A_{[3]}\sigma_k^{\gamma_{[3]}}\boldsymbol{t}_{[31]}(\lambda^q_{[12]}+\lambda^q_{[14]})\,,\; A_{[3]}\sigma_k^{\gamma_{[3]}}(\boldsymbol{t}_{[32]}\lambda^q_{[24]}+\boldsymbol{t}_{[31]}\lambda^q_{[12]})\,,\; A_{[3]}\sigma_k^{\gamma_{[3]}}(\boldsymbol{t}_{[31]}\lambda^q_{[14]}+\boldsymbol{t}_{[32]}\lambda^q_{[24]})\,,\; \mathbf{0}\,,\; \mathbf{0}\,,\; \mathbf{0}\,, \\
&\qquad A_{[4]}\sigma_k^{\gamma_{[4]}}\boldsymbol{t}_{[41]}(\lambda^q_{[12]}+\lambda^q_{[13]})\,,\; A_{[4]}\sigma_k^{\gamma_{[4]}}(\boldsymbol{t}_{[42]}\lambda^q_{[23]}+\boldsymbol{t}_{[41]}\lambda^q_{[12]})\,,\; A_{[4]}\sigma_k^{\gamma_{[4]}}(\boldsymbol{t}_{[41]}\lambda^q_{[13]}+\boldsymbol{t}_{[42]}\lambda^q_{[23]})\,,\; \mathbf{0}\,,\; \mathbf{0}\,,\; \mathbf{0}\Big) \\
\mathbf{b}^{\mathbf{q}\mathcal{Q}} &= \Big(A_{[2]}\boldsymbol{\nabla}u_h\cdot\boldsymbol{n}_{[2]}\boldsymbol{t}_{[12]} + A_{[3]}\boldsymbol{\nabla}u_h\cdot\boldsymbol{n}_{[3]}\boldsymbol{t}_{[13]} + A_{[4]}\boldsymbol{\nabla}u_h\cdot\boldsymbol{n}_{[4]}\boldsymbol{t}_{[14]}\Big)\lambda_{[1]}.
\end{aligned}
\tag{64}
$$

Note that for simplicity, the first short form of $\boldsymbol{\rho}^k_{[nm]}$ has been used (see equation (46) in Remark 12). Similar expressions can be obtained for the other two forms.

Finally, introducing equation (63) into the definition of $\boldsymbol{v}^{\nabla}$ given in equation (44) and using equation (B25) yields

$$
\boldsymbol{v}^{\nabla} = -\frac{1}{2}\frac{4}{27|\Omega_k|^3}\sum_{n=1}^{4}\sum_{m=n+1}^{4}\sum_{\substack{j=2\\ j\neq n,m}}^{4} A_{[m]}A_{[j]}\sigma_k^{\gamma_{[i]}}\boldsymbol{n}_{[m]}\left(2\alpha_{jnm}-\alpha_{jn}-\alpha_{jm}\right) = -\frac{4}{18|\Omega_k|^2}\mathbf{M}^{\mathbf{q}\nabla}\boldsymbol{\alpha}^q_k \tag{65}
$$

for

$$
\begin{aligned}
\mathbf{M}^{\mathbf{q}\nabla} = -\frac{1}{2}\Big(& -\sigma_k^{\gamma_{[2]}}A_{[2]}(A_{[3]}\boldsymbol{n}_{[3]}+A_{[4]}\boldsymbol{n}_{[4]})\,,\; -\sigma_k^{\gamma_{[2]}}A_{[2]}(A_{[3]}\boldsymbol{n}_{[3]}+A_{[4]}\boldsymbol{n}_{[4]})\,,\; -2\sigma_k^{\gamma_{[2]}}A_{[2]}A_{[4]}\boldsymbol{n}_{[4]}\,, \\
& 2\sigma_k^{\gamma_{[2]}}A_{[2]}A_{[3]}\boldsymbol{n}_{[3]}\,,\; 2\sigma_k^{\gamma_{[2]}}A_{[2]}A_{[4]}\boldsymbol{n}_{[4]}\,,\; 2\sigma_k^{\gamma_{[2]}}A_{[2]}A_{[4]}\boldsymbol{n}_{[4]}\,, \\
& -\sigma_k^{\gamma_{[3]}}A_{[3]}(A_{[2]}\boldsymbol{n}_{[2]}+A_{[4]}\boldsymbol{n}_{[4]})\,,\; -\sigma_k^{\gamma_{[3]}}A_{[3]}(A_{[2]}\boldsymbol{n}_{[2]}+A_{[4]}\boldsymbol{n}_{[4]})\,,\; -2\sigma_k^{\gamma_{[3]}}A_{[3]}A_{[4]}\boldsymbol{n}_{[4]}\,, \\
& 2\sigma_k^{\gamma_{[3]}}A_{[3]}A_{[2]}\boldsymbol{n}_{[2]}\,,\; 2\sigma_k^{\gamma_{[3]}}A_{[3]}A_{[4]}\boldsymbol{n}_{[4]}\,,\; 2\sigma_k^{\gamma_{[3]}}A_{[3]}A_{[4]}\boldsymbol{n}_{[4]}\,, \\
& -\sigma_k^{\gamma_{[4]}}A_{[4]}(A_{[2]}\boldsymbol{n}_{[2]}+A_{[3]}\boldsymbol{n}_{[3]})\,,\; -\sigma_k^{\gamma_{[4]}}A_{[4]}(A_{[2]}\boldsymbol{n}_{[2]}+A_{[3]}\boldsymbol{n}_{[3]})\,,\; -2\sigma_k^{\gamma_{[4]}}A_{[4]}A_{[3]}\boldsymbol{n}_{[3]}\,, \\
& 2\sigma_k^{\gamma_{[4]}}A_{[4]}A_{[2]}\boldsymbol{n}_{[2]}\,,\; 2\sigma_k^{\gamma_{[4]}}A_{[4]}A_{[3]}\boldsymbol{n}_{[3]}\,,\; 2\sigma_k^{\gamma_{[4]}}A_{[4]}A_{[3]}\boldsymbol{n}_{[3]}\Big).
\end{aligned}
$$

and equation (61c) is found introducing (65) into (43).

Introducing the matrix expressions for the fluxes given in equations (61) into the local squared norm $\|\boldsymbol{q}^i_k\|^2$ allows expressing the contribution of element Ω_k to the norm associated to the star as a quadratic function depending on $\boldsymbol{\alpha}^q_k$. For simplicity of presentation, the explicit quadratic expression for

$$
\|\boldsymbol{q}^i_k\|^2 = \int_{\Omega_k}(\boldsymbol{q}^i_k)^{\mathsf{T}}\boldsymbol{q}^i_k\,d\Omega = (\boldsymbol{\alpha}^q_k)^{\mathsf{T}}\mathbf{M}_k\boldsymbol{\alpha}^q_k + (\boldsymbol{\alpha}^q_k)^{\mathsf{T}}\mathbf{b}_k + \text{constant term} \tag{66}
$$

is not given here. Matrix $\mathbf{M}_k$ and vector $\mathbf{b}_k$ can be obtained explicitly by computing the norm of $\boldsymbol{q}^i_k$ using the matrix expressions given in equation (61) as done in Cases I and II. However, in this more intricate case, noting that $\boldsymbol{q}^i_k$ is a polynomial field allows exactly computing $\mathbf{M}_k$ and $\mathbf{b}_k$ using an appropriate numerical quadrature rule.

Also, Ω_k also contributes to the optimization problem with one equation coming from the constraint given in (45). Again, for simplicity of presentation the explicit expression of the weighted projected equilibration condition in terms of $\boldsymbol{\alpha}^q_k$ is not given here. However, it can easily be obtained inserting the expression of the tractions g^i_γ given in equation (37) into (45) and integrating all the terms therein.

4.5 Brief review of the algorithm to compute the upper bounds for $||e||$

The following chart describes the steps to compute upper bounds for $|||e|||$ using the new low-cost flux-free approach. The procedure is sketched as follows:

1. For each node of the mesh $\boldsymbol{x}_i$, consider its associated star ω_i and denote by n^i_{el} the number of elements in the star.

(a) Consider the global vector $\widehat{\boldsymbol{\alpha}}^i$ containing all the traction unknowns associated to the faces in Γ_i and the reaction unknowns associated to all the elements $\Omega_k \subset \omega_i$. That is $\widehat{\boldsymbol{\alpha}}^i$ contains $3 \times \text{cardinal}(\Gamma_i) + 2 \times n^i_{\text{el}}$ unknowns in Case I, $3 \times \text{cardinal}(\Gamma_i) + 5 \times n^i_{\text{el}}$ unknowns in Case II and $6 \times \text{cardinal}(\Gamma_i)$ in Case III.

(b) For each element of the star $\Omega_k \subset \omega_i$, compute the matrix $\mathbf{M}_k$ and the vector $\mathbf{b}_k$ associated to the norm of the dual estimates

$$\|\boldsymbol{q}^i_k\|^2_k + \kappa^2_k \|r^i_k\|^2_k = \widehat{\boldsymbol{\alpha}}^{\mathsf{T}}_k \mathbf{M}_k \widehat{\boldsymbol{\alpha}}_k + \widehat{\boldsymbol{\alpha}}^{\mathsf{T}}_k \mathbf{b}_k + \text{constant term},$$

where the particular form of $\mathbf{M}_k$ and $\mathbf{b}_k$ is given in equations (54), (59) and (66) for Cases I, II and III respectively, and where $\widehat{\boldsymbol{\alpha}}_k = \boldsymbol{\alpha}^q_k$ in Case III. Assemble these contributions to the global matrix and vector

$$\mathbf{M}_{\omega_i} \quad \text{and} \quad \mathbf{b}_{\omega_i}$$

associated to the global unknowns $\widehat{\boldsymbol{\alpha}}^i$.

(c) For each element of the star $\Omega_k \subset \omega_i$, compute the corresponding weighted projected equilibrated condition (55), (60) or (45). Assemble all the conditions into the linear global system of equations

$$\mathbf{A}_{\omega_i} \widehat{\boldsymbol{\alpha}}^i = \mathbf{b}_{\omega_i}. \tag{67}$$

(d) For each face γ of element $\Omega_k \subset \omega_i$ lying on the Neumann boundary, impose the boundary conditions (19b) and add these restrictions to the global system of equations given in (67).

(e) Solve the following quadratic optimization problem with only equality linear constraints

$$\begin{aligned} &\text{Minimize } (\widehat{\boldsymbol{\alpha}}^i)^{\mathsf{T}} \mathbf{M}_{\omega_i} \widehat{\boldsymbol{\alpha}}^i + (\widehat{\boldsymbol{\alpha}}^i)^{\mathsf{T}} \mathbf{b}_{\omega_i} \\ &\text{Subject to } \mathbf{A}_{\omega_i} \widehat{\boldsymbol{\alpha}}^i = \mathbf{b}_{\omega_i}. \end{aligned} \tag{68}$$

(f) For each element of the star $\Omega_k \subset \omega_i$, compute the dual estimates $\boldsymbol{q}^i_k$ and r^i_k using the values of $\widehat{\boldsymbol{\alpha}}_k$ stored in $\widehat{\boldsymbol{\alpha}}^i$, see equations (27) and (24) for Case I, (32) and (31) for Case II and (40) for Case III. Accumulate these dual estimates into the elementary fields $\boldsymbol{q}_k$ and r_k, accounting for the contributions of all stars containing Ω_k

$$\boldsymbol{q}_k = \sum_{i \in \mathcal{N}(\Omega_k)} \boldsymbol{q}^i_k \quad , \quad r_k = \sum_{i \in \mathcal{N}(\Omega_k)} r^i_k. \tag{69}$$

2. For each element of the mesh Ω_k

(a) Compute the data oscillations terms $\text{osc}_k(f)$ and $\text{osc}_\gamma(g_{\text{N}})$ given in equations (8) and (9) for the considered values of $\hat{q}$ and $\bar{q}$.

(b) Compute the local norm contributions $\|\boldsymbol{q}\|_{[\mathcal{L}^2(\Omega_k)]^3} = \|\boldsymbol{q}_k\|_k$ and $\|r\|_{\mathcal{L}^2(\Omega_k)} = \|r_k\|_k$.

(c) Compute the local error contribution η_k defined in equation (7) and add this contribution to the total upper bound for the error.

3. Return the upper bound for the norm of the error given by

$$\eta = \left(\sum_{k=1}^{n_{\text{el}}} \eta^2_k \right)^{1/2}.$$

5 A NEW MORE ACCURATE EQUILIBRATED RESIDUAL METHOD

The equilibrated residual method computes a set of equilibrated boundary tractions g_k for every element Ω_k of the mesh. These tractions are *consistent*[16] or *codiffusive*[28,33], that is

$$\begin{cases} g_k + g_{k'} = 0 & \text{on } \gamma \subset \partial\Omega_k \cap \partial\Omega_{k'} \\ g_k = \Pi^{\bar{q}}_\gamma g_{\text{N}} & \text{on } \gamma \subset \partial\Omega_k \cap \Gamma_{\text{N}}, \end{cases} \tag{70}$$

and verify the *first-order equilibration condition* for all elements of the mesh Ω_k, namely

$$\int_{\Omega_k} \left[\phi_i \Pi^{\hat{q}}_k (f - \kappa^2_k u_h) - \boldsymbol{\nabla} u_h \cdot \boldsymbol{\nabla} \phi_i \right] d\Omega + \sum_{\gamma \subset \partial\Omega_k} \int_\gamma g_k \phi_i \, d\Gamma = 0, \quad i \in \mathcal{N}(\Omega_k). \tag{71}$$

These equilibrated tractions act as local Neumann boundary conditions for the local approximated error problems: find $\boldsymbol{q}_k \in [\mathcal{V}(\Omega_k)]^3$ and $r_k \in \mathcal{V}(\Omega_k)$ such that

$$\int_{\Omega_k} \left(\boldsymbol{q}_k \cdot \boldsymbol{\nabla} v + \kappa_k^2 r_k v \right) d\Omega = R_k^{\Pi}(v) + \sum_{\gamma \subset \partial\Omega_k \setminus \Gamma_N} \int_{\gamma} g_k v \, d\Gamma \quad \text{for all } v \in \mathcal{V}(\Omega_k), \tag{72}$$

where $a_k(\cdot,\cdot)$, $R_k^{\Pi}(\cdot)$ and $\mathcal{V}(\Omega_k)$ are the restrictions of $a(\cdot,\cdot)$, $\boldsymbol{R}^{\Pi}(\cdot)$ and $\mathcal{V}$ to element Ω_k, for which the following upper bound holds

$$|||e|||^2 \leq \sum_{k=1}^{n_{\text{el}}} \left[\sqrt{\|\boldsymbol{q}_k\|_k^2 + \kappa_k^2 \|r_k\|_k^2} + \text{osc}_k(f) + \sum_{\gamma \subset \partial\Omega_k \cap \Gamma_N} \text{osc}_{\gamma}(g_N) \right]^2 .$$

Remark 16. The equilibrated tractions guarantee the solvability of the local error problems given in (72) even for $\kappa = 0$. Indeed, for $\kappa = 0$ the kernel of the left hand side of equation (72) are the constant functions and therefore solvability is ensured if the following zero-order equilibration condition holds

$$\begin{aligned} &R_k^{\Pi}(1) + \sum_{\gamma \subset \partial\Omega_k \setminus \Gamma_N} \int_{\gamma} g_k \, d\Gamma \\ &\quad = \int_{\Omega_k} \Pi_k^{\hat{q}}(f - \kappa_k^2 u_h) d\Omega + \sum_{\gamma \subset \partial\Omega_k \cap \Gamma_N} \int_{\gamma} \Pi_{\gamma}^{\bar{q}} g_N \, d\Gamma + \sum_{\gamma \subset \partial\Omega_k \setminus \Gamma_N} \int_{\gamma} g_k \, d\Gamma = 0. \end{aligned} \tag{73}$$

Adding (71) for all the nodes of an element and using both the partition of unity of the shape functions and the consistency condition (70) yields the desired result. It is also worth noting that for $\kappa \neq 0$, equation (73) along with (72) for $v = 1$ imposes a non-necessary zero mean value condition for r_k, that is $\int_{\Omega_k} r_k d\Omega = 0$.

Remark 17. If the equilibrated tractions are set to be linear functions on the faces of the mesh, the consistency and first-order equilibration conditions, equations (70) and (71) respectively, do not uniquely determine the values of the tractions. In this case, it is standard to use the average of the tractions of the finite element approximation at the inter-element faces to uniquely determine the equilibrated tractions. A vast literature exists providing different approaches to compute the equilibrated tractions, but readers are here refereed to Ainsworth et al.[34] for a very clear and concise description in the 3D convection-reaction-diffusion setting.

Remark 18. Given the set equilibrated tractions $\{g_k\}$, the local error problems (72) do not uniquely determine the dual estimates $\boldsymbol{q}_k \in [\mathcal{V}(\Omega_k)]^3$ and $r_k \in \mathcal{V}(\Omega_k)$. Sauer-Budge et al.[20,21] propose to compute piecewise polynomial dual estimates $\boldsymbol{q} \in [\widehat{\mathbb{P}}^q(\Omega)]^3$ and $r \in \widehat{\mathbb{P}}^{q-1}(\Omega)$ minimizing the squared local complementary energy norm $\|\boldsymbol{q}_k\|_k^2 + \kappa_k^2 \|r_k\|_k^2$. Alternatively, Ainsworth et al.[29,34] propose to set $r_k = 0$ and find a closed piecewise polynomial explicit expression for $\boldsymbol{q}_k$. This second approach yields bounds which are not as accurate as the ones proposed by Sauer-Budge et al.[20,21] since no norm minimization is carried out and the reaction term is not taken into account, but it provides a cheaper strategy since it does not require solving any local residual problem.

This section shows that the new technique presented in the previous sections, provides a new methodology to obtain low-cost and efficient equilibrated tractions. Following the notations introduced by Ladevèze et al.[35] this new equilibrated technique would be classified as a new *element equilibrated + star patch technique (EESPT)*.

Indeed, let $\{g_{\gamma}^i\}_{i \in \mathcal{N}}$ be a set of local weighted tractions verifying equation (19) and the unified weighted projected equilibration condition (48) and consider the global tractions obtained by adding all the weighted contributions, namely

$$g_{\gamma} = \sum_{i \in \mathcal{N}(\gamma)} g_{\gamma}^i. \tag{74}$$

Note that both g_{γ}^i and g_{γ} are associated to the arbitrary but fixed unit normal direction $\boldsymbol{n}^{\gamma}$. Then, given an element Ω_k and one of its faces $\gamma \subset \partial\Omega_k$, one can define the tractions on face γ of element Ω_k to be

$$g_k\big|_{\gamma} = \sigma_k^{\gamma} g_{\gamma}. \tag{75}$$

The key point is that the set of tractions $\{g_k\}_{k=1,\dots,n_{\text{el}}}$ defined in (75) are equilibrated, that is, they are consistent (70) and for $\kappa = 0$ they verify the zero-order equilibration condition (73). Indeed, the first consistency condition in (70) holds since on $\gamma \subset \partial\Omega_k \cap \partial\Omega_{k'}$, $g_k + g_{k'} = (\sigma_k^{\gamma} + \sigma_{k'}^{\gamma}) g_{\gamma} = (\boldsymbol{n}_k^{\gamma} + \boldsymbol{n}_{k'}^{\gamma}) \cdot \boldsymbol{n}^{\gamma} g_{\gamma} = 0$. Also, if $\gamma \in \partial\Omega_k \cap \Gamma_N$ is a face in the Neumann boundary, since $\sigma_k^{\gamma} = 1$ and using equation (19b) and the partition of unity of the linear shape functions, it holds that

$$g_k\big|_{\gamma} = g_{\gamma} = \sum_{i=1}^{n_{\text{np}}} g_{\gamma}^i = \sum_{i=1}^{n_{\text{np}}} \phi_i \Pi_{\gamma}^{\bar{q}} g_N = \Pi_{\gamma}^{\bar{q}} g_N,$$

TABLE 3 Notations for the different computed estimates.

New Flux-free			Existing		
Estimate	Case	Reaction term	Estimate	Reference	Details
η_1^0	I	$r_k^i = 0$	η^{st}	Parés et al.[14]	flux-free with full minimization ($q = 3$) including a full quadratic reaction dual estimate r
η_1^c	I	$r_k^i = r_k^{i0}$	η^{eq}	Ainsworth et al.[34]	equilibrated with explicit local solution ($q = 2$) with no reaction dual estimate $r = 0$
η_1	I	$r_k^i = \phi_i r_k^{i1} + r_k^{i0}$			
η_2^0	II	$r_k^i = 0$			
η_2^c	II	$r_k^i = r_k^{i0}$			
η_2	II	$r_k^i = \phi_i r_k^{iL} + r_k^{i0}$			
η_3^0	III	$r_k^i = 0$			

which ensures the second consistency condition in (70). Finally, for a given element Ω_k, adding (48) for $i \subset \mathcal{N}(\Omega_k)$ and using the partition of unity property of the shape functions yields

$$\begin{aligned}\sum_{i\subset\mathcal{N}(\Omega_k)} \int_{\Omega_k} \left[\phi_i \Pi_k^{\hat{q}}(f - \kappa_k^2 u_h) - \boldsymbol{\nabla} u_h \cdot \boldsymbol{\nabla}\phi_i - \kappa_k^2 r_k^i\right] d\Omega + \sum_{i\subset\mathcal{N}(\Omega_k)} \sum_{\gamma\subset\partial\Omega_k} \int_\gamma \sigma_k^\gamma g_\gamma^i \, d\Gamma \\ = \int_{\Omega_k} \left[\Pi_k^{\hat{q}}(f - \kappa_k^2 u_h) - \kappa_k^2 r_k\right] d\Omega + \sum_{\gamma\subset\partial\Omega_k} \int_\gamma g_k \, d\Gamma = 0,\end{aligned} \tag{76}$$

since for a face $\gamma \subset \partial\Omega_k$, $\mathcal{N}(\gamma) \subset \mathcal{N}(\Omega_k)$. Then, for $\kappa = 0$ and using the consistency of g_k in the Neumann boundaries, equation (76) coincides with the zero-order equilibration condition (73).

Remark 19. In the case $\kappa \neq 0$, equation (76) coincides with (72) with $\upsilon = 1$. Therefore the inclusion of the reaction term $\kappa_k^2 r_k^i$ in (48) (compare equations (48) and (71)) allows avoiding the additional condition on the reaction term r_k, while retaining the same equilibration condition for $\kappa = 0$.

6 NUMERICAL EXAMPLES

The behavior of the new flux-free equilibrated strategy presented above is analyzed in three numerical examples. Table 3 shows the notations for the various estimates compared herein, comprising all the possible different cases for the estimate given in Section 4 and also introducing some existing equilibrated error estimates.

It is worth noting that by construction it is expected that

$$\eta^{\text{st}} \leq \eta_3^0 \leq \eta_2^0 \leq \eta_1^0 \quad , \quad \eta^{\text{st}} \leq \eta_2 \leq \eta_1 \quad \text{and} \quad \eta^{\text{st}} \leq \eta_2^c \leq \eta_1^c. \tag{77}$$

These properties cannot be guaranteed since the estimates are constructed minimizing the squared norm of the dual estimates $\boldsymbol{q}_k^i$ and r_k^i in each star, whereas the global upper bound is computed by first adding the estimates $\boldsymbol{q}_k^i$ and r_k^i and then computing its squared norm, but they hold in most numerical examples showing that, as the computational cost is reduced, the bounds are usually less accurate. However, as shown in the following numerical examples, the difference in quality when reducing the computational cost is not very significant and therefore, the cheapest strategies are recommended.

In the examples where the analytical solution is known, the quality of the error estimates is measured using the standard effectivity index

$$\rho^* = \eta^* / |||e|||.$$

All the previous estimates provide local error information which can be used as an indicator for mesh adaptivity. Indeed the new flux-free estimates η^2 can be decoupled using the local elemental contributions η_k given in (7) as

$$\eta^2 = \sum_{k=1}^{n_{\text{el}}} \eta_k^2.$$

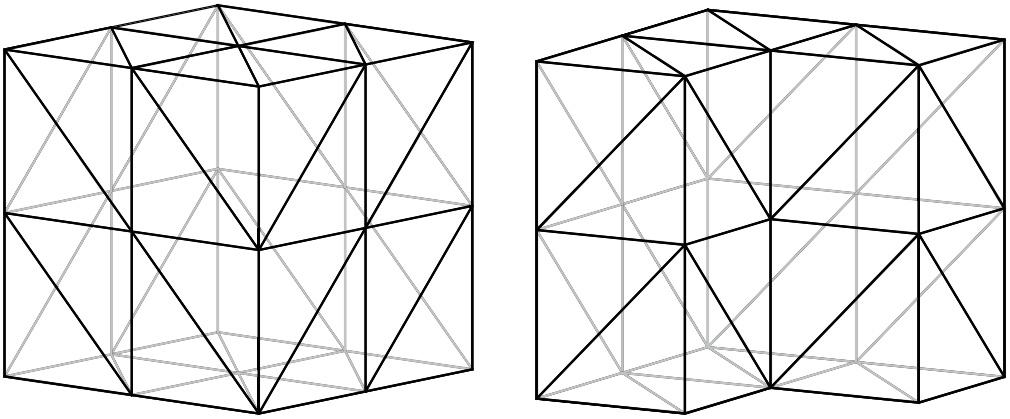

FIGURE 5 Initial mesh composed of 48 tetrahedra (left) and mesh with cut (right).

Then, the elemental contributions η_k^2 can serve as informative mesh adaptivity indicators for controlling the error in the energy norm. Note that these indicators also take into account the data oscillation errors, and therefore, the mesh is refined both in the areas most contributing to the error and in the areas where the data cannot be properly represented using its linear/constant projection.

The simulations are implemented using the MATLAB software package iFEM[36]. In some examples where the 3D longest edge bisection algorithm provided in the previous package is not able to adapt the mesh, the adaptive refinement of the meshes is done using a non-recursive version of the algorithm[37].

6.1 Poisson's equation with variable source term

The purpose of this example[38] is to both analyze the behavior of the bounds and the effect of data oscillation. Consider a diffusion problem with $\kappa = 0$ in equation (1), in the cubic domain $\Omega = (-1, 1)^3$, where the right-hand side f is such that the exact solution of the problem is

$$u(x, y, z) = e^{-10(x^2+y^2+z^2)}.$$

The boundary conditions are all Dirichlet, that is, $\Gamma_D = \partial\Omega$. Note that even though the solution is not exactly zero in the boundary of the cube, $u_D = e^{-30}$, and therefore the Dirichlet boundary conditions can be considered to be homogeneous. Thus, we will consider that there is no data error due to the interpolation of the Dirichlet boundary conditions, and therefore the upper bounds are going to be guaranteed upper bounds for the exact error. Note that $f = -\Delta u$ exhibits a large variation in Ω with oscillation within elements which forces the adaptive algorithm to refine elements due to data oscillation. It is worth noting that in this case we can only consider the new flux-free estimates η_2^0 and η_3^0, since the source term is not piecewise constant and no reaction term is present in the problem.

First the convergence of the error estimates is analyzed for a uniform mesh refinement in a series of structured meshes. The initial mesh is composed of 48 tetrahedra and in each refinement step every tetrahedron is divided into 8 similar tetrahedra (see Figure 5). The results can be found in Table 4. The results confirm that, as shown in previous literature[11,13,14,15,12], the flux-free strategies are really competitive in terms of accuracy with respect to the equilibrated strategies, since the effectivities ρ^{st} are much more closer to one than ρ^{eq}. The results also show that if the value of the error estimates is mainly given by the data oscillation error terms (two first meshes) the effectivities of both the flux-free estimates and equilibrated estimates are similar in both cases and far from one. However, when the finite element mesh properly describes the source term, the quality of the flux-free error estimates is clearly superior to the equilibrated estimates.

The predominance of the data oscillation errors in the error estimates in the first meshes is shown in Figure 6. The separate contributions to the local squared error estimate $(\eta_2^0)_k^2$ of the elements with larger error and contributing to the 90% of the error is shown in a stacked bar plot. Note that since the problem is a pure diffusion problem with no Neumann boundary conditions, the local squared contributions of η_k^2 given in equation (7) are

$$\eta_k^2 = \left[\|\boldsymbol{q}\|_k + \text{osc}_k(f)\right]^2 = \|\boldsymbol{q}\|_k^2 + (\text{osc}_k(f))^2 + 2\|\boldsymbol{q}\|_k \text{osc}_k(f). \tag{78}$$

n_{el}	$\|\|\|u_h\|\|\|$	$\|\|\|e\|\|\|$	flux-free η^{st}	flux-free η_3^0	flux-free η_2^0	equilibrated η^{eq}
48	0.56407	1.24479	5.31603	5.37791	5.38936	5.61466
384	0.98403	0.94835	2.10283	2.13369	2.13768	2.27058
3072	1.24335	0.56723	0.65742	0.66622	0.66929	1.01969
24576	1.31492	0.37237	0.40272	0.40514	0.40568	0.67717
196608	1.35355	0.18859	0.19856	0.19968	0.19965	0.33654
			ρ^{st}	ρ_3^0	ρ_2^0	ρ^{eq}
48			4.27063	4.32034	4.32954	4.51054
384			2.21737	2.24991	2.25411	2.39426
3072			1.15899	1.17451	1.17992	1.79766
24576			1.08151	1.08803	1.08947	1.81855
196608			1.05283	1.05877	1.05860	1.78448

TABLE 4 Example 1: upper bounds for the error in the energy norm and its effectivities in a series of uniformly h-refined linear tetrahedral meshes.

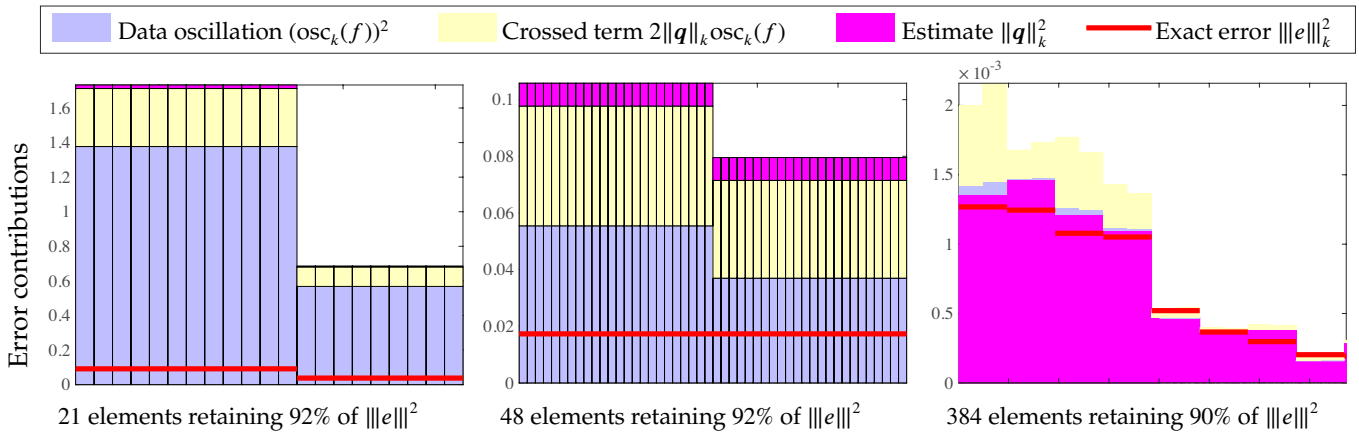

FIGURE 6 Example 1: Stacked bar plot of the contributions to the local squared total estimate $(\eta_2^0)_k^2$ of the elements with larger error for the three first meshes of 48 (left), 384 (middle) and 3072 (right) elements.

The total contributions of the error estimate η_2^0 can be seen in Table 5. As can be appreciated both in Figure 6 and in Table 5, the error estimate for the two first meshes is governed by the data oscillation error contributions resulting in a bad quality estimate η_2^0. This quality is improved in the third mesh where the data oscillation errors only affect a 22% of the error estimate. Once the error coming from the projection of the source term is not relevant, the effectivities of the flux-free estimates get really close to one while the effectivities of the equilibrated strategy are close to 1.7.

n_{el}	η_2^0	$\sum_k \|\boldsymbol{q}\|_k^2$	$\sum_k (\text{osc}_k(f))^2$	$\sum_k 2\|\boldsymbol{q}\|_k \text{osc}_k(f)$	$\sum_k \|\boldsymbol{q}\|_k^2 \%$
48	29.04517	0.31415	23.34769	5.38333	1.08%
384	4.56968	0.47346	2.22114	1.87508	10.36%
3072	0.44795	0.35104	0.00756	0.08934	78.36%
24576	0.16458	0.15131	0.00036	0.01290	91.94%

TABLE 5 Example 1: Contributions to the squared estimate $(\eta_2^0)^2$ of the data oscillation terms.

As seen by Parés and Díez[1] for the two dimensional setting, alleviating the cost of the flux-free strategy by either using η_2^0 or η_3^0 instead of η^{st} does not significantly modify the value of the effectivities. As expected, introducing

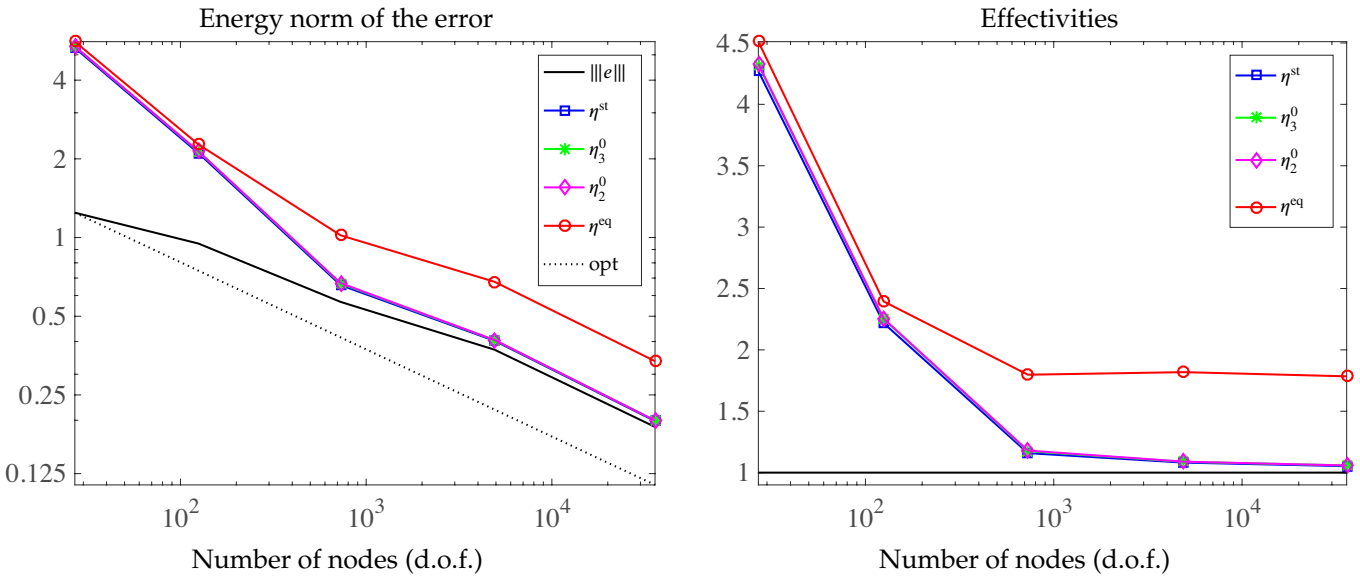

FIGURE 7 Example 1: Convergence of the upper bounds (left) and its effectivities (right) in a uniform h-refinement. The optimal decay is indicated (left) by the line with slope $-1/3$.

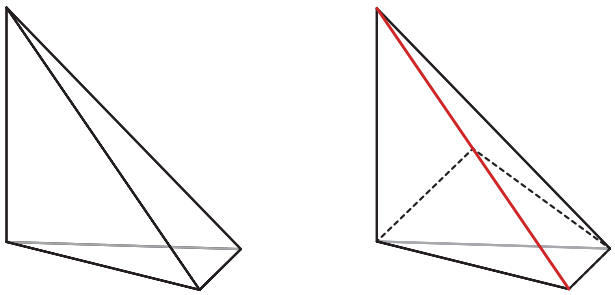

FIGURE 8 Example 1: Longest edge tetrahedron refinement for the adaptive strategy.

quadratic tractions in ρ^q provides closer results to the third order tractions implicitly computed in ρ^{st}. However, since the difference in accuracy when using linear (η_2^0) or quadratic (η_3^0) tractions is really small, it is preferable to use linear tractions which is much cheaper. Also, it is clear that the new strategy to compute the linear equilibrated tractions in the faces of the mesh (ρ_2^0) is more competitive than the standard equilibrated one (ρ^{eq}), because a much better accuracy is achieved without a significant increase in the computational cost.

Finally, Figure 7 shows the convergence of the bounds and its effectivity indices. As can be appreciated the expected optimal convergence rate of $|||e||| \propto n_{\mathrm{np}}^{-1/3}$ is achieved.

The behavior of the bounds is also analyzed for an adaptive mesh refinement. The meshes are adaptively refined using a bulk criterion[39]. In particular, the set of elements marked for refinement, denoted by $\mathcal{T}_{50\%}$, is the one which has the smallest number of elements verifying that the sum of the contributions toward the estimator from these elements exceeds 50% of the value of the estimator, namely

$$\sum_{\Omega_k \subset \mathcal{T}_{50\%}} \eta_k^2 \geq 0.5\eta^2.$$

The marked elements of the mesh are subdivided into two new ones by bisecting the longest edge of each specified tetrahedron as can be shown in Figure 8.

Figure 9 shows the results obtained using as guiding error indicators both the contributions of η_2^0 and η_3^0. As can be seen both adaptive procedures achieve the optimal rate of convergence and yield practically equal results, confirming that in this case there is no need to use the more expensive approach given by η_3^0.

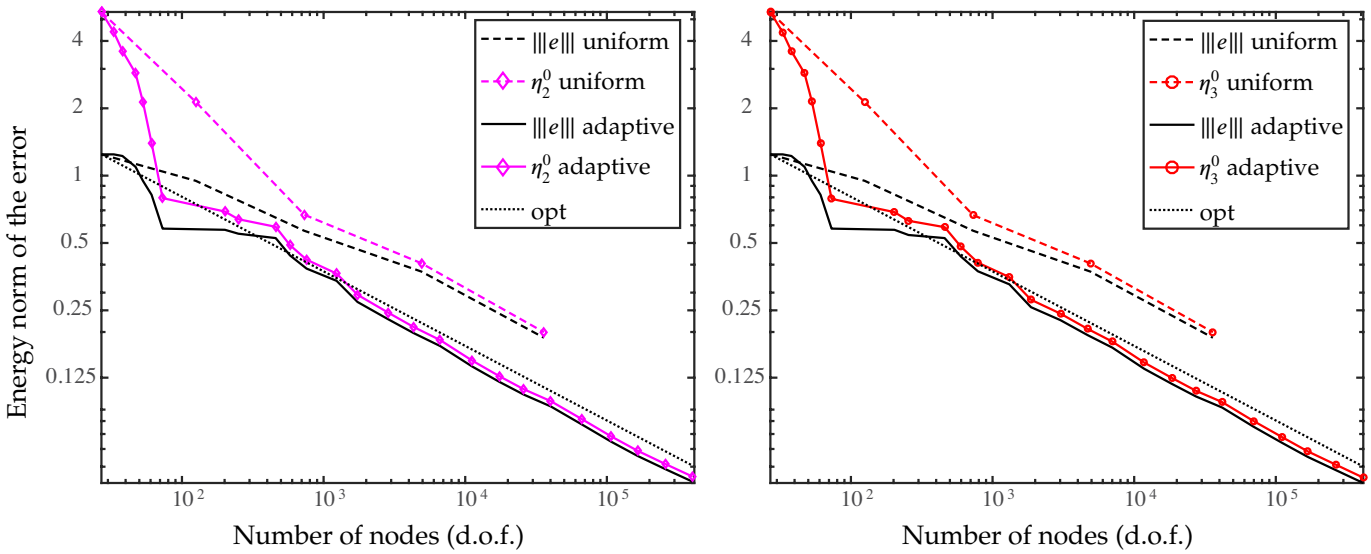

FIGURE 9 Example 1: Convergence of the upper bounds in an adaptive h-refinement, guided by the local error indicators associated to η_2^0 (left) and η_3^0 (right). The optimal decay is given by the $-1/3$ slope line.

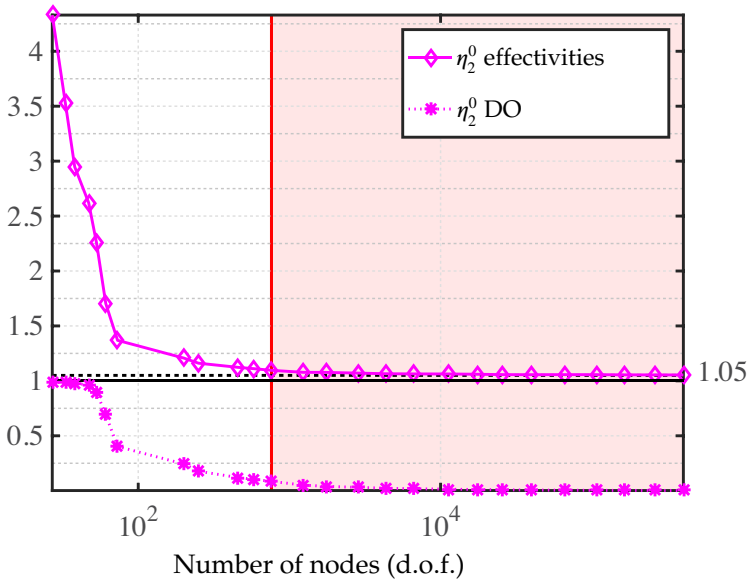

FIGURE 10 Example 1: Effectivities of the upper bounds η_2^0 in an adaptive h-refinement and influence of the data oscillation errors in the final error estimate. The red region indicates that DO $< 10\%$.

Figure 10 shows the effectivities associated to the error estimate η_2^0 along with the influence of the data oscillation in the error estimate, measured using the index DO $= (\eta_2^0 - (\sum_k \|q\|_k^2))/\eta_2^0$. It is worth noting that the DO index includes the two terms of the error decomposition given in (78) containing errors associated to the source term. That is, for a zero data oscillation error DO $= 0$ while DO $= 1$ means that all the error come from errors due to the source term. As in the uniform mesh refinement procedure, in the initial meshes the data oscillation errors are dominant and the error estimate is not very accurate. However, as the adaptive procedure advances, it refines the regions where the source term f exhibits larger variations and the effectivity indices tend to 1.05. Indeed, after only 11 refinements a mesh with only 758 nodes and 3966 elements is obtained for which $\rho_2^0 = 1.09$ and DO $= 8.5\%$. The value $\rho = 1.05$ has been highlighted in the figure since this value is representative of the effectivities in most of the final meshes.

FIGURE 11 Example 1: Adaptive meshes for the 10th (left) and 24th (middle) iterations with 2880 and 1478844 elements and zoom into the 24th mesh (right).

Finally, two intermediate meshes obtained in the adaptive procedure for the estimate η_2^0 are shown in Figure 11. The error estimate for the initial mesh is $\eta_2^0 = 5.3896$, an the meshes to be shown are selected such that its error estimate is approximately 10% and 1% of the initial error, that is $(\eta_0^2)_{\text{iter}10} = 0.48891$ and $(\eta_0^2)_{\text{iter}24} = 0.0513$. As can be seen, the adaptive procedure refines just the areas with a larger gradient of the source term, that is, the region around the center of the cube.

6.2 Building - Poisson's equation with no data oscillation errors

The second example is a pure diffusion problem with no source term $f = 0$ and constant boundary conditions[34]. The purpose of this example is to compare the performance of the explicit error estimates presented in this work with the explicit equilibrated error estimate given by Ainsworth et al.[34]. The domain and boundary conditions are shown in Figure 12 (where the symmetric splitting of the domain is marked using the red dashed line). Homogeneous Neumann boundary conditions are applied at the faces $z = 0$, $y = 20$ and $x = 5$ (symmetry condition) and on the remaining boundaries homogeneous Dirichlet boundary conditions are applied except on the building faces where $u_{\text{D}} = 1$.

The behavior of the error estimates is analyzed in an adaptive mesh refinement. Two initial meshes are considered: a very coarse initial mesh of 41 nodes and 86 tetrahedra and a finer initial mesh of 4826 nodes and 23900 tetrahedra both shown in Figure 13. The adaptive algorithm marks for refinement the elements verifying[34]

$$\eta_k \geq \frac{1}{2} \max_{k=1,\ldots,n_{\text{el}}} \{\eta_k\}. \tag{79}$$

In this example, the non-recursive version of the 3D longest edge bisection algorithm[37] is used to adapt the meshes.

Figure 14 shows the convergence of the error bounds for the two available flux-free error estimates $\eta_1^0 = \eta_2^0$ and η_3^0 starting with the two different initial meshes along with the results for the equilibrated estimate η^{eq} given by Ainsworth et al.[34]. Note that if no reaction term is present in the problem and the source term is zero, then from equations (25) and (32) $\boldsymbol{q}_k^i = \boldsymbol{q}_k^{iL}$ which yields $\eta_1^0 = \eta_2^0$.

It can be seen that all estimates decay with the optimal rate and that the new flux-free estimates are more accurate than the equilibrated one. Also as seen in the previous example, the results for $\eta_1^0 = \eta_2^0$ and η_3^0 are very close and therefore there is no gain in using quadratic tractions instead of linear.

Finally, Figure 15 shows the final mesh composed of 63963 nodes and 3396285 tetrahedra over the faces of the building obtained using the estimate $\eta_1^0 = \eta_2^0$ starting with the finer initial mesh of 4826 nodes and Figure 16 shows several section views of the mesh with fixed values in the variable y ($y \geq 3, y \geq 4, y \geq 5, y \geq 10, y \geq 15$ and $y \geq 18$). As seen by Ainsworth et al.[34] the refinement mainly takes place on the re-entrant edges.

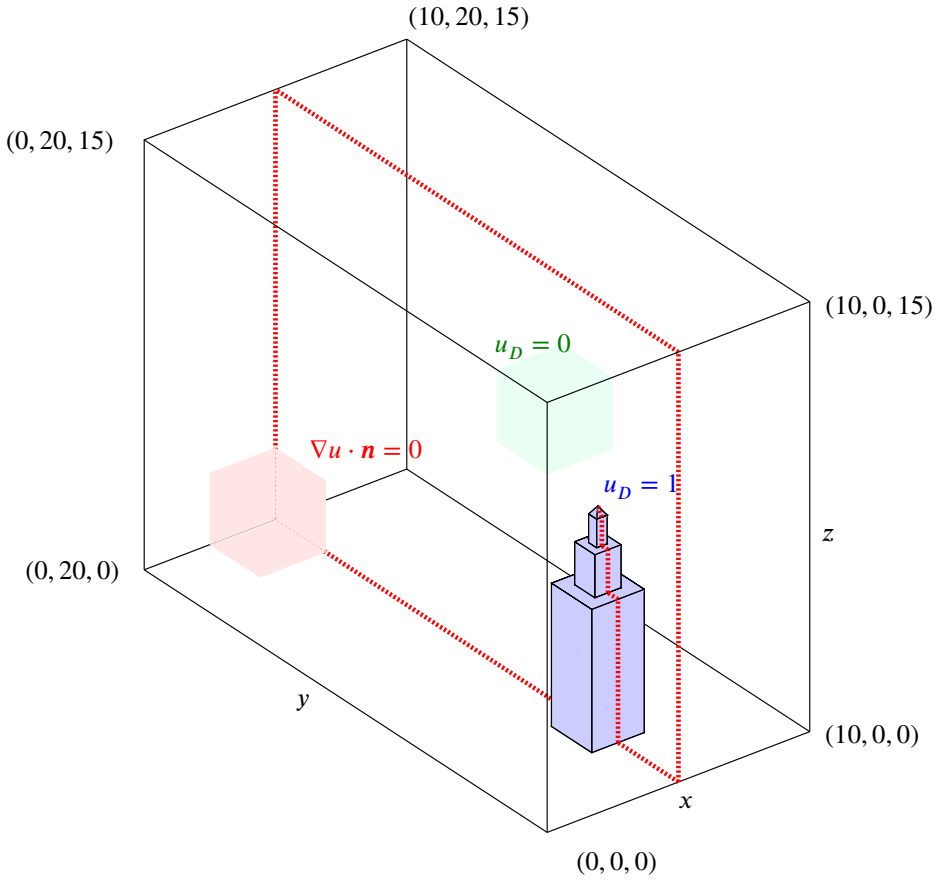

Building vertices

4	3	0	5	3	0
5	5	0	4	5	0
4	3	5	5	3	5
5	5	5	4	5	5
4.5	3.5	5	5	3.5	5
5	4.5	5	4.5	4.5	5
4.5	3.5	6.5	5	3.5	6.5
5	4.5	6.5	4.5	4.5	6.5
4.8	3.8	6.5	5	3.8	6.5
5	4.2	6.5	4.8	4.2	6.5
4.8	3.8	7.5	5	3.8	7.5
5	4.2	7.5	4.8	4.2	7.5
5	4	7.8			

FIGURE 12 Example 2: Domain geometry and boundary conditions. Neumann faces marked in red (planes $z = 0$, $y = 20$ and $x = 5$), homogeneous Dirichlet boundary conditions marked in green (planes $x = 0$, $y = 0$ and $z = 15$) and non-homogeneous Dirichlet boundary conditions marked in blue (building faces).

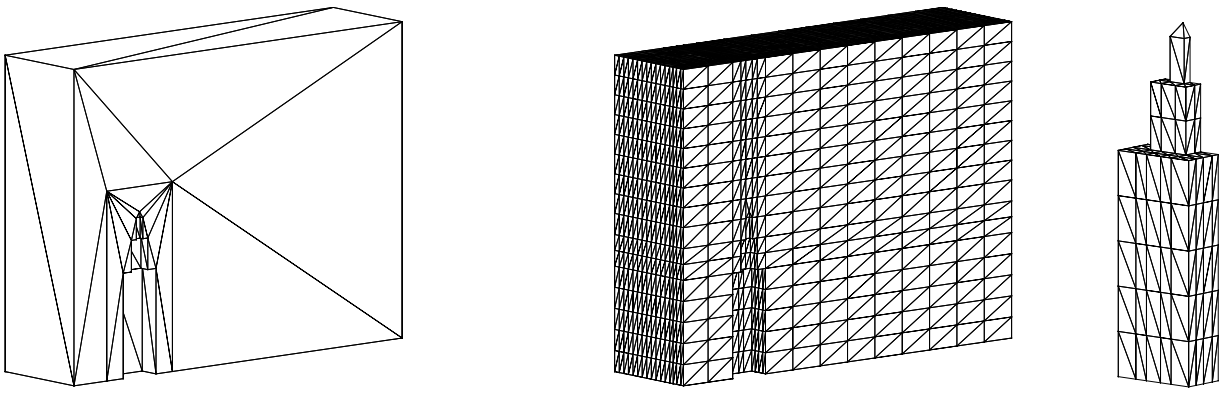

FIGURE 13 Example 2: Coarse initial mesh (left) and finer full initial mesh of the adaptive procedure (middle) and its building surface mesh (right).

6.3 Reaction-diffusion problem with analytical solution

This example illustrates the performance of the a posteriori error estimators for a reaction-diffusion problem with a discontinuous piecewise-constant reaction coefficient[29]. Consider the reaction-diffusion problem given in equation

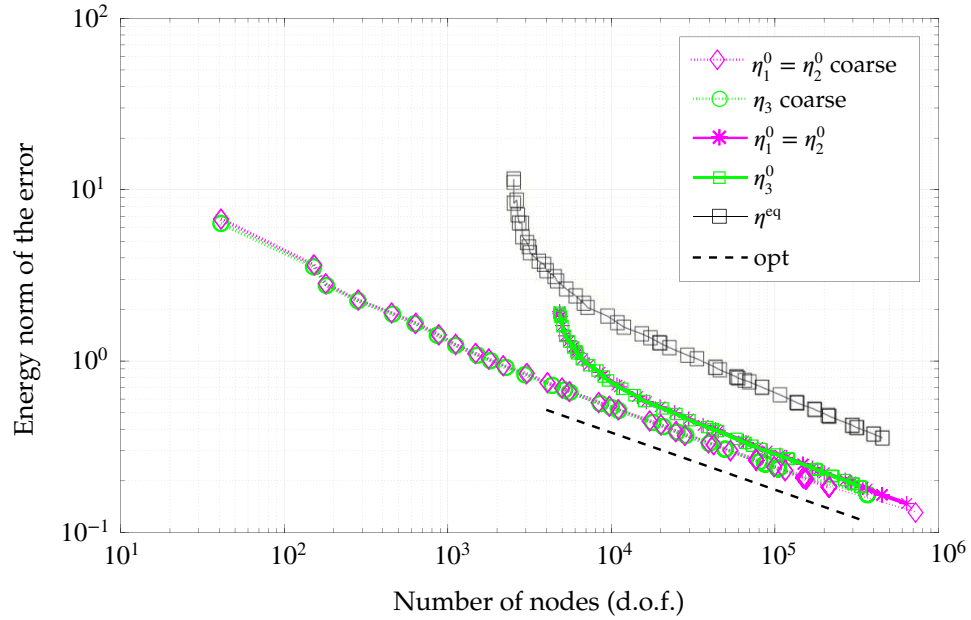

FIGURE 14 Example 2: Convergence of the new flux-free upper bounds in an adaptive *h*-refinement along with the equilibrated bounds given by Ainsworth et al.[34].

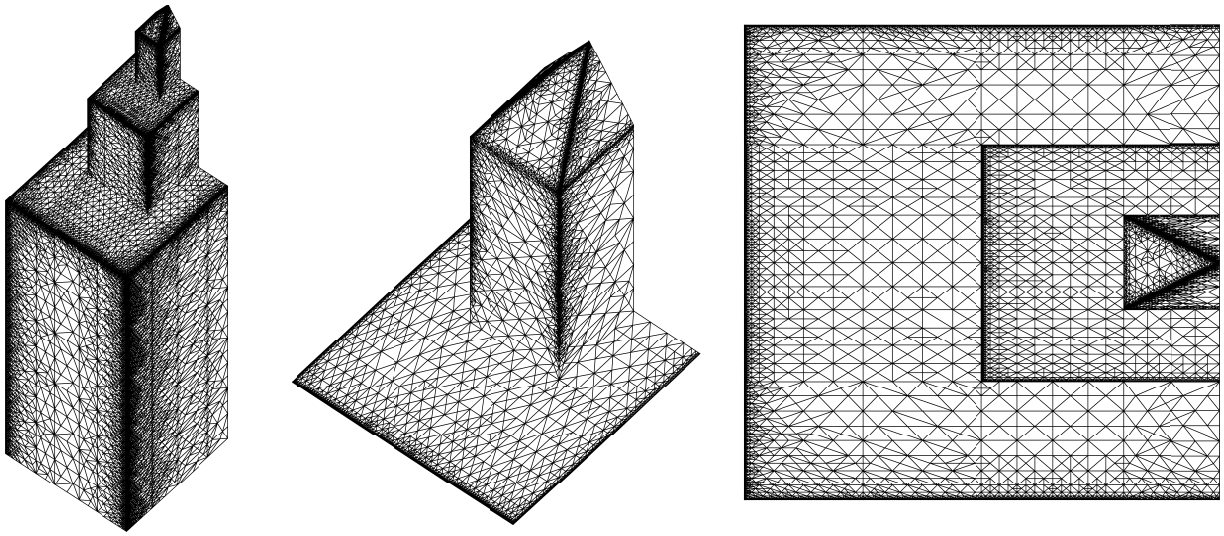

FIGURE 15 Example 2: Final mesh of the adaptive procedure starting with the finer initial mesh of 4826 nodes for the estimate $\eta_1^0 = \eta_2^0$: mesh over the building.

(1) in the cubic domain $\Omega = (-1, 1)^3$ with the piecewise-constant coefficient κ given by

$$\kappa(x, y, z) = \begin{cases} \kappa_1 \ , \ x < 0 \\ \kappa_2 \ , \ x \geq 0 \end{cases}$$

where $\kappa_2 \geq \kappa_1 > 0$ are constants and for $f = \kappa_1^2$. Homogeneous Dirichlet boundary conditions are imposed on $\Gamma_D = \{x = \pm 1\}$, that is, $u(1, y, z) = u(-1, y, z) = 0$, and homogeneous Neumann boundary conditions are prescribed elsewhere. The exact solution has a univariate nature and is given by

$$u(x, y, z) = \begin{cases} A_1 e^{-\kappa_1 x} + A_2 e^{\kappa_1 x} + 1 & , \ x < 0 \\ A_3 e^{-\kappa_2 x} + A_4 e^{\kappa_2 x} + \kappa_1^2/\kappa_2^2 \ , \ x \geq 0, \end{cases}$$

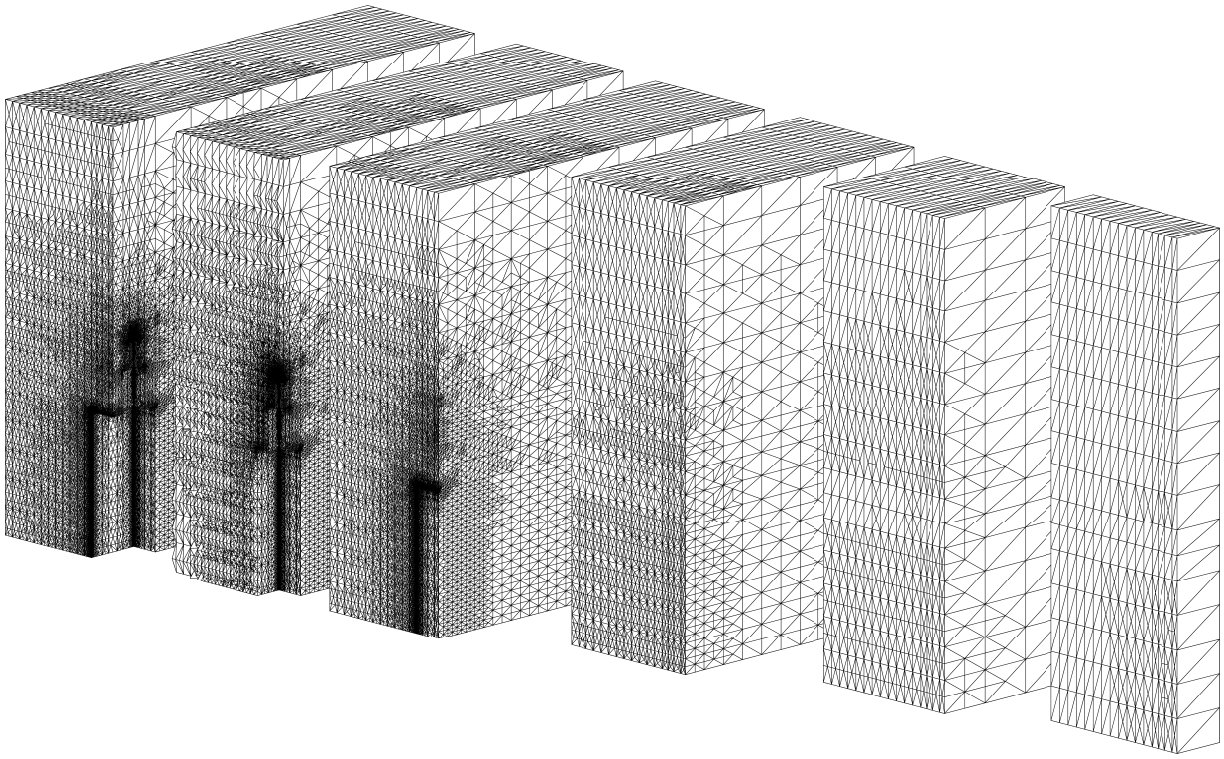

FIGURE 16 Example 2: Final mesh of the adaptive procedure starting with the finer initial mesh of 4826 nodes for the estimate $\eta_1^0 = \eta_2^0$: section views of the mesh for $y \geq 3$, $y \geq 4$, $y \geq 5$, $y \geq 10$, $y \geq 15$ and $y \geq 18$.

where the constants A_1, A_2, A_3 and A_4 are uniquely determined by the Dirichlet boundary conditions and the $\mathcal{C}^1$ continuity requirements of $u(x, y, z)$ on $x = 0$. Several solutions are plotted in Figure 17 for different values of the parameters κ_1 and κ_2 (the univariate solutions $u(x) = u(x, y, z)$ are shown).

Table 6 shows the results for a fixed regular mesh of 4913 nodes and 24576 tetrahedra (composed of 16^3 cubes subdivided into 6 tetrahedra each) for the values of κ_1 and κ_2 shown in Figure 17. It is worth noting that since the reaction term is not zero and the finite element approximation u_h is linear, $f - \kappa_k^2 u_h \neq \Pi_k^0(f - \kappa_k^2 u_h)$. Therefore, the estimate η_1^0 cannot be used and the estimates η_1^c and η_1 contain data oscillation terms. The results show that the original implicit flux-free estimate η^{st} provides very good results (with effectivities really close to 1) for all the considered values even for large values of the reaction coefficients. Also note that the data oscillation errors worsen the quality of the estimates associated to Case I (η_1 and η_1^c) and therefore it is preferable to consider the estimates associated to Case II (the tractions are linear in both cases and thus the computational cost is similar). As expected, the effectivity indices of the estimates containing a better representation of the reaction term are smaller than those having simpler or no-reaction estimates at all, that is $\rho_1 \leq \rho_1^c$ and $\rho_2 \leq \rho_2^c \leq \rho_2^0$. In particular ρ_2 provides very good results similar to η^{st} in all cases. It can also be observed that for highly reaction dominated problems the accuracy of the estimates associated to $r = 0$ (η_2^0 and η_3^0) may degenerate. Therefore when reaction is dominant robust estimates are only obtained when reaction terms are included in the expression for the estimates. Finally, as in the previous examples, the accuracy of η_2^0 and η_3^0 is very similar and therefore quadratic tractions should only be used in the elements having solvability issues.

Finally the behavior of the true error and the upper bounds is shown for a series of adapted meshes starting with a uniform regular mesh of 48 tetrahedra. The mesh is refined using the criteria given in equation (79) for the estimate η_2 (in this example, if the estimate η_1 is used for guiding the adaptive procedure the same meshes are obtained). For each mesh all the new explicit flux-free estimates are computed. The upper bounds and its effectivities are shown in Figure 18. As in the results shown in Table 6, when dealing with reaction-dominated problems it is advisable to use a full reaction term in the estimates (η_2). It is worth noting that the accuracy of η_2 is very good since its associated effectivity indices is close to 1.05 for all the meshes. However, it can also be seen that as the mesh is adaptively refined, the accuracy of the estimates with a simplified reaction term or no reaction term at all ($\eta_2^c, \eta_2^0, \eta_3^0$) improves and its effectivity indices are close to one. Again, using quadratic tractions (η_3^0) instead of linear (η_2^0)

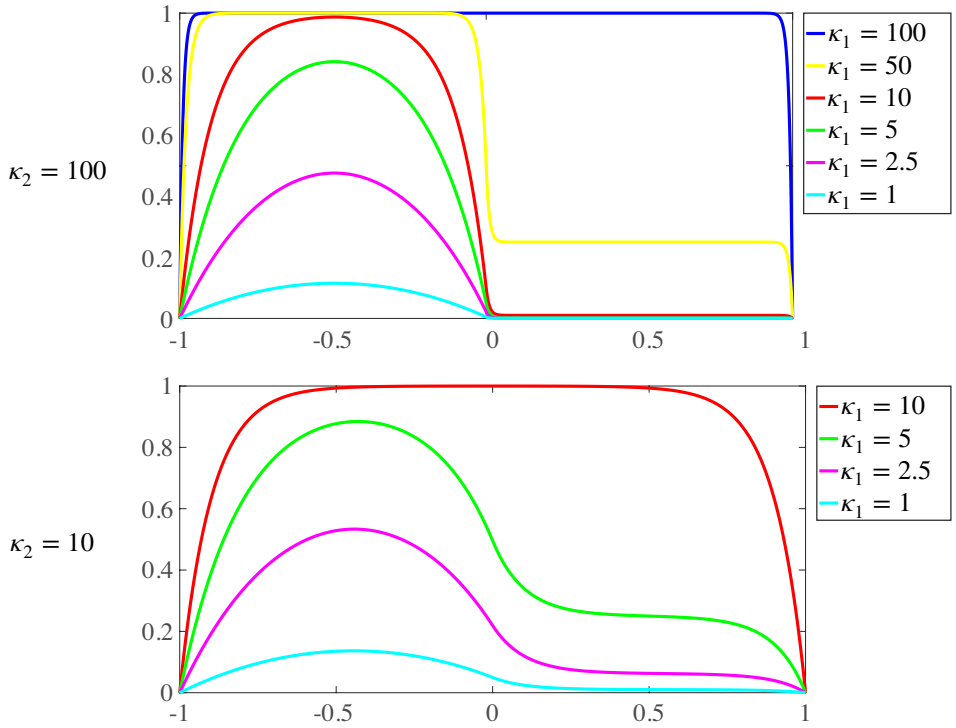

FIGURE 17 Example 3: Exact solution for different values of κ_1 and κ_2 (univariate view).

	κ_1	$\|\|\|e\|\|\|$	ρ^{st}	ρ_1	ρ_1^c	ρ_2	ρ_2^c	ρ_2^0	ρ_3^0
$\kappa_2 = 10$	1	0.09039557	1.061	1.333	1.334	1.068	1.076	1.102	1.100
	2.5	0.38187968	1.064	1.348	1.349	1.070	1.078	1.108	1.105
	5	0.85020487	1.065	1.398	1.399	1.069	1.078	1.114	1.111
	10	2.23964827	1.056	1.534	1.535	1.068	1.083	1.140	1.136
	κ_1	$\|\|\|e\|\|\|$	ρ^{st}	ρ_1	ρ_1^c	ρ_2	ρ_2^c	ρ_2^0	ρ_3^0
$\kappa_2 = 100$	1	0.10282749	1.063	1.523	1.617	1.162	1.352	1.648	1.622
	2.5	0.47334587	1.067	1.535	1.625	1.165	1.351	1.658	1.632
	5	1.15620255	1.072	1.549	1.622	1.158	1.322	1.651	1.625
	10	2.73199220	1.068	1.617	1.657	1.131	1.252	1.639	1.615
	50	19.59051014	1.013	1.531	1.552	1.059	1.317	2.649	2.602
	100	46.66672399	1.018	1.458	1.509	1.056	1.551	3.699	3.629

TABLE 6 Example 3: Effectivities of the upper bounds for the error in the energy norm for a fixed regular mesh of 4913 nodes.

does not significantly increase the quality of the bounds and therefore quadratic tractions are only advisable when solvability issues arise. Finally, it can also be seen that in this case including the reaction term in the data oscillation errors (η_1) yields worst results. Note that the only advantage of Case I estimates versus Case II estimates is that a quadratic interpolation for $\boldsymbol{q}_k^i$ and r_k^i is used instead of a cubic one since the tractions (determining the size of the linear system of equations to be solved) are linear in both cases.

Finally, the initial, final and an intermediate mesh of the adaptive procedure are shown in Figure 19.

7 CONCLUDING REMARKS

A three-dimensional extension of the new technique to compute guaranteed upper bounds for the energy norm of the error presented by Parés and Díez[1] has been introduced. The bounds are guaranteed regardless of the size of

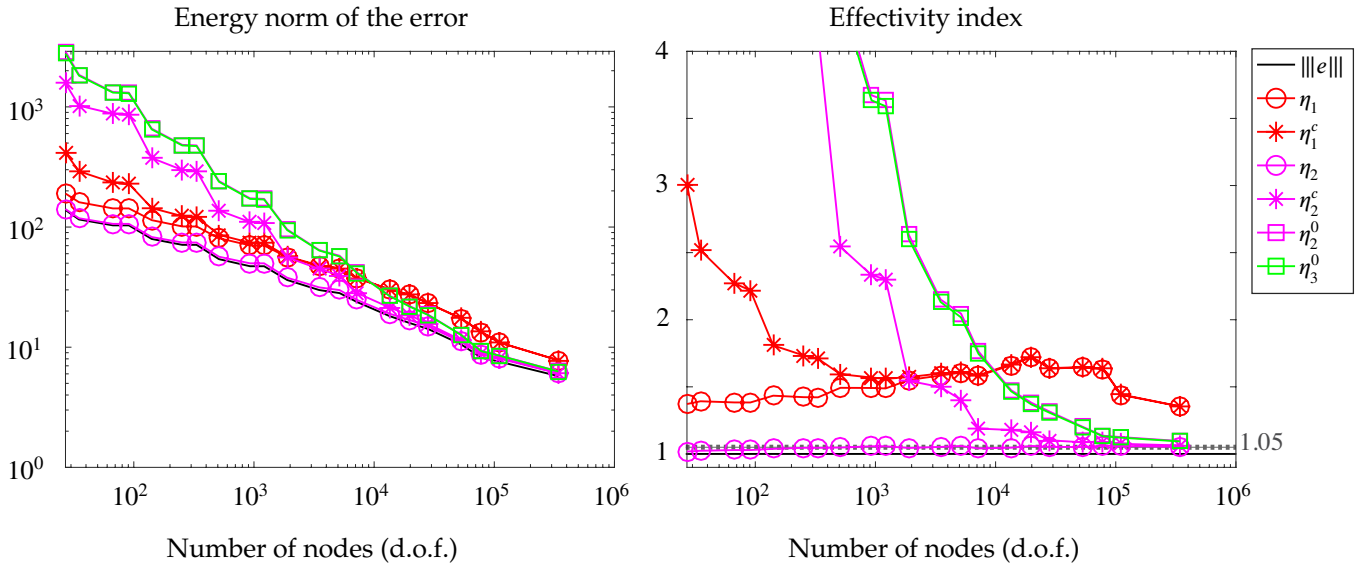

FIGURE 18 Example 3: Convergence of the new flux-free upper bounds in an adaptive *h*-refinement (left) and its effectivities (right).

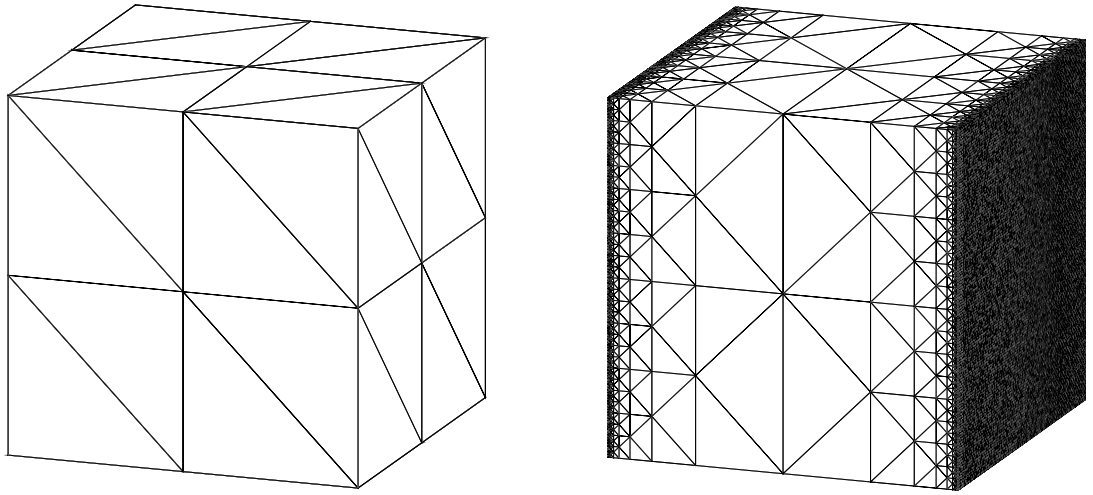

FIGURE 19 Example 3: Meshes obtained in the adaptive procedure for $\kappa_1 = \kappa_2 = 100$: initial mesh (27 nodes) and intermediate mes (77991 nodes).

the underlying finite element mesh and regardless of the kind of data (the source term and the Neumann boundary conditions are not required to be piecewise polynomial functions). This extension incorporates two novelties with respect to the two-dimensional approach: 1) the reaction term is included in the data oscillation terms so that a simplified estimate can be considered (estimates presented in Case I) and 2) the estimates incorporate a reaction term yielding estimates robust for all values of the reaction coefficient.

As in the two-dimensional case, the proposed strategy may be seen as either: (1) an improved *low-cost* version of the flux-free technique[13,14] or (2) a new more *efficient* hybrid-flux equilibrated residual method.

The new approach significantly alleviates the cost of the flux-free approach introducing only a slight difference on the accuracy of the estimates (assuming the proper version of the estimate is selected to properly deal with data oscillation errors and reaction dominated problems). It is also confirmed that the equilibrated tractions provided by the new approach yield much sharper bounds than the original equilibrated strategies. Therefore, the proposed strategy is clearly competitive to obtain guaranteed upper bounds for the error (both in accuracy and cost).

References

1. Parés N, Díez P. A new equilibrated residual method improving accuracy and efficiency of flux-free error estimates. *Comput. Methods Appl. Mech. Engrg.* 2017; 313: 785–816. doi: 10.1016/j.cma.2016.10.010

2. Díez P, Parés N, Huerta A. *Error Estimation and Quality Control*. 3(15). ch. 144: 1725–1734; John Wiley & Sons, New York . 2010

3. Chamoin L, Díez P. , eds.*Verifying calculations—forty years on*. Springer Briefs in Applied Sciences and Technology Springer, Cham . 2016. An overview of classical verification techniques for FEM simulations

4. Ainsworth M. A framework for obtaining guaranteed error bounds for finite element approximations. *J. Comput. Appl. Math.* 2010; 234(9): 2618–2632. doi: 10.1016/j.cam.2010.01.037

5. Pled F, Chamoin L, Ladevèze P. An enhanced method with local energy minimization for the robust a posteriori construction of equilibrated stress fields in finite element analyses. *Comput. Mech.* 2012; 49(3): 357–378. doi: 10.1007/s00466-011-0645-y

6. Choi HW, Paraschivoiu M. Adaptive computations of a posteriori finite element output bounds: a comparison of the "hybrid-flux" approach and the "flux-free" approach. *Comput. Methods Appl. Mech. Engrg.* 2004; 193(36–38): 4001–4033. doi: 10.1016/j.cma.2004.02.012

7. Carstensen C, Merdon C. Effective postprocessing for equilibration a posteriori error estimators. *Numer. Math.* 2013; 123(3): 425–459. doi: 10.1007/s00211-012-0494-4

8. Carstensen C, Merdon C. Estimator competition for Poisson problems. *J. Comput. Math.* 2010; 28(3): 309–330. doi: 10.4208/jcm.2009.10-m1010

9. Pled F, Chamoin L, Ladevèze P. On the techniques for constructing admissible stress fields in model verification: Performances on engineering examples. *International Journal for Numerical Methods in Engineering* 2011; 88(5): 409–441. doi: 10.1002/nme.3180

10. Parret-Fréaud A, Rey V, Gosselet P, Rey C. Improved recovery of admissible stress in domain decomposition methods—application to heterogeneous structures and new error bounds for FETI-DP. *Internat. J. Numer. Methods Engrg.* 2017; 111(1): 69–87. doi: 10.1002/nme.5462

11. Parés N, Díez P, Huerta A. Subdomain-based flux-free a posteriori error estimators. *Comput. Methods Appl. Mech. Engrg.* 2006; 195(4-6): 297–323. doi: 10.1016/j.cma.2004.06.047

12. Cottereau R, Díez P, Huerta A. Strict error bounds for linear solid mechanics problems using a subdomain-based flux-free method. *Comput. Mech.* 2009; 44(4): 533–547. doi: 10.1007/s00466-009-0388-1

13. Parés N, Santos H, Díez P. Guaranteed energy error bounds for the Poisson equation using a flux-free approach: solving the local problems in subdomains. *Internat. J. Numer. Methods Engrg.* 2009; 79(10): 1203–1244. doi: 10.1002/nme.2593

14. Parés N, Díez P, Huerta A. Exact bounds for linear outputs of the advection-diffusion-reaction equation using flux-free error estimates. *SIAM J. Sci. Comput.* 2009; 31(4): 3064–3089. doi: 10.1137/080724356

15. Parés N, Díez P, Huerta A. Computable exact bounds for linear outputs from stabilized solutions of the advection-diffusion-reaction equation. *Internat. J. Numer. Methods Engrg.* 2013; 93(5): 483–509. doi: 10.1002/nme.4396

16. Ainsworth M, Oden JT. *A posteriori error estimation in finite element analysis*. Pure and Applied Mathematics (New York)Wiley-Interscience [John Wiley & Sons], New York . 2000

17. Ainsworth M, Rankin R. Guaranteed computable bounds on quantities of interest in finite element computations. *Internat. J. Numer. Methods Engrg.* 2012; 89(13): 1605–1634. doi: 10.1002/nme.3276

18. Quarteroni A, Valli A. *Numerical approximation of partial differential equations*. 23 of *Springer Series in Computational Mathematics*. Springer-Verlag, Berlin . 1994.

19. Fraeijs de Veubeke B. Displacement and equilibrium models in the finite element method by B. Fraeijs de Veubeke, Chapter 9, pages 145–197 of *Stress Analysis*, Edited by O. C. Zienkiewicz and G. S. Holister, Published by John Wiley & Sons, 1965. *Internat. J. Numer. Methods Engrg.* 2001; 52(3): 287–342. Edited by O. C. Zienkiewicz and G. S. Holister and with introductory remarks by Zienkiewiczdoi: 10.1002/nme.339

20. Sauer-Budge AM, Bonet J, Huerta A, Peraire J. Computing bounds for linear functionals of exact weak solutions to Poisson's equation. *SIAM J. Numer. Anal.* 2004; 42(4): 1610–1630. doi: 10.1137/S0036142903425045

21. Sauer-Budge AM, Peraire J. Computing bounds for linear functionals of exact weak solutions to the advection-diffusion-reaction equation. *SIAM J. Sci. Comput.* 2004; 26(2): 636–652. doi: 10.1137/S1064827503427121

22. Haslinger J, Hlaváček I. Convergence of a finite element method based on the dual variational formulation. *Apl. Mat.* 1976; 21(1): 43–65.

23. Repin SI. A unified approach to a posteriori error estimation based on duality error majorants. *Math. Comput. Simulation* 1999; 50(1-4): 305–321. Modelling '98 (Prague)doi: 10.1016/S0378-4754(99)00081-6

24. Almeida Pereira OJB, Moitinho de Almeida JP, Maunder EAW. Adaptive methods for hybrid equilibrium finite element models. *Comput. Methods Appl. Mech. Engrg.* 1999; 176(1-4): 19–39. New advances in computational methods (Cachan, 1997)doi: 10.1016/S0045-7825(98)00328-4

25. Prager W, Synge JL. Approximations in elasticity based on the concept of function space. *Quart. Appl. Math.* 1947; 5: 241–269. doi: 10.1090/qam/25902

26. Verfürth R. *A posteriori error estimation techniques for finite element methods*. Numerical Mathematics and Scientific ComputationOxford University Press, Oxford . 2013

27. Kempeneers M, Beckers P, Moitinho de Almeida JP, Almeida Pereira OJB. Modèles équilibre pour l'analyse duale. *Revue Européenne des Éléments Finis* 2003; 12(6): 737–760. doi: 10.3166/reef.12.737-760

28. Moitinho de Almeida JP, Maunder EAW. *Equilibrium Finite Element Formulations*. Wiley-Interscience [John Wiley & Sons], New York . 2017.

29. Ainsworth M, Vejchodský T. Robust error bounds for finite element approximation of reaction-diffusion problems with non-constant reaction coefficient in arbitrary space dimension. *Comput. Methods Appl. Mech. Engrg.* 2014; 281: 184–199. doi: 10.1016/j.cma.2014.08.005

30. Ainsworth M, Vejchodský T. Corrigendum to "Robust error bounds for finite element approximation of reaction-diffusion problems with non-constant reaction coefficient in arbitrary space dimension" [Comput. Methods Appl. Mech. Engrg. 281 (2014) 184–199] [MR3262938]. *Comput. Methods Appl. Mech. Engrg.* 2016; 299: 143. doi: 10.1016/j.cma.2015.10.018

31. Brenner SC, Scott LR. *The mathematical theory of finite element methods*. 15 of *Texts in Applied Mathematics*. Springer, New York. third ed. 2008

32. Brezzi F, Fortin M. *Mixed and hybrid finite element methods*. 15 of *Springer Series in Computational Mathematics*. Springer-Verlag, New York . 1991

33. Ladevèze P, Maunder E. A general method for recovering equilibrating element tractions. *Computer Methods in Applied Mechanics and Engineering* 1996; 137(2): 111 - 151. doi: https://doi.org/10.1016/S0045-7825(96)01067-5

34. Ainsworth M, Allendes A, Barrenechea GR, Rankin R. Fully computable a posteriori error bounds for stabilised FEM approximations of convection-reaction-diffusion problems in three dimensions. *Internat. J. Numer. Methods Fluids* 2013; 73(9): 765–790.

35. Ladevèze P, Chamoin L, Florentin É. A new non-intrusive technique for the construction of admissible stress fields in model verification. *Comput. Methods Appl. Mech. Engrg.* 2010; 199(9-12): 766–777. doi: 10.1016/j.cma.2009.11.007

36. Chen L. iFEM: An integrated finite element methods package in MATLAB. tech. rep., University of California at Irvine; : 2009.

37. Shan W. Recursive longest-edge bisection. MathWorks File Exchange. https://es.mathworks.com/matlabcentral/fileexchange/24381-recursive-longest-edge-bisection; .

38. Morin P, Nochetto RH, Siebert KG. Convergence of adaptive finite element methods. *SIAM Rev.* 2002; 44(4): 631–658 (2003). Revised reprint of "Data oscillation and convergence of adaptive FEM" [SIAM J. Numer. Anal. **3**8 (2000), no. 2, 466–488 (electronic); MR1770058 (2001g:65157)]doi: 10.1137/S0036144502409093

39. Dörfler W. A convergent adaptive algorithm for Poisson's equation. *SIAM J. Numer. Anal.* 1996; 33(3): 1106–1124. doi: 10.1137/0733054

40. Dörfler W, Wilderotter O. An adaptive finite element method for a linear elliptic equation with variable coefficients. *ZAMM Z. Angew. Math. Mech.* 2000; 80(7): 481–491. doi: 10.1002/1521-4001(200007)80:7<481::AID-ZAMM481>3.0.CO;2-5

APPENDIX

A PROOF OF THEOREM 2

The proof of Theorem 2 follows the same rationale presented in Appendix C of Parés and Díez[1] and in Section 3.5 of Ainsworth and Vejchodský[29] but is included here for completeness.

Let $\boldsymbol{q}_k^i$ and r_k^i be the weighted dual estimates defined by equations (24) and (25) for a set of local tractions g_γ^i verifying (30). Then, we need to proof that $\boldsymbol{q}_k^i$ and r_k^i verify equation (18) for $\hat{q} = 0$. Taking $\hat{q} = 0$ and recalling the expression for r_k^i given in equation (24), equation (18) can be rewritten as

$$-\nabla \cdot \left(\boldsymbol{q}_k^i + \phi_i \boldsymbol{\nabla} u_h\right) = \phi_i F^0 - \kappa_k^2 r_k^{i0} - \boldsymbol{\nabla} u_h \cdot \nabla \phi_i \qquad \text{in } \Omega_k, \tag{A1a}$$

$$\left(\boldsymbol{q}_k^i + \phi_i \boldsymbol{\nabla} u_h\right) \cdot \boldsymbol{n}_k^\gamma = \sigma_k^\gamma g_\gamma^i \qquad \text{on } \gamma \subset \partial\Omega_k, \tag{A1b}$$

where recall that $F^0 = \Pi_k^0(f - \kappa_k^2 u_h) - \kappa_k^2 r_k^{i1}$.

Consider first equation (A1b) on face $\gamma_{[1]}$. On this face, since $\lambda_{[1]}|_{\gamma_{[1]}} = 0$, the normal component of the linear flux $\mathbf{q}_k^{iL}$ defined in (29) can be simplified to

$$\mathbf{q}_k^{iL} \cdot \boldsymbol{n}_{[1]} = \frac{1}{3|\Omega_k|} \sum_{n=1}^{4} \boldsymbol{\rho}_{[n]}^k \cdot \boldsymbol{n}_{[1]} \lambda_{[n]} = \frac{1}{3|\Omega_k|} \sum_{n=2}^{4} \boldsymbol{\rho}_{[n]}^k \cdot \boldsymbol{n}_{[1]} \lambda_{[n]}$$

where recall that $\boldsymbol{n}_{[1]} = \boldsymbol{n}_k^{\gamma_{[1]}}$. Moreover, taking into account that

$$\boldsymbol{t}_{[mn]}^\mathsf{T} \boldsymbol{n}_{[1]} = 0 \text{ if } m, n \neq 1 \quad \text{and} \quad A_{[1]} \boldsymbol{t}_{[1n]}^\mathsf{T} \boldsymbol{n}_{[1]} = 3|\Omega_k| \text{ for } n \neq 1 \tag{A2}$$

and the definition of $\boldsymbol{\rho}_{[n]}^k$ given in (29), yields for $n \neq 1$

$$\boldsymbol{\rho}_{[n]}^k \cdot \boldsymbol{n}_{[1]} = \sum_{\substack{m=1 \\ m \neq n}}^{4} A_{[m]} \mathcal{R}_{|\gamma_{[m]}}(\boldsymbol{x}_{[n]}) \boldsymbol{t}_{[mn]} \cdot \boldsymbol{n}_{[1]} = A_{[1]} \mathcal{R}_{|\gamma_{[1]}}(\boldsymbol{x}_{[n]}) \boldsymbol{t}_{[1n]} \cdot \boldsymbol{n}_{[1]} = 3|\Omega_k| \mathcal{R}_{|\gamma_{[1]}}(\boldsymbol{x}_{[n]}),$$

and therefore, since $\mathcal{R}_{|\gamma_{[1]}}$ is a linear function over $\gamma_{[1]}$ uniquely defined by its values at nodes $\boldsymbol{x}_{[2]}$, $\boldsymbol{x}_{[3]}$ and $\boldsymbol{x}_{[4]}$

$$\mathbf{q}_k^{iL} \cdot \boldsymbol{n}_{[1]} = \sum_{n=2}^{4} \mathcal{R}_{|\gamma_{[1]}}(\boldsymbol{x}_{[n]}) \lambda_{[n]} = \mathcal{R}_{|\gamma_{[1]}} = \sigma_k^{\gamma_{[1]}} g_{\gamma_{[1]}}^i - \phi_i \boldsymbol{\nabla} u_h \cdot \boldsymbol{n}_{[1]}.$$

Also note that the quadratic flux $\mathbf{q}_k^{iQ}$ defined in (27) has vanishing normal components on $\gamma_{[1]}$. Indeed, using the compact notations introduced in Remark 8 and noting that $\lambda_{[1]}|_{\gamma_{[1]}} = 0$ yields

$$\begin{aligned} \mathbf{q}_k^{iQ} \cdot \boldsymbol{n}_{[1]} &= \boldsymbol{n}_{[1]}^\mathsf{T} \mathbf{q}_k^{iQ} = \frac{F^0}{4} \boldsymbol{n}_{[1]}^\mathsf{T} \mathbf{M}^{\mathbf{q}} \nabla \phi_i = \frac{F^0}{4} \sum_{n=1}^{4} \sum_{\substack{m=2 \\ m>n}}^{4} \lambda_{[n]} \lambda_{[m]} \boldsymbol{n}_{[1]}^\mathsf{T} \boldsymbol{t}_{[nm]} \boldsymbol{t}_{[nm]}^\mathsf{T} \nabla \phi_i \\ &= \frac{F^0}{4} \sum_{n=2}^{4} \sum_{\substack{m=3 \\ m>n}}^{4} \lambda_{[n]} \lambda_{[m]} \boldsymbol{n}_{[1]}^\mathsf{T} \boldsymbol{t}_{[nm]} \boldsymbol{t}_{[nm]}^\mathsf{T} \nabla \phi_i = 0, \end{aligned} \tag{A3}$$

since $\boldsymbol{n}_{[1]}$ is orthogonal to $\boldsymbol{t}_{[mn]}^\mathsf{T}$ if $m, n \neq 1$.

Analogous arguments apply to the other three faces, and we conclude that since

$$\mathbf{q}_k^{iL}\cdot\boldsymbol{n}_k^{\gamma}=\sigma_k^{\gamma}g_{\gamma}^{i}-\phi_i\boldsymbol{\nabla}u_h\cdot\boldsymbol{n}_k^{\gamma}\quad\text{ and }\quad\mathbf{q}_k^{iQ}\cdot\boldsymbol{n}_k^{\gamma}=0 \tag{A4}$$

then

$$\mathbf{q}_k^{i}\cdot\boldsymbol{n}_k^{\gamma}=\mathbf{q}_k^{iL}\cdot\boldsymbol{n}_k^{\gamma}+\mathbf{q}_k^{iQ}\cdot\boldsymbol{n}_k^{\gamma}=\mathbf{q}_k^{iL}\cdot\boldsymbol{n}_k^{\gamma}=\sigma_k^{\gamma}g_{\gamma}^{i}-\phi_i\boldsymbol{\nabla}u_h\cdot\boldsymbol{n}_k^{\gamma},$$

and equation (A1b) is verified.

In order to proof the divergence condition (A1a) note that both $\boldsymbol{q}_k^{iL}$ and $\phi_i\boldsymbol{\nabla}u_h$ are linear functions and therefore they have constant divergence over Ω_k. Thus, using the divergence theorem, the fact that $\mathbf{q}_k^{iQ}$ has vanishing normal components on each face of Ω_k and equation (A1b), yields

$$\begin{aligned}\nabla\cdot(\boldsymbol{q}_k^{iL}+\phi_i\boldsymbol{\nabla}u_h)&=\frac{1}{|\Omega_k|}\int_{\Omega_k}\nabla\cdot(\boldsymbol{q}_k^{iL}+\phi_i\boldsymbol{\nabla}u_h)\,d\Omega=\frac{1}{|\Omega_k|}\int_{\partial\Omega_k}(\boldsymbol{q}_k^{iL}+\phi_i\boldsymbol{\nabla}u_h)\cdot\boldsymbol{n}_k\,d\Gamma\\&=\frac{1}{|\Omega_k|}\int_{\partial\Omega_k}(\boldsymbol{q}_k^{i}+\phi_i\boldsymbol{\nabla}u_h)\cdot\boldsymbol{n}_k\,d\Gamma=\frac{1}{|\Omega_k|}\sum_{\gamma\subset\partial\Omega_k}\int_{\gamma}\sigma_k^{\gamma}g_{\gamma}^{i}\,d\Gamma,\end{aligned} \tag{A5}$$

which can again be simplified using the projected equilibration condition (30) and the fact that F^0 and $\kappa_k^2 r_k^{i0}+\nabla u_h\cdot\nabla\phi_i$ are constant functions

$$\begin{aligned}-\nabla\cdot(\boldsymbol{q}_k^{iL}+\phi_i\boldsymbol{\nabla}u_h)&=-\frac{1}{|\Omega_k|}\sum_{\gamma\subset\partial\Omega_k}\int_{\gamma}\sigma_k^{\gamma}g_{\gamma}^{i}\,d\Gamma=\frac{1}{|\Omega_k|}\int_{\Omega_k}\left[\phi_i F^0-\kappa_k^2 r_k^{i0}-\nabla u_h\cdot\nabla\phi_i\right]\,d\Omega\\&=\frac{1}{4}F^0-\kappa_k^2 r_k^{i0}-\nabla u_h\cdot\nabla\phi_i,\end{aligned} \tag{A6}$$

since $\int_{\Omega_k}\phi_i d\Omega=|\Omega_k|/4$.

To compute the divergence of the quadratic contribution to the flux $\mathbf{q}_k^{iQ}$ the compact notations given in Remark 8 are used along with the fact that $\boldsymbol{t}_{[nm]}^{\mathsf{T}}\nabla\phi_i$ has is constant in Ω_k yielding

$$\nabla\cdot\mathbf{q}_k^{iQ}=\frac{F^0}{4}\sum_{n=1}^{4}\sum_{\substack{m=2\\m>n}}^{4}\nabla\cdot\left(\lambda_{[n]}\lambda_{[m]}\boldsymbol{t}_{[nm]}\right)\boldsymbol{t}_{[nm]}^{\mathsf{T}}\nabla\phi_i. \tag{A7}$$

Now, considering the centroid of the tetrahedron $\overline{\boldsymbol{x}}_k=(\boldsymbol{x}_{[1]}+\boldsymbol{x}_{[2]}+\boldsymbol{x}_{[3]}+\boldsymbol{x}_{[4]})/4$ and using the geometrical properties

$$\nabla\cdot(\lambda_{[n]}\lambda_{[m]}\boldsymbol{t}_{[nm]})=\lambda_{[n]}-\lambda_{[m]}\quad\text{ and }\quad\frac{1}{4}\sum_{n=1}^{4}\sum_{\substack{m=2\\m>n}}^{4}(\lambda_{[n]}-\lambda_{[m]})\boldsymbol{t}_{[nm]}^{\mathsf{T}}=(\overline{\boldsymbol{x}}_k-\boldsymbol{x})^{\mathsf{T}} \tag{A8}$$

yields

$$\nabla\cdot\mathbf{q}_k^{iQ}=F^0(\overline{\boldsymbol{x}}_k-\boldsymbol{x})^{\mathsf{T}}\nabla\phi_i=\left(\frac{1}{4}-\phi_i\right)F^0. \tag{A9}$$

The last equality in (A9) can be deduced using (A10) and that

$$\phi_i=\lambda_{[1]}=-\frac{A_{[1]}}{3|\Omega_k|}\boldsymbol{n}_{[1]}^{\mathsf{T}}(\boldsymbol{x}-\boldsymbol{x}_{[4]})\ ,\ \nabla\phi_i=-\frac{A_{[1]}}{3|\Omega_k|}\boldsymbol{n}_{[1]}\ \text{ and }\ \boldsymbol{x}_{[4]}-\overline{\boldsymbol{x}}_k=\frac{1}{4}(\boldsymbol{t}_{[14]}+\boldsymbol{t}_{[24]}+\boldsymbol{t}_{[34]}). \tag{A10}$$

Indeed, using these properties

$$\begin{aligned}(\overline{\boldsymbol{x}}_k-\boldsymbol{x})^{\mathsf{T}}\nabla\phi_i&=-\nabla\phi_i^{\mathsf{T}}(\boldsymbol{x}-\overline{\boldsymbol{x}}_k)=\frac{A_{[1]}}{3|\Omega_k|}\boldsymbol{n}_{[1]}^{\mathsf{T}}(\boldsymbol{x}-\overline{\boldsymbol{x}}_k)\\&=\frac{A_{[1]}}{3|\Omega_k|}\boldsymbol{n}_{[1]}^{\mathsf{T}}(\boldsymbol{x}-\boldsymbol{x}_{[4]})+\frac{A_{[1]}}{3|\Omega_k|}\boldsymbol{n}_{[1]}^{\mathsf{T}}(\boldsymbol{x}_{[4]}-\overline{\boldsymbol{x}}_k)\\&=-\phi_i+\frac{1}{4}\frac{A_{[1]}}{3|\Omega_k|}\boldsymbol{n}_{[1]}^{\mathsf{T}}(\boldsymbol{t}_{[14]}+\boldsymbol{t}_{[24]}+\boldsymbol{t}_{[34]})=-\phi_i+\frac{1}{4}\frac{A_{[1]}}{3|\Omega_k|}\boldsymbol{n}_{[1]}^{\mathsf{T}}\boldsymbol{t}_{[14]}=-\phi_i+\frac{1}{4},\end{aligned} \tag{A11}$$

which easily yields to equation (A9).

Finally, joining (A6) and (A9) yields

$$\begin{aligned}-\nabla\cdot(\boldsymbol{q}_k^{i}+\phi_i\boldsymbol{\nabla}u_h)&=-\nabla\cdot(\boldsymbol{q}_k^{iL}+\phi_i\boldsymbol{\nabla}u_h)-\nabla\cdot\boldsymbol{q}_k^{iQ}\\&=\frac{1}{4}F^0-\kappa_k^2 r_k^{i0}-\nabla u_h\cdot\nabla\phi_i-\left(\frac{1}{4}-\phi_i\right)F^0\\&=\phi_i F^0-\kappa_k^2 r_k^{i0}-\nabla u_h\cdot\nabla\phi_i\end{aligned}$$

and therefore equation (A1a) holds. □

B PROOF OF THEOREM 3

Let $\boldsymbol{q}_k^i$ and r_k^i be the weighted dual estimates defined by equations (31) and (32) for a set of local tractions g_γ^i verifying (36). Then, we need to proof that $\boldsymbol{q}_k^i$ and r_k^i verify equation (18) for $\hat{q} = 1$. Taking $\hat{q} = 1$ and recalling the expression for r_k^i given in equation (31), equation (18) can be rewritten as

$$-\boldsymbol{\nabla} \cdot \left(\boldsymbol{q}_k^i + \phi_i \boldsymbol{\nabla} u_h\right) = \phi_i F^1 - \kappa_k^2 r_k^{i0} - \boldsymbol{\nabla} u_h \cdot \boldsymbol{\nabla} \phi_i \qquad \text{in } \Omega_k \tag{B12a}$$

$$\left(\boldsymbol{q}_k^i + \phi_i \boldsymbol{\nabla} u_h\right) \cdot \boldsymbol{n}_k^\gamma = \sigma_k^\gamma g_\gamma^i \qquad \text{on } \gamma \subset \partial\Omega_k, \tag{B12b}$$

where recall that from equation (35), $F^1 = \Pi_k^1(f - \kappa_k^2 u_h) - \kappa_k^2 r_k^{iL}$.

Let's first start proving that the boundary conditions given in (B12b) hold. As seen in equation (A4) of Appendix A, the value of $\mathbf{q}_k^{iL}$ defined in (26) at the faces of Ω_k is given by $\mathbf{q}_k^{iL} \cdot \boldsymbol{n}_k^\gamma = \sigma_k^\gamma g_\gamma^i - \phi_i \boldsymbol{\nabla} u_h \cdot \boldsymbol{n}_k^\gamma$, and, following an analogous rationale as the one used in equation (A3), that is, using that

$$\boldsymbol{n}_{[i]}^\mathsf{T} \mathbf{M}^{\mathbf{q}}\Big|_{\gamma_{[i]}} = \mathbf{0},$$

it is trivial to see that $\mathbf{q}_k^{iC}$ defined in (33) also has vanishing normal components on each face of Ω_k. Hence

$$\mathbf{q}_k^i \cdot \boldsymbol{n}_k^\gamma = \mathbf{q}_k^{iL} \cdot \boldsymbol{n}_k^\gamma + \mathbf{q}_k^{iC} \cdot \boldsymbol{n}_k^\gamma = \sigma_k^\gamma g_\gamma^i - \phi_i \boldsymbol{\nabla} u_h \cdot \boldsymbol{n}_k^\gamma,$$

and equation (B12b) is verified.

To proof the divergence condition (B12a), first the same reasoning used in (A5) is applied here, since again $\boldsymbol{q}_k^{iL}$ and $\phi_i \boldsymbol{\nabla} u_h$ are linear functions and $\mathbf{q}_k^{iC}$ has vanishing normal components on the faces of Ω_k. Therefore, using equation (A5) along with the projected equilibration condition (36) yields

$$\begin{aligned} -\nabla \cdot (\boldsymbol{q}_k^{iL} + \phi_i \boldsymbol{\nabla} u_h) &= -\frac{1}{|\Omega_k|} \sum_{\gamma \subset \partial\Omega_k} \int_\gamma \sigma_k^\gamma g_\gamma^i \, d\Gamma = \frac{1}{|\Omega_k|} \int_{\Omega_k} \left[\phi_i F^1 - \kappa_k^2 r_k^{i0} - \nabla u_h \cdot \nabla \phi_i\right] \, d\Omega \\ &= \frac{1}{20}\left(2F_{[1]}^1 + F_{[2]}^1 + F_{[3]}^1 + F_{[4]}^1\right) - \kappa_k^2 r_k^{i0} - \nabla u_h \cdot \nabla \phi_i, \end{aligned} \tag{B13}$$

where in the last step, the integral of the quadratic function $\phi_i F^1$ has been computed and simplified.

To compute the divergence of the cubic flux $\mathbf{q}_k^{iC}$ given in equation (33)

$$\nabla \cdot \mathbf{q}_k^{iC} = \frac{1}{4} \sum_{n=1}^{4} \sum_{\substack{m=2 \\ m>n}}^{4} \nabla \cdot \left(\lambda_{[n]} \lambda_{[m]} \boldsymbol{t}_{[nm]} \boldsymbol{t}_{[nm]}^\mathsf{T} \nabla v^Q\right)$$

it is worth noting that $\lambda_{[n]} \lambda_{[m]} \boldsymbol{t}_{[nm]} \boldsymbol{t}_{[nm]}^\mathsf{T} \nabla v^Q$ is a vector function which can be split into the product of the scalar function $c = \boldsymbol{t}_{[nm]}^\mathsf{T} \nabla v^Q$ and the vector $\boldsymbol{v} = \lambda_{[n]} \lambda_{[m]} \boldsymbol{t}_{[nm]}$. Then, using the basic divergence property $\nabla \cdot (c\boldsymbol{v}) = c \nabla \cdot \boldsymbol{v} + \boldsymbol{v}^\mathsf{T} \nabla c$ yields

$$\nabla \cdot \mathbf{q}_k^{iC} = \frac{1}{4} \sum_{n=1}^{4} \sum_{\substack{m=2 \\ m>n}}^{4} (\boldsymbol{t}_{[nm]}^\mathsf{T} \nabla v^Q) \nabla \cdot (\lambda_{[n]} \lambda_{[m]} \boldsymbol{t}_{[nm]}) + \frac{1}{4} \sum_{n=1}^{4} \sum_{\substack{m=2 \\ m>n}}^{4} \lambda_{[n]} \lambda_{[m]} \boldsymbol{t}_{[nm]}^\mathsf{T} \nabla (\boldsymbol{t}_{[nm]}^\mathsf{T} \nabla v^Q). \tag{B14}$$

Let's first simplify the first term in the previous summation. Using the relations given in (A8) it follows that

$$\frac{1}{4} \sum_{n=1}^{4} \sum_{\substack{m=2 \\ m>n}}^{4} (\boldsymbol{t}_{[nm]}^\mathsf{T} \nabla v^Q) \nabla \cdot (\lambda_{[n]} \lambda_{[m]} \boldsymbol{t}_{[nm]}) = \frac{1}{4} \sum_{n=1}^{4} \sum_{\substack{m=2 \\ m>n}}^{4} (\lambda_{[n]} - \lambda_{[m]}) \boldsymbol{t}_{[nm]}^\mathsf{T} \nabla v^Q = (\overline{\boldsymbol{x}}_k - \boldsymbol{x})^\mathsf{T} \nabla v^Q. \tag{B15}$$

Now, to compute the gradient of the quadratic function v^Q defined in equation (34), first note that introducing the vector $\mathbf{F}^1 = (F_{[1]}^1, F_{[2]}^1, F_{[3]}^1, F_{[4]}^1)^\mathsf{T}$ and the matrix

$$\mathbf{M}_1^{v^Q} = \begin{pmatrix} 4 & 0 & 0 & 0 \\ 0 & 0 & -1 & -1 \\ 0 & -1 & 0 & -1 \\ 0 & -1 & -1 & 0 \end{pmatrix} \tag{B16}$$

then

$$v^Q = \frac{2}{5} \phi_i F^1 + \frac{1}{10} (\lambda_{[1]} \, \lambda_{[2]} \, \lambda_{[3]} \, \lambda_{[4]}) \mathbf{M}_1^{v^Q} \mathbf{F}^1. \tag{B17}$$

Also note that since

$$\nabla \lambda_{[j]} = -\frac{\boldsymbol{A}_{[j]} \boldsymbol{n}_{[j]}}{3|\Omega_k|}, \tag{B18}$$

the gradient of a linear function $v^L = v_{[1]}\lambda_{[1]} + v_{[2]}\lambda_{[2]} + v_{[3]}\lambda_{[3]} + v_{[4]}\lambda_{[4]}$, described by its associated vector $\boldsymbol{v}^L = \left(v_{[1]}, v_{[2]}, v_{[3]}, v_{[4]}\right)^\mathsf{T}$ containing the nodal values of the function, can be rewritten as a matrix vector multiplication

$$\nabla v^L = -\frac{1}{3|\Omega_k|}\boldsymbol{\nabla}^L\boldsymbol{v}^L, \tag{B19}$$

where $\boldsymbol{\nabla}^L = \left(A_{[1]}\boldsymbol{n}_{[1]}, A_{[2]}\boldsymbol{n}_{[2]}, A_{[3]}\boldsymbol{n}_{[3]}, A_{[4]}\boldsymbol{n}_{[4]}\right)$. Therefore using the product rule for the gradient and rearranging terms yields

$$\begin{aligned}
\nabla v^Q &= \frac{2}{5}(\nabla\phi_i F^1 + \phi_i\nabla F^1) + \frac{1}{10}\nabla\left((\lambda_{[1]}\ \lambda_{[2]}\ \lambda_{[3]}\ \lambda_{[4]})\mathbf{M}_1^{v^Q}\mathbf{F}^1\right)\\
&= -\frac{2}{15|\Omega_k|}\boldsymbol{\nabla}^L\begin{pmatrix}F^1\\0\\0\\0\end{pmatrix} - \frac{2\lambda_{[1]}}{15|\Omega_k|}\boldsymbol{\nabla}^L\mathbf{F}^1 - \frac{1}{30|\Omega_k|}\boldsymbol{\nabla}^L\mathbf{M}_1^{v^Q}\mathbf{F}^1\\
&= -\frac{1}{30|\Omega_k|}\boldsymbol{\nabla}^L(4\mathbf{M}_2^{v^Q} + 4\lambda_{[1]}\mathbf{I}_4 + \mathbf{M}_1^{v^Q})\mathbf{F}^1,
\end{aligned} \tag{B20}$$

where $\mathbf{I}_4$ is the 4×4 identity matrix and

$$\mathbf{M}_2^{v^Q} = \begin{pmatrix}\lambda_{[1]} & \lambda_{[2]} & \lambda_{[3]} & \lambda_{[4]}\\ 0 & 0 & 0 & 0\\ 0 & 0 & 0 & 0\\ 0 & 0 & 0 & 0\end{pmatrix}. \tag{B21}$$

Finally, taking $\phi_i = \lambda_{[1]}$ into (B18) and (A11) yields $A_{[1]}(\overline{\boldsymbol{x}}_k - \boldsymbol{x})^\mathsf{T}\boldsymbol{n}_{[1]} = 3|\Omega_k|(\lambda_{[1]} - 1/4)$, which also holds for all the other shape functions, namely $A_{[j]}(\overline{\boldsymbol{x}}_k - \boldsymbol{x})^\mathsf{T}\boldsymbol{n}_{[j]} = 3|\Omega_k|(4\lambda_{[j]} - 1)/4$. Using this property along with the partition of unity $\lambda_{[1]} + \lambda_{[2]} + \lambda_{[3]} + \lambda_{[4]} = 1$ and after carefully simplifying the resulting expressions yields

$$\begin{aligned}
(\overline{\boldsymbol{x}}_k - \boldsymbol{x})^\mathsf{T}\nabla v^Q &= -\frac{1}{30|\Omega_k|}(\overline{\boldsymbol{x}}_k - \boldsymbol{x})^\mathsf{T}\boldsymbol{\nabla}^L(4\lambda_{[1]}\mathbf{I}_4 + \mathbf{M}_1^{v^Q} + 4\mathbf{M}_2^{v^Q})\\
&= -\frac{1}{40}\left(4\lambda_{[1]} - 1, 4\lambda_{[2]} - 1, 4\lambda_{[3]} - 1, 4\lambda_{[4]} - 1\right)(4\lambda_{[1]}\mathbf{I}_4 + \mathbf{M}_1^{v^Q} + 4\mathbf{M}_2^{v^Q})\\
&= -\frac{4}{5}\lambda_{[1]}F^1 - \frac{1}{5}\lambda_{[1]}F^1_{[1]} + \frac{1}{20}(2F^1_{[1]} + F^1_{[2]} + F^1_{[3]} + F^1_{[4]}).
\end{aligned} \tag{B22}$$

To simplify the second summation in equation (B14), let's first note that if $\mathbf{H}(v^Q)$ denotes the Hessian matrix associated to the function v^Q, then

$$\nabla(\boldsymbol{t}_{[nm]}^\mathsf{T}\nabla v^Q) = \mathbf{H}(v^Q)\boldsymbol{t}_{[nm]} = \frac{2}{5}\mathbf{H}(\phi_i F^1)\boldsymbol{t}_{[nm]}, \tag{B23}$$

since the Hessian matrix of the linear part of v^Q is the null matrix. This expression can be further simplified applying the property of the Hessian of a product of functions and recalling that F^1 and ϕ_i are linear functions

$$\mathbf{H}(\phi_i F^1) = \mathbf{H}(\phi_i)F^1 + \nabla\phi_i(\nabla F^1)^\mathsf{T} + \nabla F^1(\nabla\phi_i)^\mathsf{T} + \mathbf{H}(F^1)\phi_i = \nabla\phi_i(\nabla F^1)^\mathsf{T} + \nabla F^1(\nabla\phi_i)^\mathsf{T}$$

which again can be rewritten using equations (B18) and (B19) as

$$\mathbf{H}(\phi_i F^1) = \frac{A_{[1]}}{9|\Omega_k|^2}\left(\boldsymbol{n}_{[1]}(\mathbf{F}^1)^\mathsf{T}(\boldsymbol{\nabla}^L)^\mathsf{T} + \boldsymbol{\nabla}^L\mathbf{F}^1\boldsymbol{n}_{[1]}^\mathsf{T}\right). \tag{B24}$$

Then, joining equations (B23) and (B24) yields

$$\begin{aligned}
\boldsymbol{t}_{[nm]}^\mathsf{T}\nabla(\boldsymbol{t}_{[nm]}^\mathsf{T}\nabla v^Q) &= \frac{2A_{[1]}}{45|\Omega_k|^2}\left(\boldsymbol{t}_{[nm]}^\mathsf{T}\boldsymbol{n}_{[1]}(\mathbf{F}^1)^\mathsf{T}(\boldsymbol{\nabla}^L)^\mathsf{T}\boldsymbol{t}_{[nm]} + \boldsymbol{t}_{[nm]}^\mathsf{T}\boldsymbol{\nabla}^L\mathbf{F}^1\boldsymbol{n}_{[1]}^\mathsf{T}\boldsymbol{t}_{[nm]}\right)\\
&= \frac{4A_{[1]}}{45|\Omega_k|^2}\boldsymbol{t}_{[nm]}^\mathsf{T}\boldsymbol{n}_{[1]}(\mathbf{F}^1)^\mathsf{T}(\boldsymbol{\nabla}^L)^\mathsf{T}\boldsymbol{t}_{[nm]}.
\end{aligned}$$

Finally, using that

$$A_{[l]}\boldsymbol{n}_{[l]}\cdot\boldsymbol{t}_{[nm]} = 3|\Omega_k|(\delta_{ln} - \delta_{lm}) \tag{B25}$$

then

$$\boldsymbol{t}_{[nm]}^\mathsf{T}\boldsymbol{\nabla}^L = 3|\Omega_k|\left(\delta_{1n} - \delta_{1m}\,,\ \delta_{2n} - \delta_{2m}\,,\ \delta_{3n} - \delta_{3m}\,,\ \delta_{4n} - \delta_{4m}\right)$$

and it holds that

$$\boldsymbol{t}_{[nm]}^\mathsf{T}\nabla(\boldsymbol{t}_{[nm]}^\mathsf{T}\nabla v^Q) = \frac{4}{5}(\delta_{1n} - \delta_{1m})(\mathbf{F}^1)^\mathsf{T}\left(\delta_{1n} - \delta_{1m}\,,\ \delta_{2n} - \delta_{2m}\,,\ \delta_{3n} - \delta_{3m}\,,\ \delta_{4n} - \delta_{4m}\right)^\mathsf{T}.$$

Therefore the second summation in equation (B14) can be simplified noting first that $\delta_{1m} = 0$ since $m > 1$ and that $\delta_{1n} = 0$ unless $n = 1$ as

$$\begin{aligned}\frac{1}{4}\sum_{n=1}^{4}\sum_{\substack{m=2\\m>n}}^{4}\lambda_{[n]}\lambda_{[m]}\boldsymbol{t}_{[nm]}^{\mathsf{T}}\nabla(\boldsymbol{t}_{[nm]}^{\mathsf{T}}\nabla v^{Q}) &= \frac{1}{5}\sum_{\substack{m=2\\m>n}}^{4}\lambda_{[1]}\lambda_{[m]}(\mathbf{F}^{1})^{\mathsf{T}}\left(1\,,\,-\delta_{2m}\,,\,-\delta_{3m}\,,\,-\delta_{4m}\right)^{\mathsf{T}}\\ &= \frac{1}{5}\lambda_{[1]}(\mathbf{F}^{1})^{\mathsf{T}}\left(\lambda_{[2]}(1\,,\,-1\,,\,0\,,\,0)^{\mathsf{T}}+\lambda_{[3]}(1\,,\,0\,,\,-1\,,\,0)^{\mathsf{T}}+\lambda_{[4]}(1\,,\,0\,,\,0\,,\,-1)^{\mathsf{T}}\right)\\ &= \frac{1}{5}\lambda_{[1]}\left(F^{1}_{[1]}-F^{1}\right)\end{aligned} \tag{B26}$$

where to obtain the last equality, the partition of unity of the shape functions has been used.

Introducing equations (B15), (B22) and (B26) into (B14) and simplifying the expression allows obtaining that

$$\nabla\cdot\mathbf{q}_k^{iC} = -\phi_i F^1 + \frac{1}{20}(2F^1_{[1]}+F^1_{[2]}+F^1_{[3]}+F^1_{[4]}), \tag{B27}$$

and joining equations (B27) and (B13) after simplifying the common terms yields

$$-\nabla\cdot(\boldsymbol{q}_k^i+\phi_i\boldsymbol{\nabla}u_h) = -\nabla\cdot(\boldsymbol{q}_k^{iL}+\phi_i\boldsymbol{\nabla}u_h)-\nabla\cdot(\boldsymbol{q}_k^{iC}) = \phi_i F^1-\kappa_k^2 r_k^{i0}-\nabla u_h\cdot\nabla\phi_i,$$

which proofs equation (B12a). □

C NOTATIONS FOR THE MATRICES AND VECTORS APPEARING IN THE LOCAL SQUARED NORMS $\|\boldsymbol{q}_k^i\|_k^2+\kappa_k^2\|r_k^i\|_k^2$

This section provides the detailed expressions of the matrices, vectors and constants appearing in the local squared norms given in equation (49) for Cases I and II. These expressions are derived by explicitly computing and simplifying the integrals involved in the norms and scalar products given in equations (53) and (58), but these computations are not included here for brevity.

C.1 Case I. Piecewise constant projection of the data $\hat{q} = \bar{q} = 0$

The local norms of the dual estimates given in equations (53) and (54) are defined using the following matrices, vectors and constants:

$$\widehat{\mathbf{M}}_k^L = \begin{bmatrix}\mathbf{M}_k^L & \mathbf{0}_{9\times2}\\ \mathbf{0}_{2\times9} & \mathbf{0}_{2\times2}\end{bmatrix},\ \widehat{\mathbf{M}}_k^{LQ} = -\frac{\kappa_k^2}{2}\begin{bmatrix}\mathbf{0}_{9\times9} & \mathbf{b}_k^{LQ} & \mathbf{0}_{9\times1}\\ (\mathbf{b}_k^{LQ})^{\mathsf{T}} & 0 & 0\\ \mathbf{0}_{1\times9} & 0 & 0\end{bmatrix},\ \widehat{\mathbf{M}}_k^{Q} = \begin{bmatrix}\mathbf{0}_{9\times9} & \mathbf{0}_{9\times1} & \mathbf{0}_{9\times1}\\ \mathbf{0}_{1\times9} & \kappa_k^4\mathrm{c}_k^Q & 0\\ \mathbf{0}_{1\times9} & 0 & 0\end{bmatrix},$$

$$\widehat{\mathbf{b}}_k^L = \begin{bmatrix}\mathbf{b}_k^L\\ \mathbf{0}_{2\times1}\end{bmatrix},\ \widehat{\mathbf{b}}_k^{LQ} = \begin{bmatrix}\Pi_k^0(f-\kappa_k^2u_h)\mathbf{b}_k^{LQ}\\ -\kappa_k^2\mathrm{c}_k^{LQ}\\ 0\end{bmatrix},\ \widehat{\mathbf{b}}_k^{Q} = \begin{bmatrix}\mathbf{0}_{9\times1}\\ -2\kappa_k^2\Pi_k^0(f-\kappa_k^2u_h)\mathrm{c}_k^Q\\ 0\end{bmatrix},$$

and

$$\mathrm{c}_k^L = \frac{1}{90|\Omega_k|}(\mathbf{b}^{\mathbf{q}L})^{\mathsf{T}}\mathbf{b}^{\mathbf{q}L},\ \mathrm{c}_k^{LQ} = -\frac{1}{720}(\boldsymbol{t}_{[12]}+\boldsymbol{t}_{[13]}+\boldsymbol{t}_{[14]})\mathbf{b}^{\mathbf{q}L},$$
$$\mathrm{c}_k^Q = \frac{|\Omega_k|}{3360}\Big(\ell^2_{[12]}+\ell^2_{[13]}+\ell^2_{[14]}+\boldsymbol{t}_{[12]}^{\mathsf{T}}\boldsymbol{t}_{[13]}+\boldsymbol{t}_{[12]}^{\mathsf{T}}\boldsymbol{t}_{[14]}+\boldsymbol{t}_{[13]}^{\mathsf{T}}\boldsymbol{t}_{[14]}\Big),$$

for

$$\mathbf{M}_k^L = \frac{1}{180|\Omega_k|}\begin{bmatrix}2&1&1&2&1&1&2&1&1\\1&2&1&1&1&1&1&1&2\\1&1&2&1&1&2&1&1&1\\2&1&1&2&1&1&2&1&1\\1&1&1&1&2&1&1&2&1\\1&1&2&1&1&2&1&1&1\\2&1&1&2&1&1&2&1&1\\1&1&1&1&2&1&1&2&1\\1&2&1&1&1&1&1&1&2\end{bmatrix}\otimes\left((\mathbf{M}^{\mathbf{q}L})^{\mathsf{T}}\mathbf{M}^{\mathbf{q}L}\right),$$

$$\mathbf{b}_k^{LQ} = -\frac{1}{2880}\mathbf{\Lambda}^{LQ}\begin{bmatrix} 8 & 2 & 2 & -2 & -2 & 0 \\ 4 & -4 & 0 & -1 & -1 & 1 \\ 4 & 0 & -4 & -1 & -1 & 1 \\ 2 & 8 & 2 & -2 & 0 & -2 \\ -4 & 4 & 0 & -1 & 1 & -1 \\ 0 & 4 & -4 & -1 & 1 & -1 \\ 2 & 2 & 8 & 0 & -2 & -2 \\ -4 & 0 & 4 & 1 & -1 & -1 \\ 0 & -4 & 4 & 1 & -1 & -1 \end{bmatrix}\begin{pmatrix} \ell^2_{[12]} \\ \ell^2_{[13]} \\ \ell^2_{[14]} \\ \ell^2_{[23]} \\ \ell^2_{[24]} \\ \ell^2_{[34]} \end{pmatrix},$$

$$\mathbf{b}_k^{L} = \frac{1}{90|\Omega_k|}\mathbf{diag}(2,1,1,2,1,1,2,1,1)(\mathbf{M}^{\mathbf{q}L})^{\mathsf{T}}\mathbf{b}^{\mathbf{q}L},$$

and

$$\mathbf{\Lambda}^{LQ} = \mathbf{diag}(A_{[2]}\sigma_k^{\gamma_{[2]}}, A_{[2]}\sigma_k^{\gamma_{[2]}}, A_{[2]}\sigma_k^{\gamma_{[2]}}, A_{[3]}\sigma_k^{\gamma_{[3]}}, A_{[3]}\sigma_k^{\gamma_{[3]}}, A_{[3]}\sigma_k^{\gamma_{[3]}}, A_{[4]}\sigma_k^{\gamma_{[4]}}, A_{[4]}\sigma_k^{\gamma_{[4]}}, A_{[4]}\sigma_k^{\gamma_{[4]}}),$$

where the operator $\otimes$ refers to the element-by-element matrix product and the length of the edge of the tetrahedron joining nodes $\boldsymbol{x}_{[m]}$ and $\boldsymbol{x}_{[n]}$ has been denoted by $\ell_{[mn]} = |\boldsymbol{t}_{[mn]}|^2$.

C.2 Case II. Mixed piecewise linear/constant projection of the data $\hat{q} = 1, \bar{q} = 0$

The local norms of the dual estimates given in equations (58) and (59) are defined using the following matrices and vectors:

$$\widehat{\mathbf{M}}_k^L = \begin{bmatrix} \mathbf{M}_k^L & \mathbf{0}_{9\times5} \\ \mathbf{0}_{5\times9} & \mathbf{0}_{5\times5} \end{bmatrix},\ \widehat{\mathbf{M}}_k^{LC} = -\frac{\kappa_k^2}{2}\begin{bmatrix} \mathbf{0}_{9\times9} & \mathbf{M}_k^{LC} & \mathbf{0}_{9\times1} \\ (\mathbf{M}_k^{LC})^{\mathsf{T}} & \mathbf{0}_{4\times4} & \mathbf{0}_{4\times1} \\ \mathbf{0}_{1\times9} & \mathbf{0}_{1\times4} & 0 \end{bmatrix},$$

$$\widehat{\mathbf{M}}_k^C = \kappa_k^4\begin{bmatrix} \mathbf{0}_{9\times9} & \mathbf{0}_{9\times4} & \mathbf{0}_{9\times1} \\ \mathbf{0}_{4\times9} & \mathbf{M}_k^C & \mathbf{0}_{4\times1} \\ \mathbf{0}_{1\times9} & \mathbf{0}_{1\times4} & 0 \end{bmatrix},\ \widehat{\mathbf{M}}_k^r = \begin{bmatrix} \mathbf{0}_{9\times9} & \mathbf{0}_{9\times5} \\ \mathbf{0}_{5\times9} & \mathbf{M}_k^r \end{bmatrix},$$

and

$$\widehat{\mathbf{b}}_k^L = \begin{bmatrix} \mathbf{b}_k^L \\ \mathbf{0}_{5\times1} \end{bmatrix},\ \widehat{\mathbf{b}}_k^{LC} = \begin{bmatrix} \mathbf{M}_k^{LC}\mathbf{\Pi}^1 \\ \mathbf{b}_k^{LC} \\ 0 \end{bmatrix},\ \widehat{\mathbf{b}}_k^C = -2\kappa^2\begin{bmatrix} \mathbf{0}_{9\times1} \\ \mathbf{b}_k^C \\ 0 \end{bmatrix},$$

where the expressions for $\mathbf{M}_k^L$ and $\mathbf{b}_k^L$ are given in the previous subsection C.1 and

$$\mathbf{M}_k^{LC} = \mathbf{diag}(A_{[2]}\sigma_k^{\gamma_{[2]}}, A_{[2]}\sigma_k^{\gamma_{[2]}}, A_{[2]}\sigma_k^{\gamma_{[2]}}, A_{[3]}\sigma_k^{\gamma_{[3]}}, A_{[3]}\sigma_k^{\gamma_{[3]}}, A_{[3]}\sigma_k^{\gamma_{[3]}}, A_{[4]}\sigma_k^{\gamma_{[4]}}, A_{[4]}\sigma_k^{\gamma_{[4]}}, A_{[4]}\sigma_k^{\gamma_{[4]}})\,\mathbf{D}^1\mathbf{M}^1,$$

$$\mathbf{M}_k^C = \mathbf{M}^2 - \mathbf{M}^3,\ \mathbf{M}_k^r = \frac{|\Omega_k|}{420}\begin{bmatrix} 12 & 3 & 3 & 3 & 42 \\ 3 & 2 & 1 & 1 & 21 \\ 3 & 1 & 2 & 1 & 21 \\ 3 & 1 & 1 & 2 & 21 \\ 42 & 21 & 21 & 21 & 420 \end{bmatrix},$$

$$\mathbf{b}_k^{LC} = \frac{\kappa_k^2}{100800}\begin{pmatrix} 104(\boldsymbol{t}_{[12]}^{\mathsf{T}} + \boldsymbol{t}_{[13]}^{\mathsf{T}} + \boldsymbol{t}_{[14]}^{\mathsf{T}}) \\ -8\boldsymbol{t}_{[12]}^{\mathsf{T}} + 22(\boldsymbol{t}_{[13]}^{\mathsf{T}} + \boldsymbol{t}_{[14]}^{\mathsf{T}}) + 15(\boldsymbol{t}_{[23]}^{\mathsf{T}} + \boldsymbol{t}_{[24]}^{\mathsf{T}}) \\ 22(\boldsymbol{t}_{[12]}^{\mathsf{T}} + \boldsymbol{t}_{[14]}^{\mathsf{T}}) - 8\boldsymbol{t}_{[13]}^{\mathsf{T}} + 15(\boldsymbol{t}_{[34]}^{\mathsf{T}} - \boldsymbol{t}_{[23]}^{\mathsf{T}}) \\ 22(\boldsymbol{t}_{[12]}^{\mathsf{T}} + \boldsymbol{t}_{[13]}^{\mathsf{T}}) - 8\boldsymbol{t}_{[14]}^{\mathsf{T}} - 15(\boldsymbol{t}_{[24]}^{\mathsf{T}} + \boldsymbol{t}_{[34]}^{\mathsf{T}}) \end{pmatrix}\mathbf{b}^{\mathbf{q}L},\ \mathbf{b}_k^C = \mathbf{M}^2\mathbf{\Pi}^1,$$

for matrices $\mathbf{D}^1 \in \mathbb{R}^{9\times27}$ and $\mathbf{M}^1 \in \mathbb{R}^{27\times4}$ given by

$$\mathbf{D}^1 = -\frac{1}{100800}\mathbf{diag}(\boldsymbol{t}_{[21]}^{\mathsf{T}}, \boldsymbol{t}_{[23]}^{\mathsf{T}}, \boldsymbol{t}_{[24]}^{\mathsf{T}}, \boldsymbol{t}_{[31]}^{\mathsf{T}}, \boldsymbol{t}_{[32]}^{\mathsf{T}}, \boldsymbol{t}_{[34]}^{\mathsf{T}}, \boldsymbol{t}_{[41]}^{\mathsf{T}}, \boldsymbol{t}_{[42]}^{\mathsf{T}}, \boldsymbol{t}_{[43]}^{\mathsf{T}}),$$

$$\mathbf{M}^1 = \begin{bmatrix} 416(\overline{\boldsymbol{x}}_k - \boldsymbol{x}_{[1]}) & 148\overline{\boldsymbol{x}}_k - 73\boldsymbol{x}_{[1]} - 75\boldsymbol{x}_{[2]} & 148\overline{\boldsymbol{x}}_k - 73\boldsymbol{x}_{[1]} - 75\boldsymbol{x}_{[3]} & 148\overline{\boldsymbol{x}}_k - 73\boldsymbol{x}_{[1]} - 75\boldsymbol{x}_{[4]} \\ 44(4\overline{\boldsymbol{x}}_k - 5\boldsymbol{x}_{[1]} + \boldsymbol{x}_{[3]}) & 11(-12\overline{\boldsymbol{x}}_k + 7\boldsymbol{x}_{[3]} + 5\boldsymbol{x}_{[4]}) & 148\overline{\boldsymbol{x}}_k - 75\boldsymbol{x}_{[1]} - 73\boldsymbol{x}_{[3]} & 11(-12\overline{\boldsymbol{x}}_k + 5\boldsymbol{x}_{[2]} + 7\boldsymbol{x}_{[3]}) \\ 44(4\overline{\boldsymbol{x}}_k - 5\boldsymbol{x}_{[1]} + \boldsymbol{x}_{[4]}) & 11(-12\overline{\boldsymbol{x}}_k + 5\boldsymbol{x}_{[3]} + 7\boldsymbol{x}_{[4]}) & 11(-12\overline{\boldsymbol{x}}_k + 5\boldsymbol{x}_{[2]} + 7\boldsymbol{x}_{[4]}) & 148\overline{\boldsymbol{x}}_k - 75\boldsymbol{x}_{[1]} - 73\boldsymbol{x}_{[4]} \\ 416(\overline{\boldsymbol{x}}_k - \boldsymbol{x}_{[1]}) & 148\overline{\boldsymbol{x}}_k - 73\boldsymbol{x}_{[1]} - 75\boldsymbol{x}_{[2]} & 148\overline{\boldsymbol{x}}_k - 73\boldsymbol{x}_{[1]} - 75\boldsymbol{x}_{[3]} & 148\overline{\boldsymbol{x}}_k - 73\boldsymbol{x}_{[1]} - 75\boldsymbol{x}_{[4]} \\ 44(4\overline{\boldsymbol{x}}_k - 5\boldsymbol{x}_{[1]} + \boldsymbol{x}_{[2]}) & 148\overline{\boldsymbol{x}}_k - 75\boldsymbol{x}_{[1]} - 73\boldsymbol{x}_{[2]} & 11(-12\overline{\boldsymbol{x}}_k + 7\boldsymbol{x}_{[2]} + 5\boldsymbol{x}_{[4]}) & 11(-12\overline{\boldsymbol{x}}_k + 7\boldsymbol{x}_{[2]} + 5\boldsymbol{x}_{[3]}) \\ 44(4\overline{\boldsymbol{x}}_k - 5\boldsymbol{x}_{[1]} + \boldsymbol{x}_{[4]}) & 11(-12\overline{\boldsymbol{x}}_k + 5\boldsymbol{x}_{[3]} + 7\boldsymbol{x}_{[4]}) & 11(-12\overline{\boldsymbol{x}}_k + 5\boldsymbol{x}_{[2]} + 7\boldsymbol{x}_{[4]}) & 148\overline{\boldsymbol{x}}_k - 75\boldsymbol{x}_{[1]} - 73\boldsymbol{x}_{[4]} \\ 416(\overline{\boldsymbol{x}}_k - \boldsymbol{x}_{[1]}) & 148\overline{\boldsymbol{x}}_k - 73\boldsymbol{x}_{[1]} - 75\boldsymbol{x}_{[2]} & 148\overline{\boldsymbol{x}}_k - 73\boldsymbol{x}_{[1]} - 75\boldsymbol{x}_{[3]} & 148\overline{\boldsymbol{x}}_k - 73\boldsymbol{x}_{[1]} - 75\boldsymbol{x}_{[4]} \\ 44(4\overline{\boldsymbol{x}}_k - 5\boldsymbol{x}_{[1]} + \boldsymbol{x}_{[2]}) & 148\overline{\boldsymbol{x}}_k - 75\boldsymbol{x}_{[1]} - 73\boldsymbol{x}_{[2]} & 11(-12\overline{\boldsymbol{x}}_k + 7\boldsymbol{x}_{[2]} + 5\boldsymbol{x}_{[4]}) & 11(-12\overline{\boldsymbol{x}}_k + 7\boldsymbol{x}_{[2]} + 5\boldsymbol{x}_{[3]}) \\ 44(4\overline{\boldsymbol{x}}_k - 5\boldsymbol{x}_{[1]} + \boldsymbol{x}_{[3]}) & 11(-12\overline{\boldsymbol{x}}_k + 7\boldsymbol{x}_{[3]} + 5\boldsymbol{x}_{[4]}) & 148\overline{\boldsymbol{x}}_k - 75\boldsymbol{x}_{[1]} - 73\boldsymbol{x}_{[3]} & 11(-12\overline{\boldsymbol{x}}_k + 5\boldsymbol{x}_{[2]} + 7\boldsymbol{x}_{[3]}) \end{bmatrix},$$

and for the symmetric matrix $\mathbf{M}^2 \in \mathbb{R}^{4\times4}$ and the anti-symmetric matrix $\mathbf{M}^3 \in \mathbb{R}^{4\times4}$ given by

$$\mathbf{M}^2 = \frac{|\Omega_k|}{12096000}\begin{bmatrix} m_{11} & \text{SYM} & & \\ m_{21} & m_{22} & & \\ m_{31} & m_{32} & m_{33} & \\ m_{41} & m_{42} & m_{43} & m_{44} \end{bmatrix}$$

and

$$\mathbf{M}^3 = -\frac{|\Omega_k|}{672000}\begin{bmatrix} 0 & & \text{ANTI-SYM} & \\ 6\ell^2_{[12]} + \ell^2_{[13]} + \ell^2_{[14]} - \ell^2_{[23]} - \ell^2_{[24]} & 0 & & \\ \ell^2_{[12]} + 6\ell^2_{[13]} + \ell^2_{[14]} - \ell^2_{[23]} - \ell^2_{[34]} & 0 & 0 & \\ \ell^2_{[12]} + \ell^2_{[13]} + 6\ell^2_{[14]} - \ell^2_{[24]} - \ell^2_{[34]} & 0 & 0 & 0 \end{bmatrix},$$

where for $\boldsymbol{\ell}^2 = (\ell^2_{[12]}, \ell^2_{[13]}, \ell^2_{[14]}, \ell^2_{[23]}, \ell^2_{[24]}, \ell^2_{[34]})^\mathsf{T}$,

$$\begin{pmatrix} m_{11} \\ m_{21} \\ m_{22} \\ m_{31} \\ m_{32} \\ m_{33} \\ m_{41} \\ m_{42} \\ m_{43} \\ m_{44} \end{pmatrix} = \begin{pmatrix} 3648 & 3648 & 3648 & -912 & -912 & -912 \\ -456 & 924 & 924 & -24 & -24 & -300 \\ -198 & 237 & 237 & 237 & 237 & -158 \\ 924 & -456 & 924 & -24 & -300 & -24 \\ 12 & 12 & 222 & -262 & 4 & 4 \\ 237 & -198 & 237 & 237 & -158 & 237 \\ 924 & 924 & -456 & -300 & -24 & -24 \\ 12 & 222 & 12 & 4 & -262 & 4 \\ 222 & 12 & 12 & 4 & 4 & -262 \\ 237 & 237 & -198 & -158 & 237 & 237 \end{pmatrix} \boldsymbol{\ell}^2.$$

Remark 20. The value of the constants c_k^L, c_k^{LC} and c_k^C appearing in equation (58) is not needed for minimization purposes and therefore are omitted here for brevity.

Remark 21. The notation for the matrices and vectors associated to the linear flux, namely $\widehat{\mathbf{M}}_k^L$ and $\widehat{\mathbf{b}}_k^L$, is the same as in Case I even though they are slightly different (they contain more zero elements). However, the authors believe that this notation simplifies the reading since they are easily differentiated by the case.

D DEDUCTION OF THE EXPRESSIONS FOR THE WEIGHTED PROJECTED EQUILIBRATION CONDITIONS (47)

This section is devoted to provide a compact expression for the constraints of the local optimization problems (47) in terms of the local unknowns of the problem for Cases I and II. That is, equations (55) and (60) are derived by explicitly computing and simplifying the integrals involved in equations (30) and (36).

D.1 Case I. Piecewise constant projection of the data $\hat{q} = \bar{q} = 0$

After some algebraic manipulations, the projected equilibration condition (30) can be rewritten as

$$|\Omega_k|\left(\frac{1}{4}\Pi_k^0(f-\kappa_k^2 u_h)-\nabla u_h\cdot\nabla\phi_i\right)-\kappa_k^2|\Omega_k|\left(\frac{1}{4}r_1+r_0\right)$$
$$+\frac{1}{3}A_{[2]}\sigma_k^{\gamma_{[2]}}(\alpha_{21}+\alpha_{23}+\alpha_{24})+\frac{1}{3}A_{[3]}\sigma_k^{\gamma_{[3]}}(\alpha_{31}+\alpha_{32}+\alpha_{34})+\frac{1}{3}A_{[4]}\sigma_k^{\gamma_{[4]}}(\alpha_{41}+\alpha_{42}+\alpha_{43})=0.$$

Indeed, since F^0 and $\kappa_k^2 r_0+\nabla u_h\cdot\nabla\phi_i$ are constant functions and since $\int_{\Omega_k}\phi_i d\Omega = |\Omega_k|/4$, it follows that the first term of equation (30) is

$$\begin{aligned}\int_{\Omega_k}\left[\phi_i F^0-\kappa_k^2 r_0-\nabla u_h\cdot\nabla\phi_i\right]\,d\Omega &= |\Omega_k|\left(\frac{1}{4}F^0-\kappa_k^2 r_0-\nabla u_h\cdot\nabla\phi_i\right)\\ &= |\Omega_k|\left(\frac{1}{4}\Pi_k^0(f-\kappa_k^2 u_h)-\nabla u_h\cdot\nabla\phi_i\right)-\kappa_k^2|\Omega_k|\left(\frac{1}{4}r_1+r_0\right).\end{aligned}\tag{D28}$$

Also, introducing the values of the tractions g_γ^i given in equation (22) into the second term of equation (30) yields, after explicitly computing the integrals over the faces of the tetrahedron involved therein,

$$\begin{aligned}\sum_{\gamma\subset\partial\Omega_k}\int_\gamma\sigma_k^\gamma g_\gamma^i\,d\Gamma &= \sum_{j=2}^4\int_{\gamma_{[j]}}\sigma_k^\gamma g_{\gamma_{[j]}}^i\,d\Gamma = \sum_{j=2}^4\sum_{\substack{l=1\\l\neq j}}^4\sigma_k^\gamma\alpha_{jl}\int_{\gamma_{[j]}}\lambda_{[l]}\,d\Gamma = \frac{1}{3}\sum_{j=2}^4\sum_{\substack{l=1\\l\neq j}}^4\sigma_k^\gamma\alpha_{jl}A_{[j]}\\ &= \frac{1}{3}A_{[2]}\sigma_k^{\gamma_{[2]}}(\alpha_{21}+\alpha_{23}+\alpha_{24})+\frac{1}{3}A_{[3]}\sigma_k^{\gamma_{[3]}}(\alpha_{31}+\alpha_{32}+\alpha_{34})+\frac{1}{3}A_{[4]}\sigma_k^{\gamma_{[4]}}(\alpha_{41}+\alpha_{42}+\alpha_{43}),\end{aligned}\tag{D29}$$

proving the desired result.

D.2 Case II. Mixed piecewise linear/constant projection of the data $\hat{q} = 1, \bar{q} = 0$

After some algebraic manipulations, the projected equilibration condition (36) can be rewritten as

$$\frac{|\Omega_k|}{20}\left(2F_{[1]}^1+F_{[2]}^1+F_{[3]}^1+F_{[4]}^1-20\kappa_k^2 r_0-20\nabla u_h\cdot\nabla\phi_i\right)$$
$$+\frac{1}{3}A_{[2]}\sigma_k^{\gamma_{[2]}}(\alpha_{21}+\alpha_{23}+\alpha_{24})+\frac{1}{3}A_{[3]}\sigma_k^{\gamma_{[3]}}(\alpha_{31}+\alpha_{32}+\alpha_{34})+\frac{1}{3}A_{[4]}\sigma_k^{\gamma_{[4]}}(\alpha_{41}+\alpha_{42}+\alpha_{43})=0.$$

Indeed, since the tractions in Cases I and II are the same, the boundary term of equation (36) coincides with the one given in (D29). Also, using that $\kappa_k^2 r_k^{i0}+\nabla u_h\cdot\nabla\phi_i$ is constant along with $\int_{\Omega_k}\phi_i\lambda_{[j]}d\Omega = |\Omega_k|(1+\delta_{ij})/20$ allows rewriting the volume integral of equation (36) as

$$\begin{aligned}\int_{\Omega_k}\left[\phi_i F^1-\kappa_k^2 r_k^{i0}-\nabla u_h\cdot\nabla\phi_i\right]\,d\Omega &\\ = \frac{|\Omega_k|}{20}(2F_{[1]}^1+F_{[2]}^1+F_{[3]}^1+F_{[4]}^1)-|\Omega_k|(\kappa_k^2 r_k^{i0}+\nabla u_h\cdot\nabla\phi_i),&\end{aligned}$$

concluding the proof.

E VARIABLE REACTION COEFFICIENT

Let $\kappa\in\mathcal{L}^\infty(\Omega)$ be a function varying in Ω not necessarily piecewise-constant and denote by $\kappa_k^{\min}$ the essential infimum of the function $\kappa_k = \kappa|_{\Omega_k}$ where it is assumed that

$$0\le\kappa_k^{\min} = \operatorname*{essinf}_{x\in\Omega_k}\kappa_k(x)<\infty.$$

Then, upper bounds for the energy norm of the error can be obtained using the following more general version of Theorem 1.

Theorem 4. Let $\boldsymbol{q}\in[\mathcal{L}^2(\Omega)]^3$ and $r\in\mathcal{L}^2(\Omega)$ be a pair of dual estimates verifying

$$\int_\Omega\left(\boldsymbol{q}\cdot\boldsymbol{\nabla}v+\bar{\kappa}^2 rv\right)d\Omega = R^\Pi(v)\quad\forall v\in\mathcal{V},\tag{E30}$$

where $\bar{\kappa}\in\mathcal{L}^\infty(\Omega)$ is such that for all $v\in\mathcal{V}(\Omega_k)$, $\|\bar{\kappa}_k v\|_k\le\|\kappa_k v\|_k$. Then, the following upper bound follows

$$|||e|||^2\le\sum_{k=1}^{n_{\text{el}}}\left(\sqrt{\|\boldsymbol{q}\|^2_{[\mathcal{L}^2(\Omega_k)]^3}+\|\bar{\kappa}_k r\|^2_{\mathcal{L}^2(\Omega_k)}}+\operatorname{osc}_k(f)+\sum_{\gamma\subset\partial\Omega_k\cap\Gamma_{\text{N}}}\operatorname{osc}_\gamma(g_{\text{N}})\right)^2,$$

where the data oscillation constants C_0 and C_1 appearing in equations (8) and (9) are replaced by

$$C_0 = \min\left\{\frac{h_k}{\pi}, \frac{1}{\kappa_k^{\min}}\right\} \quad , \quad C_1^2 = \frac{|\gamma|}{3|\Omega_k|}\frac{1}{\kappa_k^{\min}}\sqrt{(2\max_{\boldsymbol{x}\in\gamma}|\boldsymbol{x}-\boldsymbol{x}_\gamma|)^2 + (3/\kappa_k^{\min})^2}.$$

In this case, the flux free local problems given in equation (18) become: find $\boldsymbol{q}_k^i \in [\mathbb{P}^q(\Omega_k)]^3$ and $r_k^i \in \mathbb{P}^{q-1}(\Omega_k)$ such that

$$-\boldsymbol{\nabla}\cdot\left(\boldsymbol{q}_k^i + \phi_i\boldsymbol{\nabla}u_h\right) + \bar{\kappa}_k^2 r_k^i = \phi_i\Pi_k^{\hat{q}}(f-\kappa_k^2 u_h) - \boldsymbol{\nabla}u_h\cdot\boldsymbol{\nabla}\phi_i \qquad \text{in } \Omega_k, \tag{E31a}$$

$$\left(\boldsymbol{q}_k^i + \phi_i\boldsymbol{\nabla}u_h\right)\cdot\boldsymbol{n}_k^\gamma = \sigma_k^\gamma g_\gamma^i \qquad \text{on } \gamma\subset\partial\Omega_k. \tag{E31b}$$

It is worth noting that if $\bar{\kappa}_k^2 \notin \mathbb{P}^{q-1}(\Omega_k)$, equation (18a) can only be verified for $r_k^i = 0$. Then, the authors suggest to use the following values for $\bar{\kappa}$:

1) if $\kappa_k^2 \in \mathbb{P}^{q-1}(\Omega_k)$, take either $\bar{\kappa}_k = \kappa_k$ or $\bar{\kappa}_k = \kappa_k^{\min}$ and the desired compatible form for r_k^i,
2) otherwise, either take $\bar{\kappa}_k = \kappa_k^{\min}$ and the desired compatible form for r_k^i or $\bar{\kappa}_k = \kappa_k$ and $r_k^i = 0$.

Alternatively, one could use the ideas introduced in Dörfler and Wilderotter[40] to work with a projected polynomial reaction term by means of introducing new terms in the final upper bound.